Inaugural dissertation

for

obtaining the doctoral degree

of the

Combined Faculty of Mathematics, Engineering and Natural Sciences

of the

Ruprecht – Karls – University

Heidelberg

Presented by

M. Sc. Lena Roling

born in: Coesfeld (Germany)

Oral examination: 21.12.2022

Investigating the importance of exported proteins for survival and host cell modification in asexual blood stages of *Plasmodium falciparum*

Referees: Prof. Dr. Michael Lanzer

Prof. Dr. Jude Przyborski

Acknowledgments

A special thanks goes to my supervisor Prof. Jude Przyborski for letting me do my PhD in his laboratory, his advice, and his infectious passion for the malaria parasite. I am very grateful for the opportunity to work in Heidelberg and Giessen and to fly around the world to attend a conference in Australia. A also thank my first supervisor and TAC member Prof. Michael Lanzer for his ideas and discussions during our meetings.

I also thank my TAC member and examiner Prof. Matthias Mayer for his advice, especially in protein biochemistry, and Dr. Alessia Ruggieri for agreeing to be my fourth examiner.

I thank Dr. Ross Douglas for sharing his knowledge and for letting me use his cell culture in times of need. I also thank Sebastian Weber (EMCF Heidelberg) for his help in electron microscopy and Dr. Monika Langlotz (FFCF Heidelberg) who answered all my questions regarding flow cytometry.

Big thanks to all colleagues in Heidelberg and Giessen, for the nice working atmosphere, for sharing their knowledge, and for countless scientific and non-scientific discussions in and outside of the lab. A special thanks to the original Heidelberg group with Sonja Engels, Mathias Diehl, and Ardin Ouayoue who introduced me to the field of protein export in Plasmodium, and thanks to Violeta Pancakova with whom I also attended the MAM2020 conference in Australia.
I would also like to thank my Bachelor and Master students who helped to optimize some of my experiments and thanks to all technical assistants and secretaries who were very helpful after our move to the new lab in Giessen.

Last but not least I thank my family and friends for their support and patience during this time.

Thank you,

Lena

Abstract

The malaria parasite *Plasmodium falciparum* has a unique, complex life cycle and exports a variety of proteins into the erythrocyte to alter the physiological properties of its host cell. These modifications are crucial for survival and they render the parasite a master of immune evasion, which is one of the main reasons why there has not been developed an efficient vaccine to eradicate this devastating disease. Many exported proteins are thought to play a crucial role in protein export and host cell modifications. However, scientific breakthroughs in this field were hampered due to a lack of efficient genetic systems for the blood stages of the parasite. Over the last years, several new genetic tools were established for *P. falciparum* that allow the investigation of essential genes. In this study, four predicted essential proteins were analyzed using the *glmS* ribozyme system, an inducible knockdown method on mRNA level that is activated by glucosamine-6-phosphate. Coupled with selection-linked integration (SLI), it allows faster generation of transgenic cell lines than conventional subcloning methods. The *glmS* system worked efficiently in all cell lines studied with significant downregulation of the proteins of interest with 2.5 mM glucosamine. Concerning the development and morphology of the parasites, there was no growth defect observed via microscopy or SybrGreen-based growth assays. PF3D7_0220300 and PF3D7_0220600 are predicted to be membrane-bound proteins partly co-localizing with the Maurer's clefts marker SBP1, and the erythrocyte membrane, respectively. PF3D7_0113300 and PF3D7_0301600 are predicted to be soluble proteins with the second partly co-localizing with SBP1. Using an *in vitro* static cytoadherence assay, I could show that binding to chondroitin sulfate A was significantly reduced in all cell lines except CS2PF3D7_0113300^{glmS} with the strongest effect observed upon downregulation of PF3D7_0301600 and PF3D7_0220300. Quantification of the mean fluorescence intensities of PfEMP1 VAR2CSA via flow cytometry only showed significantly less signal after downregulation of PF3D7_0220300, further demonstrating the importance of the studied exported proteins in host cell modification, specifically cytoadherence and presentation of PfEMP1 on knobs. These results should be further investigated to get a more comprehensive understanding of the parasites' biology. Moreover, inducible knockout systems using a dimerizable Cre recombinase could circumvent some disadvantages of the *glmS* system resulting from remaining protein levels or the cytotoxicity of glucosamine and should be considered in further studies.

Zusammenfassung

Der Malariaparasit *Plasmodium falciparum* hat einen einzigartigen, komplexen Lebenszyklus und exportiert eine große Anzahl an Proteinen, um die physiologischen Eigenschaften seiner Wirtszelle zu verändern. Diese Modifikationen sind überlebenswichtig und machen den Parasiten zu einem Meister der Immunumgehung, was einer der Hauptgründe dafür ist, dass bis jetzt noch kein ausreichend wirksamer Impfstoff entwickelt werden konnte, um Malaria weltweit auszurotten. Viele teils essentielle exportierte Proteine scheinen eine entscheidende Rolle während des Proteinexports und der Wirtszellmodifizierung zu haben. Allerdings wurden wissenschaftliche Fortschritte bis jetzt dadurch erschwert, dass es keine effizienten genetischen Systeme für die Untersuchung von Blutstadien des Parasiten gab. Während der letzten Jahre wurden einige neue genetische Methoden für *P. falciparum* entwickelt, welche eine Untersuchung von essentiellen Genen ermöglichen. In dieser Arbeit wurden vier potentiell essentielle Proteine mit Hilfe des *glmS* Ribozym-Systems charakterisiert, was eine induzierbare Knockdown-Methode auf Ebene der mRNA ist und durch Glukosamin-6-Phosphat aktiviert werden kann. Gekoppelt mit *Selection-linked Integration* (SLI) können transgene Zelllinien schneller generiert werden, als mit konventionellen Methoden. Das *glmS*-System hat in allen Zelllinien effizient funktioniert und zeigte eine signifikante Herunterregulierung der untersuchten Proteine durch 2,5 mM Glukosamin. In mikroskopischen Untersuchungen und *SybrGreen*-basierten Wachstumsassays konnte kein Defekt der Parasiten festgestellt werden. PF3D7_0220300 und PF3D7_0220600 sind potentiell membrangebundene Proteine, die teilweise mit SBP1, einem Markerprotein der Maurer'schen Spalten, ko-lokalisieren beziehungsweise an der Erythrozytenmembran lokalisiert sind. PF3D7_0113300 und PF3D7_0301600 hingegen sind potentiell lösliche Proteine und PF3D7_0301600 ko-lokalisiert ebenfalls teilweise mit SBP1. Ein statischer *in vitro* Zytoadherenzassay zeigte, dass die Bindung an Chondroitinsulfat A bei allen Zelllinien bis auf CS2PF3D7_0113300^{glmS} signifikant reduziert war. Quantifizierungen der Fluoreszenzintensitäten von PfEMP1 VAR2CSA in durchflusszytometrischen Experimenten zeigten lediglich bei PF3D7_0220300 signifikant reduzierte Signale, was die Funktion der untersuchten Proteine für Wirtszellmodifikation, insbesondere für Zytoadherenz und die Präsentation von PfEMP1 auf den Knobs verdeutlicht. Diese Ergebnisse sollten weiter untersucht werden, um ein besseres Verständnis über physiologische Zusammenhänge zu erlangen. Außerdem sollten induzierbare Knockout-Systeme zum Beispiel mit Hilfe der dimerisierbaren *Cre*-Rekombinase für zukünftige Arbeiten in Erwägung gezogen werden, da diese mögliche Nachteile des *glmS*-Systems als Folge von Restprotein oder Zytotoxizität des Glukosamins umgehen können.

Table of contents

4 Material and Methods

4.1 Material

4.2 Molecular methods

4.3 Biochemical methods

4.4 Cell biology methods

4.5 Microscopy-based methods

List of Figures

List of Tables

List of Supplements

List of abbreviations

ACT	Artemisinin-based combination therapy
AmpR	Ampicillin resistance
APS	Ammonium persulfate
ASP5	Aspartyl Protease 5
aTc	Anhydrotetracycline
bp	Base pair
BSA	Bovine serum albumin
CO_2	Carbon dioxide
COVID-19	Coronavirus Disease 2019
CRISPR	Clustered regularly interspaced short palindromic repeats
CS	Circumsporozoite
CSA	Chondroitin sulphate A
CSC	Stress-gated ion channel
DAPI	4',6-diamidino-2-phenylindole
DD	Destabilization domain
DDD	DHFR destabilization domain
ddH_2O	Double destilled water
DiCre	Dimerizable cyclization recombinase
DMSO	Dimethyl sulfoxide
DNA	Deoxyribonucleic acid
DOZI	Development of zygote inhibited
DTT	Dithiothreitol
ECL	Enhanced chemoluminescence
EDTA	Ethylenediaminetetraacetic acid
EGTA	Ethylene glycol tetraacetic acid
EM	Erythrocyte membrane
EMP1	Erythrocyte membrane protein 1
EMP3	Erythrocyte membrane protein 3
ER	Endoplasmatic reticulum
EXP	Exported protein
FKBP	FK506 binding protein
FRB	FKBP12-rapamycin-binding domain
g	Gravitational force
GA	Glutaraldehyde
gDNA	Genomic DNA
GlcN	Glucosamine
glmS	Glucosamine-6-phosphate ribozyme
GOI	Gene of interest
GPI	Glycosylphosphatidylinositol
HA	Hemagglutinin
h	Hour
HbS	Sickel hemoglobin
HCl	Hydrochloric acid
hDHFR	human dihydrofolate reductase
HDR	Homology-directed repair
HEPES	4-(2-hydroxyethyl)-1-piperazineethanesulfonic acid
HRP	Horse radish peroxidase
Hsp	Heat shock protein
HT	Host-targeting

IFA	Immunofluorescence assay
IRS	Indoor residual spraying
ITN	insecticide-treated mosquito net
iRBC	Infected red blood cell
KAHRP	Knob-associated histidine-rich protein
KCl	Potassium chloride
KOH	Potassium hydroxide
KD	Knockdown
kDa	Kilo Dalton
LB	Lysogeny broth
MAHRP	Membrane-associated histidine-rich protein
MC	Maurer's cleft
Mg	Milligramm
Min	Minute
mM	Millimolar
mRNA	Messenger RNA
N_2	Nitrogen
NeoR	Neomycin resistance
NHEJ	Non-homologous end joining
nm	Nanometer
NPP	New permeability pathway
O_2	Oxygen
OMPP	Outer membrane pore-forming protein
PBS	Phosphate buffered saline
PCR	Polymerase chain reaction
PEXEL	*Plasmodium* export element
PFA	Paraformaldehyde
PIC	Protease inhibitor cocktail
PMSF	Phenylmethylsulfonyl fluoride
PNEP	PEXEL-negative exported protein
POI	Protein of interest
PPM	Parasite plasma membrane
PTEX	*Plasmodium* transporter of exported proteins
PV	Parasitophorous vacuole
PvDBP	*Plasmodium vivax* Duffy-binding protein
PVM	Parasitophorous vacuole membrane
RBC	Red blood cell
REX	Ring exported protein
RNA	Ribonucleic acid
SBP1	Skeleton binding protein 1
SDS	Sodium dodecyl sulfate
SEM	Scanning electron microscopy
SLI	Selection-linked integration
SP	Signal peptide
TAE	Tris acetate EDTA
TCA	Trichloroacetic acid
TGD	Targeted gene disruption
TE	Tris EDTA
TEM	Transmission electron microscopy
TEMED	N,N,N',N'-Tetramethyl ethylenediamine
TetR	Tetracycline repressor

TM	Transmembrane
U	Unit
UTR	Untranslated region
V	Volt
WHO	World Health Organization
µg	Micrograms
µl	Microliter
µm	Micrometer
°C	Degree Celsius

1. Introduction

1.1 Malaria – a parasitic disease

Malaria is one of the most dangerous infectious diseases worldwide with 241 million cases and 627,000 deaths in 2020. Contrary to the positive trend over the last decades, the number of deaths increased by 69,000 compared to 2019, which is mainly caused by service disruptions during the COVID-19 pandemic. Malaria is endemic in 85 countries whereof the African region accounted for 95% of all deaths followed by the South-East Asia region (2%) and America (Figure 1). As many malaria endemic countries are developing countries, the disease poses a significant threat to socioeconomic growth and the health system. The majority of fatal infections occur in children under the age of five and infections during pregnancy often result in low birth weight which is an additional risk factor for neonatal and childhood mortality (WHO, 2021).

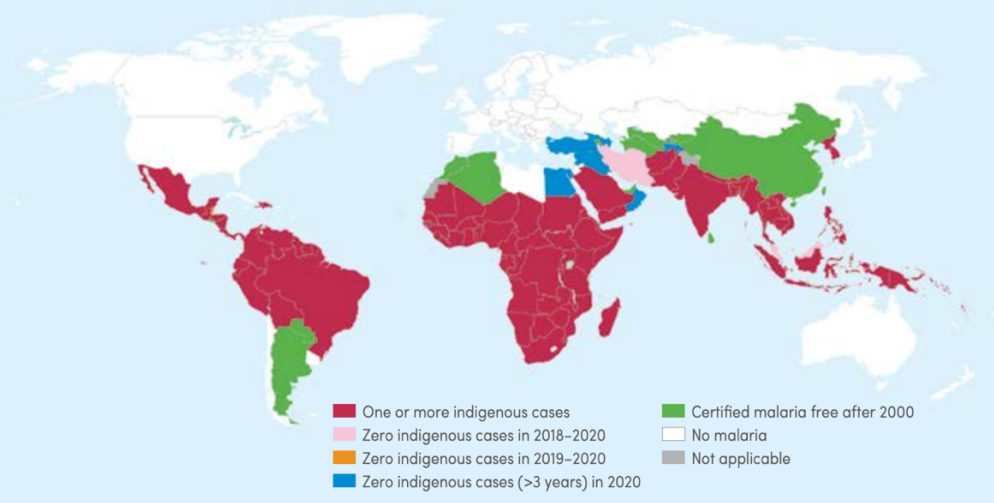

Fig. 1: Global distribution of malaria cases in 2000 and 2020. Countries with no reported malaria cases over the last three years are declared malaria-free (WHO, 2021).

The term malaria comes from the Italian words *mal aria* (spoiled air) as the symptoms were originally linked to the putrid smell in marshland and swamps. In 1980, the French physician Alfonse Laveran could show that malaria is caused by an infection of a protozoan parasite of the genus *Plasmodium*. Later, Giovanni B. Grassi, Amico Bignami, Giuseppe Bastianelli, Angelo Celli, Camillo Golgi, and Ettore Marchiafava discovered the crucial vector which is an *Anopheles* mosquito that transmits the parasite to humans during a blood meal (Cox, 2010).

To this day, there are five human pathogenic *Plasmodium* species known – *P. falciparum*, *P. vivax*, *P. ovale*, *P. malariae,* and *P. knowlesi. P. knowlesi* is a simian species that typically infects macaques but is able to infect humans and is the main source of zoonotic malaria in South-East Asia. However, transmission between humans has not been reported yet (Sato, 2021; WHO, 2021).

P. falciparum is responsible for 74% of infections worldwide, followed by *P. vivax* with 26%. It causes the most dangerous form of malaria that is predominant in sub-Saharan Africa while *P. vivax* infection is less severe (Sato, 2021; WHO, 2021). However, *P. vivax* produces hypnozoites that can lead to relapse even months after the parasites have been eliminated from the blood which needs to be considered when new drugs are generated to eradicate malaria (Thurnburn Manson, 1901; Korteweg, 1902; Sato, 2021).

Humans in malaria endemic regions have developed several polymorphisms due to the evolutionary pressure of *Plasmodium* species that partly protect them from infection or severe malaria symptoms (Sato et al., 2021). For a long time, a Duffy-negative phenotype was considered to fully protect from infection by *P. vivax* as the Duffy protein is the receptor for the Duffy binding protein PvDBP (Horuk et al., 1993; Chitnis & Miller, 1994). However, since the first verified *P. vivax* infection in Duffy-negative individuals was reported in 2010, more and more cases are reported suggesting that this phenotype alone is not the only trait important for invasion, but Duffy-independent mechanisms remain elusive (Ménard et al., 2010; Popovici et al., 2020). Another prominent polymorphism is a hemoglobinopathy, the sickle cell trait, that is presented in nearly 80% of sub-Saharan African individuals (Piel et al., 2013, Taylor et al., 2013)). A mutation in the beta-globin gene leads to the generation of sickle hemoglobin (HbS) and heterologous carriers (sickle cell trait) exhibit up to 90% protection from severe *P. falciparum* malaria (Allison, 1954; Williams et al., 2005). The exact mechanism has yet to be discovered but a leading hypothesis is that the erythrocyte membrane protein PfEMP1 is less expressed leading to reduced cytoadherence of infected red blood cells to endothelium receptors (Cholera et al., 2008). Moreover, polymerization of HbS in tissues with low oxygen levels seems to be a major reason for severely reduced parasite growth in individuals with sickle cell trait and observed mild symptoms (Taylor et al., 2013; Archer et al., 2018). It was observed that actin polymerization is inhibited in HbS erythrocytes likely due to enriched oxidation products leading to the generation of an aberrant actin cytoskeleton. This, together with aberrant MCs, can interfere with the protein trafficking of exported proteins that are important for cytoadherence which further demonstrates the protective role of HbS against malaria (Cyrklaff et al., 2011).

Typically, *falciparum* malaria is characterized by heavy influenza-like symptoms such as headache, chills, myalgia, nausea, vomiting, and diarrhea with periodically reoccurring episodes of fever and increasing anemia that are linked to the asexual blood cycle (Bartoloni & Zammarchi, 2012). The disease progression ranges from asymptomatic infections in some patients with acquired immunity to severe complications like cerebral or placental malaria (Rogerson et al., 2018; Sato, 2021; Tu et al., 2021). This is due to the cytoadherence of erythrocytes infected with

P. falciparum to endothelium receptors. Among other effects like systemic inflammatory responses, the sequestration in various organs leads to vascular congestion, impaired perfusion, and a prothrombotic state (MacPherson et al., 1985; Clemens et al., 1994; Elhassan et al., 1994; Turner et al., 1998; Tu et al., 2021). However, the severity varies from individual to individual and depends on age, immune and pregnancy status, and the parasite itself (species and genotype) (Desai et al., 2007; Rogerson et al., 2018).

As one of the most important preventative measures the WHO still recommends the use of insecticide-treated mosquito nets (ITN) and further indoor residual spraying (IRS) to reduce transmission (WHO, 2021). For global first-line treatment, an artemisinin-based combination therapy (ACT) is commonly used which contains the potent artemisinin component and a second long-lasting partner drug. The combination of several drugs is highly efficient even if they are not as effective on their own, which was further shown in a recent study using triple ACT. (van der Pluijm et al., 2020; WHO, 2021; van der Pluijm et al., 2021). However, emerging resistances against insecticides and antimalarial drugs are of great concern and emphasize the importance to develop new tools for malaria control (WHO, 2021).

In 1987, the development of the first vaccine against *P. falciparum* infection -RTS,S - which contains a sequence of the circumsporozoite (CS) protein, hepatitis B surface antigens, and the immunogenic adjuvant AS01, was initiated. After several clinical studies, it was classified as safe but unfortunately, a phase III randomized trial in sub-Saharan countries between 2009 and 2014 showed that the efficacy decreased significantly over time. Three doses with an additional booster dose had an efficacy of 36% in children (5-17 months of age) and only 26% in infants (6-12 weeks of age) against clinical malaria (Tinto et al., 2015; Arora et al., 2021). A series of pilot introductions in selected African countries since 2016 verified those findings in real-life settings. In 2021, the WHO recommended the use of RTS,S for children in moderate to high transmission regions. Even though it significantly reduces severe clinical malaria and more than 2.3 million doses have been administered in Africa so far, this vaccine alone cannot eradicate global malaria (WHO, 2021). New and adjusted vaccines are under investigation to achieve better and long-lasting protection against genetically diverse parasites and other species (Arora et al., 2021).

1.2 Apicomplexa and the life cycle of *P. falciparum*

The genus *Plasmodium* belongs to the phylum Apicomplexa whose members are mainly obligate parasites that cause various infectious diseases in humans and animals. Important apicomplexan parasites that are relevant for human health and can also infect other vertebrates are *Toxoplasma gondii* and *Cryptosporidium spp.* causing toxoplasmosis and cryptosporidiosis,

respectively. Other Apicomplexans such as *Babesia*, *Theileria*, *Eimeria,* and *Sarcocystis* cause infectious diseases in animals making apicomplexan parasites a threat to economic growth and health systems in affected countries (Arisue & Hashimoto, 2015; Sato et al., 2021).

Apicomplexa are closely related to dinoflagellates which also belong to the superphylum Alveolata that has a characteristic apical complex, hence the name Apicomplexa, which is crucial for host cell invasion (Fast et al., 2002; Arisue & Hashimoto, 2015). Most apicomplexan parasites have a small plastid called apicoplast, which is derived from secondary endosymbiosis of a red algae but has lost its photosynthetic abilities (Janouskovec et al, 2010). However, it plays a role in type II fatty acid biosynthesis, isoprenoid synthesis, and heme synthesis and is a target of many antimalarial drugs like fluoroquinolones, aminocoumarins, and doxycycline (Surolia & Padmanaban, 1992; Yu et al., 2008; Yeh & DeRisi, 2011; Arisue & Hashimoto, 2015; Biddau & Sheiner, 2019). It is essential for parasite development in mosquitoes and the liver while it seems to be non-essential in the blood stage development *in vitro* as long as the isoprenoid precursor isopentenyl pyrophosphate is added to the culture medium. This further shows that the generation of isoprenoid precursors is a crucial function of the apicoplast in blood stages (Vaughan et al., 2009; Yeh & DeRisi, 2011; van Schajjk et al., 2014). There are also some exceptions like *Cryptosporidium* that does not have an apicoplast and recently discovered apicomplexan chromerids with photosynthetic plastids (Zhu et al., 2000; Moore et al., 2008; Oborník et al., 2011; Oborník et al., 2012). The parasite ingests and metabolizes 80% of the erythrocyte hemoglobin as a source of nutrients and converts it into toxic heme that is subsequently detoxified and stored in the food vacuole as crystalline hemozoin. Some antimalarial drugs like chloroquine affect this process by inhibiting the detoxification which results in the death of the parasite (Francis et al., 1997; Lingelbach & Joiner, 1998).

All human pathogenic *Plasmodium* species share a similar, complex life cycle with a host change between a human and an *Anopheles* mosquito as a final host. After transmission of the parasite to the human host during a mosquito's blood meal, the parasite first infects hepatocytes, followed by an intraerythrocytic phase that is divided into asexual and sexual blood stage development (Figure 2) (Sato et al., 2021).

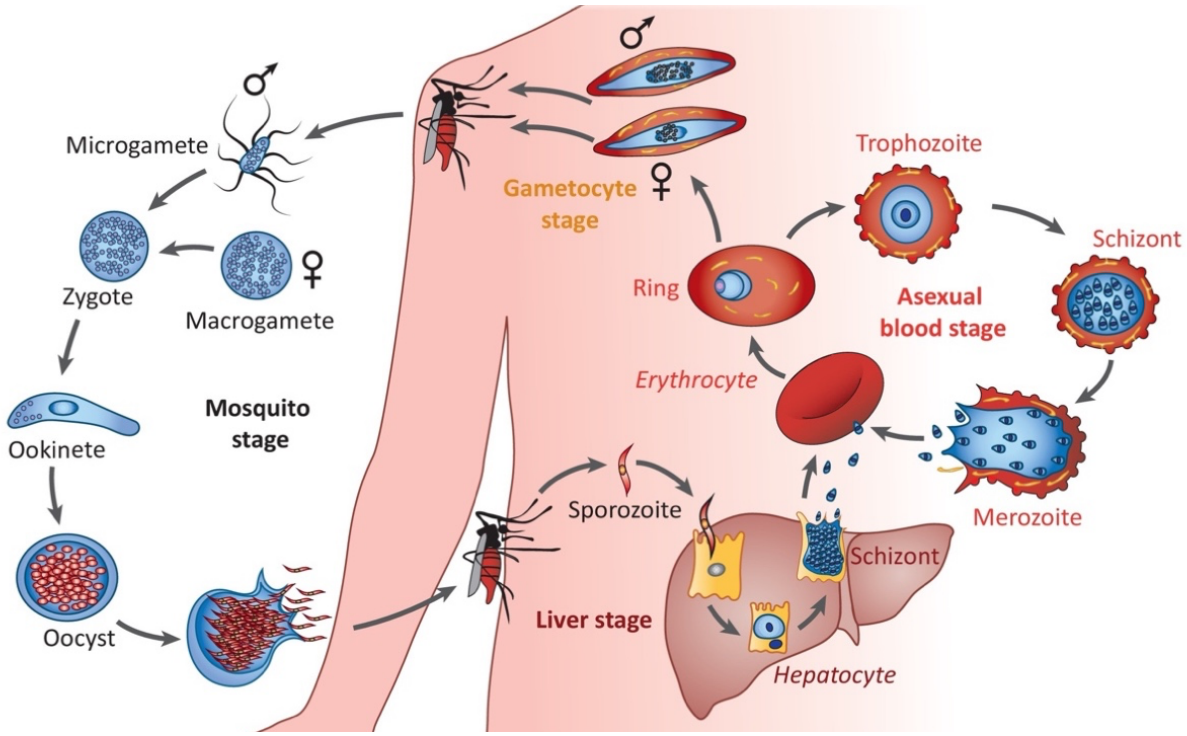

Fig. 2: Life cycle of the human pathogenic parasite *P. falciparum*. A female *Anopheles* mosquito injects sporozoites into the skin of the human host that quickly migrate into blood vessels. They first infect hepatocytes and asexually develop until merozoites are released into the bloodstream and invade erythrocytes where the asexual blood cycle takes place. Some parasites develop into sexual blood stages and the mature gametocytes are taken up by an *Anopheles* mosquito. Here, sexual reproduction takes place until sporozoites are formed and the whole life cycle starts again (Maier et al., 2019).

The complex life cycle starts with a bite of an infected female *Anopheles* mosquito that injects sporozoites into the skin of the human host from where they actively penetrate dermal blood vessels and spread throughout the blood system (Sidjanski & Vanderberg, 1997). Only 35% of the injected sporozoites reach blood vessels while about 50% remain in the skin and can be removed by phagocytes (Amino et al., 2006, 2008). Some parasites get to liver sinusoids where they invade their first host cells, the hepatocytes after traversing Kupffer cells and multiple hepatocytes (Tavares et al., 2013). In an asexual developmental process called liver schizogony, the nuclei divide multiple times to form mature liver schizonts that takes about 6-15 days depending on the species (Prudêncio et al., 2006). Merozoites leave the hepatocytes inside vesicle structures called merosomes that protect them from the hosts' immune system and rupture once they have reached the lung capillaries releasing up to 1000 merozoites (Baer et al., 2007; Shears et al., 2019). Those merozoites invade erythrocytes via an apical complex that is specific for apicomplexan parasites. It is made up of several organelles like secretory vesicles, micronemes, dense granules, and rhoptries that release proteins important for invasion (Cowman et al., 2012). In blood and liver stages, a so-called parasitophorous vacuole (PV) is formed during

invasion when the force of the parasites' actomyosin motor leads to invagination of the host cell membrane. The additional PV membrane (PVM) therefore isolates the parasite from the erythrocyte (Baum et al., 2006; Matz et al., 2020). During the 48 h asexual blood cycle, the parasites first develop into ring stages, followed by trophozoites and schizonts that eventually rupture and release 16-36 invasive daughter merozoites into the bloodstream that can infect new erythrocytes. This intraerythrocytic cycle is the reason for most of the pathology associated with malaria (Salmon et al., 2001; Bartoloni & Zammarchi, 2012). Quickly after invasion, the parasite induces crucial host cell modifications that ensure immune evasion and the survival of the parasite which is discussed in more detail in chapter 1.4. Some parasites differentiate into sexual forms called gametocytes which can be triggered by stress factors like high parasitemia (Carter & Miller, 1979; Billker et al., 1998). During gametocytogenesis, the parasite goes through five developmental stages until mature, crescent-shaped gametocytes are formed after about 12 days (Hawking et al., 1971; Bennink et al., 2016). Immature gametocytes sequester in the bone marrow and once they are mature, they circulate in the peripheral blood and can be taken up by a female *Anopheles* mosquito during a blood meal (Aguilar et al., 2014; Joice et al., 2014). In the midgut of the mosquito, the female macrogametocytes and male microgametocytes develop into gametes. A change in temperature, pH, and xanthurenic acid in the midgut trigger egress and exflagellation of male microgametes that then fertilize female macrogametes and form diploid zygotes (Billker et al., 1997; Billker et al., 1998; Sinden et al., 2010; Bennink et al., 2016). These develop into motile ookinetes that penetrate the midgut epithelium and further develop into oocysts (Vinez, 2005). Invasive sporozoites are formed inside oocysts that eventually rupture and release thousands of sporozoites into the hemolymph from which they enter salivary glands (Sterling et al., 1973; Pimenta et al., 1994; Sato et al., 2021). When these infected *Anopheles* mosquitoes feed on humans, the sporozoites in the saliva are injected into the hosts' skin initiating a new parasite life cycle (Figure 2) (Sidjanski & Vanderberg, 1997; Amino et al., 2006, 2008).

1.3 Protein export in asexual blood stages of *P. falciparum*

Plasmodium parasites live within an erythrocyte and are surrounded by an additional membrane, the PVM, that is formed during invasion (Baum et al., 2006; Matz et al., 2020). Mature erythrocytes are very simple cells without any organelles, including a nucleus, and mainly consist of hemoglobin. Given this special host cell environment, the parasite needs to remodel its host cell to survive and avoid clearance by the spleen and immune system (Maier et al., 2009). Important host cell modifications and their functions are discussed in more detail in chapter 1.4. However, in order to modify its host cell for complete takeover, the parasite solely relies on its own proteins

that need to be exported and it builds a new protein transport machinery that allows the transport and export of virulence proteins up to the erythrocyte membrane (EM) (Przyborski et al., 2016).

The genome of *P. falciparum* codes for about 5,365 genes and so far, the function is only known for a fraction of them which demonstrates the importance of further research (Gardner et al., 2002; Antorini et al., 2012). As *P. falciparum* heavily depends on protein export, it is no wonder that the proteome consists of a remarkable number of exported proteins, more specifically about 10% of parasite proteins are part of the exportome (Gabriela et al., 2022).

Typically, a hydrophobic sequence close to the N-terminus of a protein is a signal to enter the secretory pathway, which is recessed from the N-terminal end in mostly soluble secreted *P. falciparum* proteins (Albano et al., 1999; Przyborski et al., 2016). Secreted membrane proteins however, usually contain canonical signal sequences at the N-terminal end (Deponte et al., 2012). These hydrophobic N-terminal sequences are a default signal for targeting proteins to the PV via the secretory pathway but they are not sufficient for export into the host cell, as the proteins need to cross the PVM, as well (Waller et al., 2000; Adisa et al., 2003).

Exported proteins can be divided into two groups: those that contain an N-terminal export signal called *Plasmodium* Export Element (PEXEL) or Host-Targeting (HT) motif and those that lack this signal (Hiller et al., 2004; Marti et al., 2004; Mayer et al., 2021). Most PEXEL-negative exported proteins (PNEPs) consist of an internal transmembrane domain (TM) that directs them to the endoplasmatic reticulum (ER) via a Sec61/62/63-SPC25-PMV translocon and some even have a standard N-terminal signal sequence but PNEPs are not as prevalent as PEXEL proteins (Heiber et al., 2013; Marapana et al., 2018; Matthews et al., 2018). However, due to the lack of a characteristic sequence, it is hard to predict their exact number. Current data suggest the presence of >50 PNEPs and around 246 PEXEL proteins, not including proteins from large multigene families of *rifin* (PEXEL), *stevor* (PEXEL), *pfemp1* (PNEP), and PEXEL-containing proteins that were shown to be not exported *in vitro* (Jonsdottir et al., 2021).

All PEXEL proteins share the pentameric signal sequence RxLxE/Q/D that is cleaved by the protease Plasmepsin V (PMV) at the conserved leucine residue during translation in the ER. The mature N-terminus is acetylated (Ac-xE/Q/D) and the protein is transported in secretory vesicles to the plasma membrane followed by secretion into the PV (Boddey et al., 2009; Boddey et al., 2010; Russo et al., 2010). Soluble proteins are possibly transported in vesicles and directly released into the PV, while transmembrane proteins might either be transported in a chaperoned, soluble state or are first inserted into the parasite plasma membrane (PPM) like PNEPS (Matthews et al., 2018).

To cross the PVM, a complex structure called *Plasmodium* translocon of exported proteins (PTEX) is needed, that actively transports unfolded proteins into the erythrocyte cytosol using ATP hydrolysis as an energy source. The three core components of PTEX are the pore-forming protein EXP2 (Exported protein 2), the AAA+ ATPase Hsp101 (Heat shock protein 101), and PTEX150 which has a structural function (de Koning-Ward et al., 2009; Elsworth et al., 2014; Beck et al., 2014; Elsworth et al., 2016). Recent studies show, that Hsp101 also localizes in the ER and a portion of it is secreted into the PV in ring to mid-trophozoite stage parasites which is the period of active protein export. Gabriela et al. hypothesize that Hsp101 interacts with PEXEL proteins in the ER and chaperones them through the EM and PV to the PVM, where they bind to the rest of PTEX (Figure 3) (Gabriela et al., 2022).

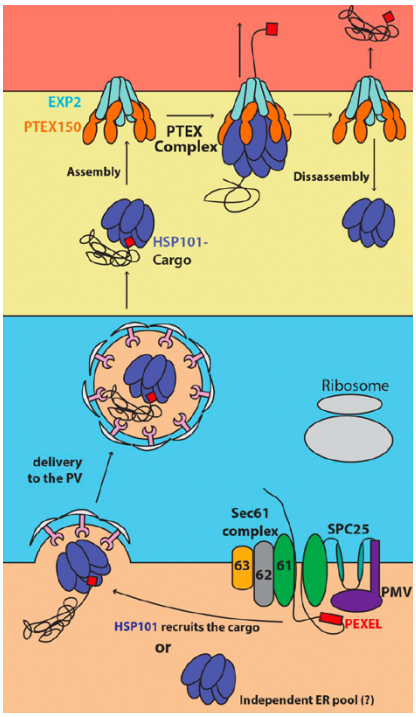

Fig. 3: Hsp101 chaperones PEXEL proteins from the ER to PTEX for protein export into the erythrocyte cytosol. PEXEL proteins reach the ER lumen via a Sec61/62/63-SPC25-PMV translocon and are then recruited by Hsp101 and chaperoned through the parasitophorous vacuole to the rest of PTEX. At the parasitophorous vacuole membrane, the Hsp101-cargo complex binds to the PTEX150-Exp2 subcomplex leading to the translocation of the protein. ER: endoplasmatic reticulum; PMV: Plasmepsin V; PEXEL: *Plasmodium* Export Element; PV: parasitophorous vacuole; PTEX: *Plasmodium* translocon of exported proteins (modified from: Gabriela et al., 2022)

Proteins that have passed PTEX will either be refolded by exported parasite and/or human chaperones and stay in the erythrocyte cytosol or they are transported further to their destination in Maurer's clefts (MC), the membrane skeleton, or the EM (Figure 4) (de Koning-Ward et al., 2016; Mayer et al., 2021). *P. falciparum* codes for many more heat-shock proteins (Hsps) than other *Plasmodium* species which might be needed for the crucial trafficking of PfEMP1 (Sargeant et al., 2006; Külzer et al., 2010; Külzer et al., 2012; Jonsdottir et al., 2021). The role of PfEMP1 in the cytoadherence of infected erythrocytes to endothelial receptors is explained in more detail in chapter 1.4. It is assumed that parasite proteins destined for the EM either pass directly through the cytosol in chaperone-associated complexes called J-dots or via MCs, which are parasite-

derived organelles that presumably act as sorting units and pack proteins into vesicles for further trafficking (Figure 4) (Deponte et al., 2012; de Koning-Ward et al., 2016). Several PNEPs like MAHRP (Membrane-associated histidine-rich protein), REX1 (Ring exported protein 1), REX2, and SBP1 (Skeleton binding protein 1) are MC resident proteins that have N-terminal regions that are important for export. Studies have shown that these regions of SBP1, REX2, and MAHRP can even be exchanged while still keeping their ability for export (Spycher et al., 2008; Dixon et al., 2008; Haase et al., 2009; Saridaki et al., 2009). The PEXEL protein KAHRP (Knob-associated histidine-rich protein), in complex with PfEMP1 (erythrocyte membrane protein 1) and PfEMP3, also transiently associates with MC via its histidine-rich region (Wickham et al., 2001). The PNEP PfEMP1 does not have a defined N-terminal signal sequence but a putative TM domain, PEXEL-like motifs, and an N-terminal head structure that are important for trafficking (Knuepfer et al., 2005a). A knockout of several MC resident proteins (SBP1, MAHRP1) has an impact on the MC structure and/or transport of PfEMP1 from MCs to the erythrocyte surface (Spycher et al., 2008; Maier et al., 2008; Cooke et al., 2006). How proteins are transported from MC to their final destination and the role of membranous structures associated with MCs is still very poorly understood (de Koning-Ward et al., 2016).

Interestingly, some parts of the export system of *P. falciparum* are conserved in other Apicomplexans like *T. gondii*, *Babesia,* and *Cryptosporidium*. They all have PEXEL-like motifs and proteases that resemble Plasmepsin V of *P. falciparum* (Matthews et al., 2018). However, in *T. gondii* the Aspartyl Protease 5 (ASP5) cleaves the PEXEL-like motif (called *Toxoplasma* export element (TEXEL)) in the Golgi instead of the ER, and the motif is not always located at the N-terminus. Moreover, TEXEL proteins are not necessarily exported but can also be localized at the PVM which has not been observed for PEXEL proteins (Hsiao et al., 2013; Hammoudi et al., 2015; Curt-Varesano et al., 2016; Coffey et al., 2016;). The translocon PTEX is only found in *Plasmodium*, while other Apicomplexans have a distant homolog of EXP2, which is only used as a pore for small molecules (Gold et al., 2015, Matthews et al., 2018). As *Babesia* loses its PVM quickly after invasion, it is not surprising that it does not have a translocon and does not need PEXEL-like motifs for export (Rudzinska et al., 1976). However, the motif seems to be important for the correct localization to spherical bodies before export (Pellé et al., 2015). There are still a lot of steps in protein export of Apicomplexans that need further research and it can help to discover potential drug targets for future malaria treatments.

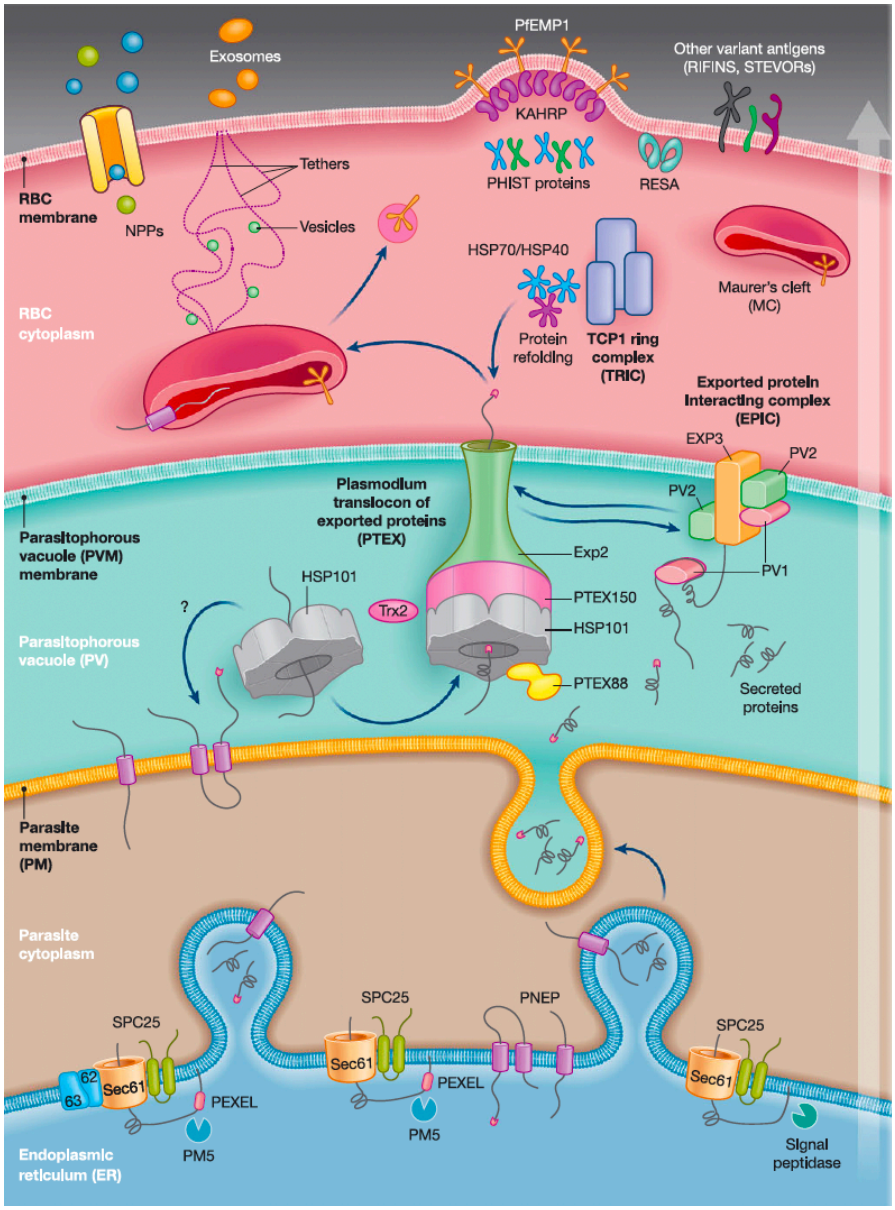

Fig. 4: Model of protein export in *P. falciparum*. Proteins enter the endoplasmatic reticulum (ER) via a Sec61-SPC25 translocon (Sec62-dependent or -independent) where the PEXEL motif is cleaved by the endoprotease Plasmepsin V (PMV). Acetylated and mature soluble PEXEL proteins are transported in secretory vesicles to the parasitophorous vacuole (PV) while transmembrane proteins might be transported in a soluble, chaperoned state or are inserted into the membrane for trafficking like PNEPS. The unfolded proteins are actively exported into the RBC cytoplasm via the *Plasmodium* translocon of exported proteins (PTEX). In the RBC cytoplasm, the proteins need to be refolded by heat shock proteins (Hsp70/Hsp40), then stay in the cytosol or are transported to their destination in Maurer's clefts (MC), the cytoskeleton or the RBC membrane. Most exported proteins are trafficked via MCs. PEXEL: *Plasmodium* export element; PNEP: PEXEL-negative exported proteins; RBC: red blood cell. (Matthews et al., 2018).

1.4 *P. falciparum* induced host cell modifications

Host cells of *P. falciparum* are hepatocytes and terminally differentiated erythrocytes that have lost their nucleus during maturation and are therefore not able to synthesize new proteins. The main component of erythrocytes is hemoglobin which is important for O_2 and CO_2 transport. As

the membrane skeleton is very flexible, erythrocytes are highly deformable cells that can penetrate 1-2 µm interendothelial slits between the splenic chord and venous sinuses (An & Mohandas, 2008; Maier et al., 2009). Most importantly, the parasite induces changes in permeability for sufficient nutrient supply from the blood plasma and modifies the adhesive properties to endothelial receptors by presenting PfEMP1 on protrusions (knobs) on the cell surface. This way, the parasite can avoid clearance by the spleen that detects changes on the surface and in rigidity (Dondorp et al., 1999; Maier et al., 2009; Beck and Ho, 2021).

The whole asexual blood cycle of *P. falciparum* takes ~48 h and is characterized by time-specific stages (ring, trophozoite, schizont) and host cell modifications that can be observed in light and electron microscopy (Figure 5) (Maier et al., 2009). During the first 5 minutes, merozoites invade the host cell by manipulating the biomechanical properties of the EM and using the parasites' actomyosin motor for penetration. After the first contact and correct reorientation of the merozoite with its apical end towards the EM, the EM surface is deformed to enable easier parasite invasion (Baum et al., 2006; Groomes et al., 2022). Final attachment to EM receptors is mediated by adhesive ligands like erythrocyte-binding like (EBL), reticulocyte binding homologous (Rh), or AMA1 ligands (apical membrane antigen) that are released from secretory organelles in the apical end of the merozoite while the erythrocyte recovers its normal, biconcave shape (Maier et al., 2009; Baum et al., 2009; Treeck et al., 2009.)

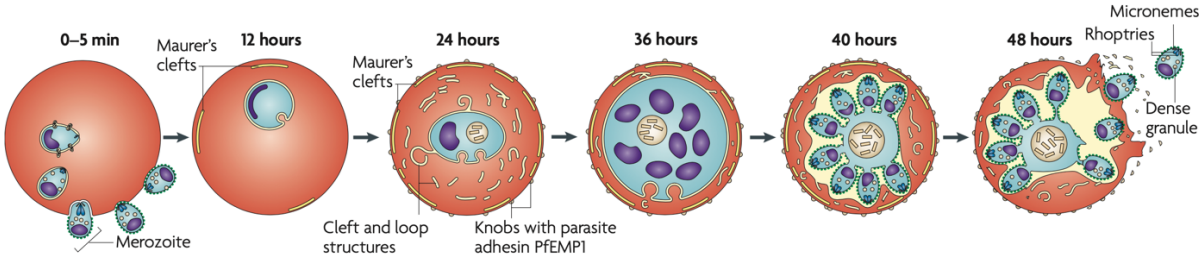

Fig. 5: Asexual blood cycle of *P. falciparum*. After merozoites invade erythrocytes, the parasite goes through different developmental stages -ring (0-24 hpi), trophozoite (24-36 hpi), and schizont stage (40-48 hpi)- before the mature schizont ruptures and releases 16-32 invasive merozoites. Between 12 and 24 hpi, membranous structures called Maurer's clefts and knobby protrusions (knobs) presenting PfEMP1 on the erythrocyte surface are formed. hpi: hours post invasion (Maier et al., 2009).

The active force of invasion leads to an invagination of the EM that eventually pinches off, resulting in the formation of the PVM (Figure 6A) (Baum et al., 2006; Matz et al., 2020). Phospholipids from the EM and parasite-derived lipids contribute to the biogenesis of the PVM, as it was shown that fluorescently labeled probes of both origins are incorporated into the PVM (Mikkelsen et al., 1988; Ward et al., 1993). Even though the EM and PVM form a continuous membrane structure during invasion, the EM area after invasion is not changed, further indicating

a major share of parasite phospholipids (Dluzewski et al., 1995). About 24 hours post invasion (hpi), membrane whorls, loops, and vesicles are formed that extend from the PVM far into the erythrocyte cytosol (Figures 5 and 6B). This so-called tubovesicular network (TVN) is a continuous PVM system that seems to be important for molecular organization in protein exporting parasite stages (Elmendorf & Haldar, 1994; Behari & Haldar, 1994; Hanssen et al., 2010; Matz et al., 2020).

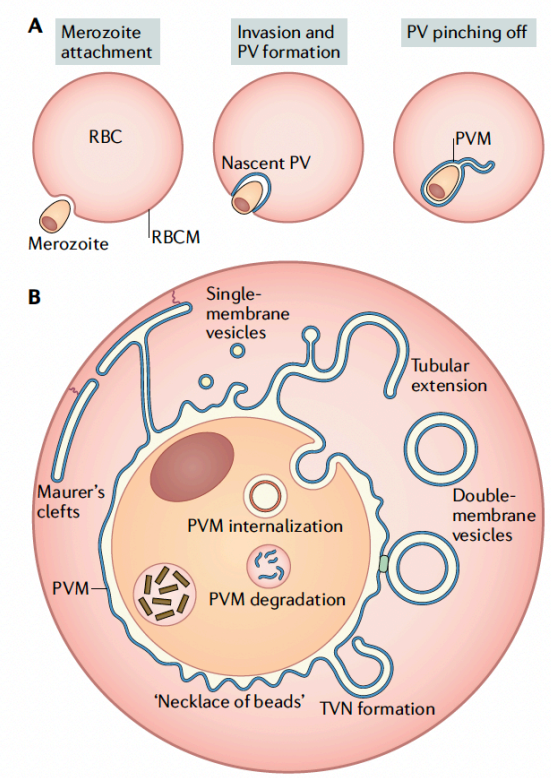

Fig. 6: The parasitophorous vacuole of *P. falciparum*. A) The parasitophorous vacuole (PV) is formed during the invasion of a merozoite and an invagination of the erythrocyte membrane that ultimately pinches off. **B)** The parasite modifies its host cell by forming membrane whorls, loops, and vesicles that extend from the PV membrane into the erythrocyte cytosol. The tubovesicular network (TVN) and Maurer's clefts play a crucial role in protein exporting parasite stages. RBCM: red blood cell membrane (modified from: Matz et al., 2020).

About 12 hpi, other membranous structures in the erythrocyte cytosol, so-called Maurer's clefts (MC), can be observed (Figure 5 and 7) (Maurer, 1902; Maier et al., 2009). MCs are disc-shaped organelles up to 1 µm in length with electron-dense coats that are attached via tethers to the EM and PVM and are thought to serve as trafficking and sorting platforms for proteins that are exported to the EM (Przyborski et al., 2003; Lanzer et al., 2006; Hanssen et al., 2008a; DeKoning-Ward et al., 2016). Data suggest that MCs originate from the PVM as they seem to be part of a continuous membrane network (Lanzer et al., 2006). Knockout and knockdown studies of several MC-resident proteins have shown functions in the correct formation of MCs and efficient delivery

of exported proteins to the EM, especially PfEMP1 (DeKoning-Ward et al., 2016). As an example, truncation of REX1 leads to stacked MCs, impaired trafficking of PfEMP1 to the EM and therefore reduced cytoadherence (Hanssen et al., 2008b; McHugh et al., 2015). And parasites lacking GEXP07 (Gametocyte-exported protein 07) show fragmented MCs, reduced PfEMP1 surface exposure with reduced EMP1-mediated cytoadherence, and aberrant knob formation (McHugh et al., 2020).

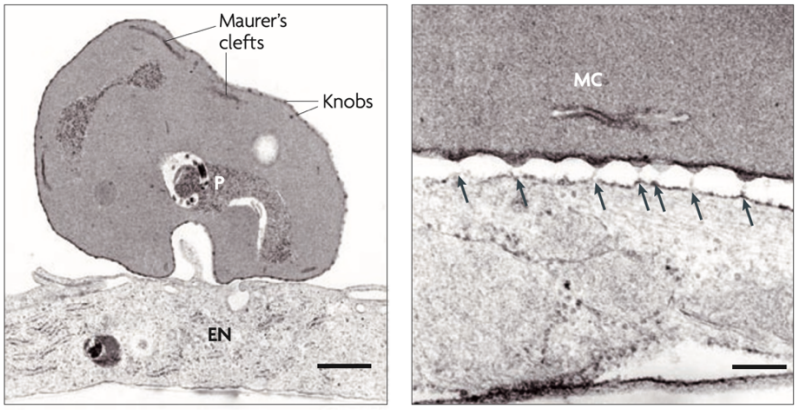

Fig. 7: Cytoadherence of erythrocytes infected with *P. falciparum* to endothelial receptors. Images of transmission electron microscopy of an infected erythrocyte that is adhering to the endothelium (EN). A detailed image shows the contact between the infected cell and the endothelium with electron-dense strands that connect the cells (arrows). MC: Maurer's cleft. Left scale bar 1 µm. Right scale bar 100 nm (Maier et al., 2009).

Moreover, there are two types of vesicles that are associated with the TVN and MCs and seem to play a role in protein transport: the uncoated 25 nm vesicle and the coated 80 nm vesicle that is additionally localized in the erythrocyte cytosol independent of the TVN/MCs (Hanssen et al., 2010). Other structures important for protein transport are J-dots. These membranous structures of about 30 nm are highly mobile and are associated with chaperone complexes that transport proteins such as PfEMP1 to the EM (Külzer et al., 2010; Külzer et al., 2012; Zhang et al., 2017).

A specific feature of erythrocytes infected with mature stages of *P. falciparum* is the cytoadherence to endothelial receptors. This strain-specific host cell modification is mediated by PfEMP1 that is presented on knobby protrusions on the surface of infected erythrocytes called knobs which can be observed in EM images about 16 hpi (Figure 7 and 8) (Baruch et al., 1995; Smith et al., 1995; Su et al., 1995; Maier et al., 2009). Contrary to earlier expectations, each knob only presents 3.3 ± 1.7 PfEMP1 VAR2CSA molecules in the wildtype strain FCR3 which are mainly located around the tip of the knob (Sanchez et al., 2019). The main protein that is crucial for the knob structure is KAHRP as a knockout leads to a knobless phenotype and a highly reduced level of cytoadherence under flow conditions while it does not impair the export of PfEMP1 to the surface (Crabb et al., 1997). KAHRP molecules are associated with components

of the membrane cytoskeleton and they form a spiral scaffold with 4-5 turns and ~32 nm in height underneath the knobs. This also reduces the elasticity of infected erythrocytes (Sanchez et al., 2021).

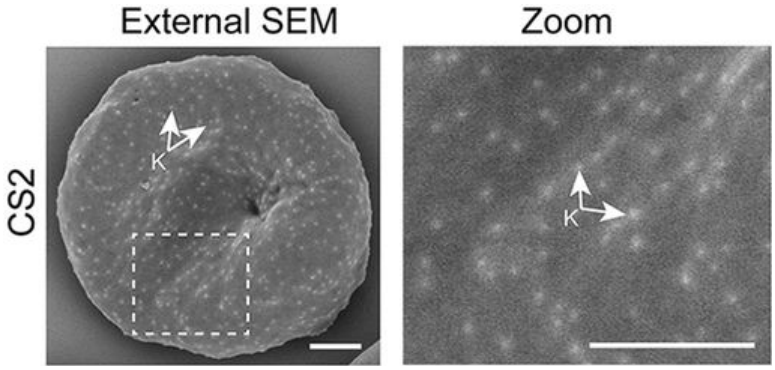

Fig. 8: Knobs on the surface of infected erythrocytes. Scanning electron microscopy (SEM) reveals knobs (K) on the surface of erythrocytes infected with the *P. falciparum* strain CS2. Scale bar: 1 µm (modified from: McHugh et al., 2020).

PfEMP1 is a variant surface antigen that is encoded by about 60 *var* genes with mutual exclusive expression and binds to endothelial receptors (Baruch et al., 1995; Smith et al., 1995; Su et al., 1995; Gardner et al., 2002). Due to this antigenic variation, the parasite can evade the immune system as it cannot adapt fast enough to identify and attack infected cells (Chen et al., 1998; Scherf et al., 1998; Introini et al., 2022). Even though *var* genes have a high sequence similarity and the expression can be lost in long-term cell culture, it is possible to express a single *var* gene using genetic approaches or select for binding to specific receptors (Omelianczyk et al., 2020). The different PfEMP1 variants mediate binding to receptors of non-infected erythrocytes leading to rosetting or they mediate binding to endothelial receptors such as ICAM-1, EPCR, CR1, or CD36 with VAR2CSA binding specifically to the endothelial receptor CSA that is predominantly expressed in the placenta (Fried & Duffy, 1996; Beeson et al., 1998; Cockburn et al., 2004; Ochola et al., 2011; Turner et al., 2013; Wahlgren et al., 2017). Cytoadherence prevents clearance by the spleen to ensure the parasites' survival and their development into gametocytes but it can also disrupt the microvascular blood flow which can lead to hypoxia in tissues and organs. Binding to endothelial receptors via PfEMP1 is specific for *P. falciparum* and this is also the reason that it causes the most severe form of malaria with dangerous complications like cerebral or placental malaria (Dondorp et al., 2008; Wahlgren et al., 2017; Introini et al., 2022).

Mature erythrocytes mainly contain hemoglobin that is used by the parasite as a nutrient supply. However, as hemoglobin lacks isoleucine and methionine is not sufficiently available, the parasite needs to acquire these amino acids from the human serum (Hill et al., 1962; Counihan et al., 2021). Moreover, *P. falciparum* cannot synthesize its own purines and pantothenate, which

is an important precursor of coenzyme A and both are essential for parasite growth (Saliba et al., 1998; Downie et al., 2008). Other growth-limiting factors like thiamine, folate, and lipid building blocks (fatty acids, choline, ethanolamine, serine) are also obtained from the serum, as *P. falciparum* is not able to produce sufficient amounts (Wrenger et al., 2006; Wang et al., 2007; O'Neal et al., 2020). All those nutrients need to be included in the medium for *in vitro* cultivation of *P. falciparum* (Divo et al., 1985).

To import these necessary nutrients, the parasite increases its permeability for smaller, anionic, and non-polar solutes by establishing new permeability pathways (NPPs) in the EM which are attractive drug targets (Ginsburg et al., 1983; Dickerman et al., 2016). The exact molecular composition of those NPP channels remains elusive as there is no functional evidence so far. However, a heterotrimeric complex of CLAG3 (cytoadherence linked asexual gene 3), RhopH2 (rhoptry protein H2), and RhopH3 is thought to form the NPP channel with CLAG3 likely being the pore-forming protein (Schureck et al., 2021). Another possibility is that an endogenous channel is activated by the RhopH complex. Parasitic anion-selective channels that might also play a role in NPPs without an auxiliary RhopH complex are calcium-dependent, stress-gated ion channels (CSCs) or outer membrane pore-forming proteins (OMPPs) (Reddy & Saier Jr., 2016; Counihan et al., 2021). To further cross the PVM, a nutrient-permeable channel made of EXP2, which also forms the pore of PTEX, is required. The essential protein EXP1 interacts with EXP2 to ensure its function as a nutrient channel and the correct distribution in the PVM (Figure 9) (Mesen-Ramirez et al., 2019; Counihan et al., 2021).

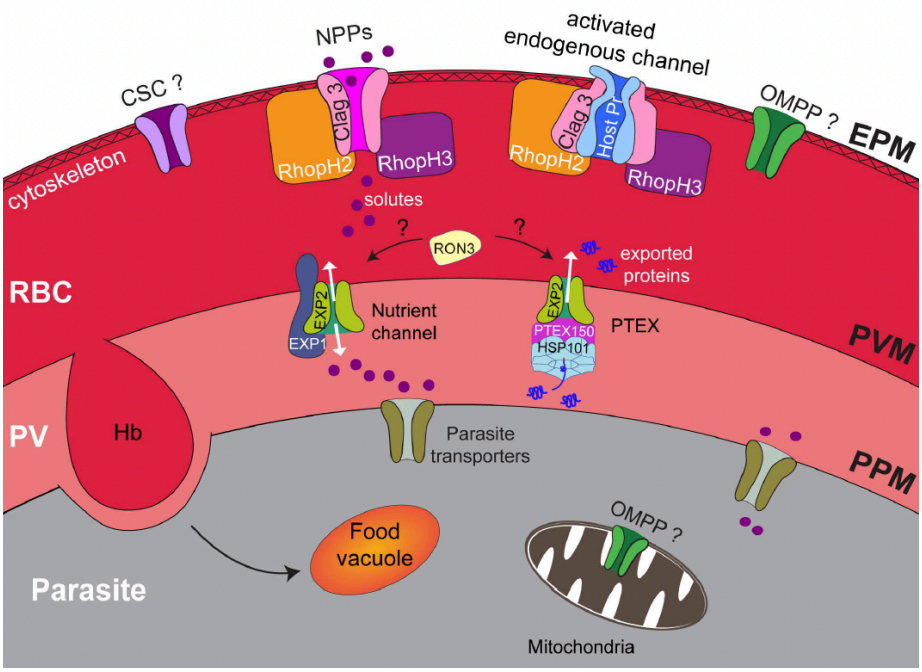

Fig. 9: Host cell modifications of *P. falciparum* that enable acquisition of crucial nutrients. Nutrients are imported into the parasitophorous vacuole (PV) via new permeability pathways (NPP), activated endogenous channels, or other protein channels in the erythrocyte plasma membrane (EPM). NPPs are made of a pore protein CLAG3 that is associated with RhopH2 and 3. Alternatively, there might be an unknown pore protein that is activated by the RhopH-complex. A nutrient-permeable channel made of EXP2 enables transport through the PV membrane (PVM). EXP2 is also a core component of the Plasmodium translocon of exported proteins (PTEX) that is important for protein export. To further transport nutrients into the parasite, the parasite plasma membrane (PPM) also contains several transporters. CSC: stress-gated ion channels; OMPP: outer membrane pore-forming protein; Hb: hemoglobin (Counihan et al., 2021).

1.5 Methods and tools to analyze the function of exported proteins and host cell modifications

Knockout and/or knockdown cell lines of candidate exported genes can be used to analyze their function in blood stages of *P. falciparum in vitro*. During this study, the main focus was on the effect of a downregulated gene on growth, host cell modifications, cytoadherence, and protein localization and distribution. In order to analyze those factors, several methods and tools were used.

The growth and development were mainly analyzed microscopically in Giemsa-stained blood smears by comparing the morphology of different developmental stages at several time points after starting the knockdown (4.4.2). This can reveal a possible arrest at a specific stage and even slight delays in development due to a downregulated gene. Images of mature schizonts were used to count the number of merozoites which highly influences the growth factor. To quantify the growth itself, double-stranded DNA was labeled with SybrGreenI and the emission was measured at 530±40 nm (excitation 482±16 nm) (4.4.11). As the emission corresponds to

the parasitemia, it allows rapid analyses of the parasite development in 96-well plates (Bennett et al., 2004).

Immunofluorescence assays are a nice method to get more information about the localization and distribution of various proteins by analyzing fluorescence microscopy images (4.5.1). As the POIs are tagged with 3xHA, α-HA antibodies can specifically bind to this tag and a fluorophore-coupled secondary antibody can be used to visualize the POIs. Additional co-localization studies with antibodies against SBP1 can demonstrate a localization at MCs, which was shown to be a stopover for many proteins that are exported to the host cell membrane (DeKoning-Ward et al., 2016). Predicted transmembrane domains suggest a membrane-bound form that can be verified by hypotonic lysis of enriched infected erythrocytes and subsequent analysis via Western Blot (4.4.7, 4.3.2). After lysis, soluble proteins are in the supernatant fraction while membrane-bound proteins are in the pellet fraction and specific known proteins serve as a control for successful lysis in the Western Blot.

Some very obvious host cell modifications like knobs on the surface of infected erythrocytes or Maurer's clefts can be observed via electron microscopy (4.5.2, 4.5.3). Having a closer look at cytoadherence, a crucial factor is the expression and correct presentation of PfEMP1 on knobs. As *P. falciparum* codes for about 60 *var* genes with mutual exclusive expression that also have different preferences for specific human receptors, it is impossible to analyze them all (Biggs et al., 1991). However, it is possible to select parasites that express VAR2CSA. This EMP1 variant specifically binds to CSA, an endothelial receptor found in the human placenta, which can be used in experiments *in vitro* (Wahlgren et al., 2017). The parasite strain used in this study, *P. falciparum* CS2, is known to express VAR2CSA after selection and rarely switches between EMP1 variants (Beeson et al., 1998; Reeder et al., 1999). Static binding assays can analyze the number of infected erythrocytes that have bound to CSA by covering a plate with soluble CSA and allowing infected erythrocytes to bind before washing away the unbound cells, staining with Giemsa, and taking images (4.4.13). A more direct approach is the measurement of PfEMP1 via flow cytometry (4.4.14). VAR2CSA-specific antibodies bind to EMP1 on the surface of infected erythrocytes and are labeled with a fluorophore-conjugated secondary antibody that is used to measure the mean fluorescence intensity (Figure 10). Together with the experimental results of electron microscopy and static CSA-binding assays, this can give important hints to the function of the POIs in protein export and host cell modification.

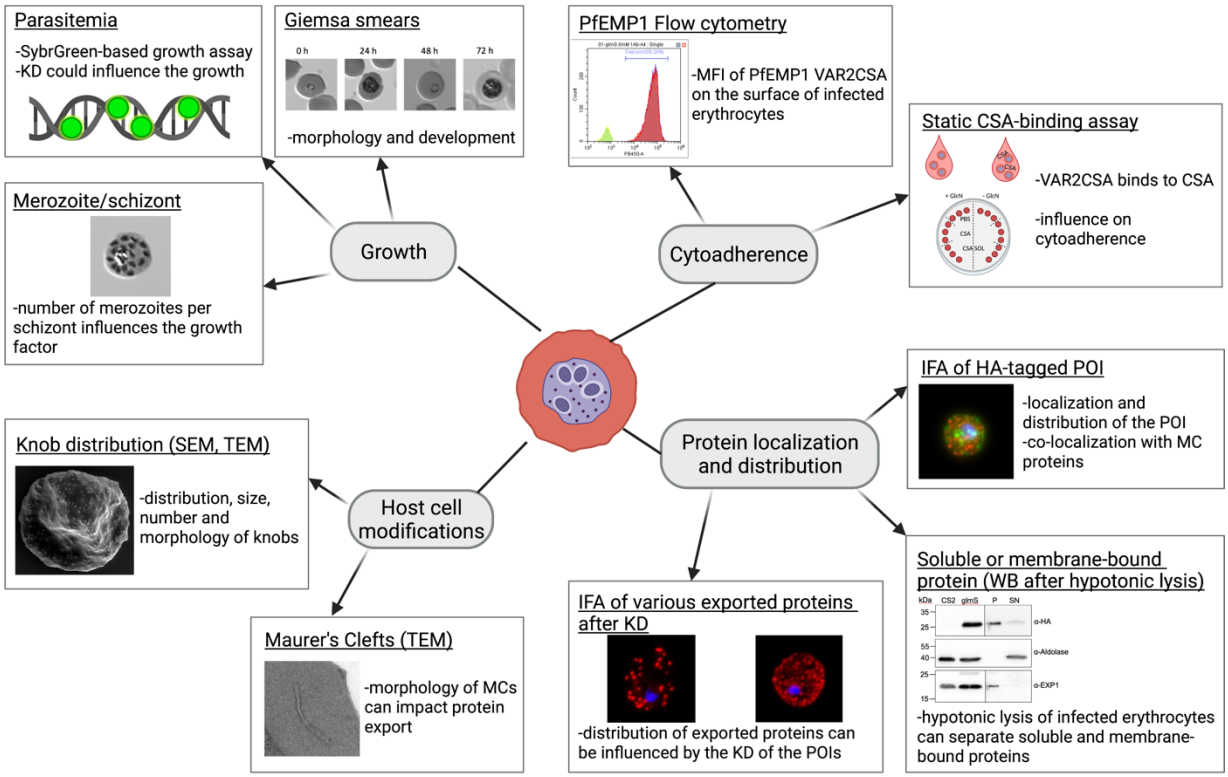

Fig. 10: Methods and tools used in this study to characterize the phenotype of knockdown cell lines. Several experiments were performed to analyze the growth, cytoadherence, host cell modifications, and protein distribution. KD: knockdown; MFI: mean fluorescence intensity; POI: protein of interest **(made with BioRender).**

1.6 Genetic systems to study essential genes in *P. falciparum*

Genetic systems to modify genes *in vitro* in *P. falciparum* blood stages are crucial to elucidate the cellular and biochemical function of proteins. In 1993, the first successful transient transfection was described and only since 1997, reasonably efficient stable transfection methods using single crossover homologous recombination are possible (Goonewardene et al., 1993; Wu et al., 1995; Wu et al., 1996; Crabb et al., 1997, Menard et al., 1997). Early transfection methods relied on single-crossover homologous recombination and the establishment of double crossover homologous recombination allowed large deletions and the removal of unwanted recombination events via an additional negative selection marker (Duraisingh et al., 2002; Maier et al., 2006). In 2002, the genome of *P. falciparum* was published and it has been constantly expanded with information about known or putative functions that opened up whole new possibilities (Gardner et al., 2002; Böhme et al., 2019).

Due to the haploid nature of *Plasmodium* blood stages, the study of essential genes relies on conditional knockout and knockdown systems (Kudyba et al., 2021). There are several systems for conditional protein knockout or knockdown studies that initially target DNA, RNA, or protein levels which will be further described in this chapter.

DNA level:

The adapted DiCre system allows for control of transcription by inducible excision or inversion of DNA sequences that have been flanked with specific Cre recombinase recognition sites called *loxP* sites. The Cre recombinase is split into two proteins that are fused to rapamycin-binding proteins FK506 binding protein 12 (FKBP) or FKBP12-rapamycin-binding domain (FRB). By adding rapamycin, those proteins dimerize leading to an active Cre recombinase that detects floxed (flanked by *loxP* sites) DNA (Figure 11 A) (Collins et al., 2013; Kudyba et al., 2021). To modify exons or specific domains, l*oxP* sites that are cloned into an artificial intron (l*oxPint*) can be used (Jones et al., 2016; Knuepfer et al., 2017). Knuepfer et al. generated DiCre expressing cell lines in a *P. falciparum* 3D7 strain by inserting the DiCre cassette into the *Pfs47* and *p230p* loci. These genes are dispensable for blood stage development and transmission to mosquitoes, making those cell lines a great tool for conditional gene knockouts (Knuepfer et al., 2017).

RNA level:

A system for inducible knockdown on mRNA level uses the self-cleaving *glmS* ribozyme which is originally from Gram-positive bacteria and specifically needs glucosamine-6-phosphate as a co-factor (Winkler et al., 2004). It is inserted at the 3' end of the coding region of the gene of interest (GOI) leading to the expression of a chimeric mRNA. The addition of glucosamine actively induces knock-down on mRNA level by activating the *glmS* ribozyme that self-cleaves the mRNA. Without the Poly(A)-tail the rest of the mRNA is unprotected and quickly degraded which should lead to a lower abundance of the target protein depending on the glucosamine concentration (Figure 11 B1). However, glucosamine can be toxic at high concentrations which could lead to misinterpretation of results without proper controls. As a control serves an inactive M9 cell line whose single-point mutation in the ribozyme sequence prevents mRNA cleavage (Prommana et al., 2013; Kudyba et al., 2021).

Another system to control translation uses a tetracycline repressor protein (TetR) that is fused to a *Plasmodium* RNA helicase called DOZI (development of zygote inhibited). TetR-aptamer sequences are inserted at the 3' and/or 5' untranslated regions (UTR) of the GOI that can be recognized and bound by TetR-DOZI. However, interaction is only possible when anhydrotetracycline (aTc) is removed from the culture as it inhibits the binding (Goldfless et al., 2014; Ganesan et al., 2016; Kudyba et al., 2021). Upon binding, the RNA is relocated to P-bodies ultimately leading to the repression of translation and an inducible protein knockdown (Figure 11 B2) (Kudyba et al., 2021). Rajaram et al. improved the stability of the aptamers by adding unique

spacers after aptamer truncations were frequently observed that decreased knockdown efficiency (Rajaram et al., 2020).

Protein level:

Contrary to the previously described knockdown and knockout methods that affect transcription or translation, a knockdown on protein level is a much more direct and fast-acting process. One method uses a destabilization domain (DD) that is fused to the protein of interest (POI) and leads to misfolding and ultimately proteasome degradation if the stabilizing ligand Shld1 is removed (Figure 11 C1) (Banaszynski et al., 2006; Armstrong & Goldberg, 2007). However, it needs to be considered that the genetic manipulation of the N- or C-terminus could have an effect on the protein structure and the ligand Shld1 can be toxic to asexual blood stages. (Kudyba et al., 2021).

Another approach is the directed mislocalization of a POI, a method called knock sideways, that also uses rapamycin-binding FKBP and FRB domains. The parasite cell line expresses a fusion protein with a FRB domain and a signal that leads to localization to the nucleus or the plasma membrane. Upon addition of rapamycin, the FKBP-coupled POI binds to the mislocalizer protein, trapping it in the wrong cellular department and therefore inhibiting its native function (Figure 11 C2) (Birnbaum et al., 2017; Kudyba et al., 2021).

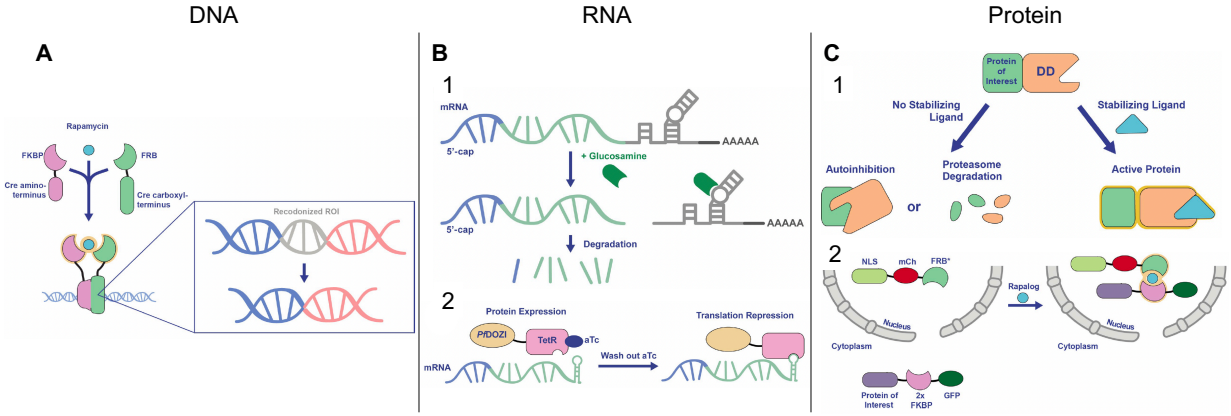

Fig. 11: Selected conditional knockout and knockdown systems in *P. falciparum*. A) Control of transcription with the DiCre system. Rapamycin leads to dimerization of the recombinase that excises or inverts the DNA sequence flanked with loxP sites. **B1)** Gene knockdown on mRNA level using the *glmS* ribozyme system. Glucosamine activates the *glmS* ribozyme leading to its self-cleavage and degradation of the mRNA. **B2)** *Pf*DOZI-TetR system. Removal of anhydrotetracycline leads to binding of the TetR-DOZI fusion protein to TetR aptamers and inhibits the translation. **C1)** Protein knockdown using the destabilization domain. Without the stabilizing ligand Shld1, the DD-tagged POI is degraded in the proteasome. **C2)** Knock sideways approach. The POI is mislocalized by using rapamycin-binding proteins FKBP and FRB and specific mislocalization signals. FKBP: FK506 binding protein 12; FRB: FKBP12-rapamycin-binding domain; *Pf*DOZI: development of zygote inhibited (*Pf* helicase); TetR: Tetracycline repressor; aTC: anhydrotetracycline; DD: destabilization domain; NLS: nuclear localization signal; mCh: mcherry tag (modified from: Kudyba et al., 2021).

Recent advances:

Modified genomic loci can be integrated via single or double crossover homologous recombination which is a passive, time-consuming, and quite an inefficient method in *P. falciparum*. This was massively improved with the introduction of selection-linked integration (SLI) which enables the selection of integrated clones with an additional selectable marker and therefore decreasing the time to generate modified cell lines. The second selection gene is expressed under the promotor of the protein of interest but it is joined through a skip-peptide resulting in the expression of two separate proteins: the protein of interest and the second resistance marker. Therefore, the first resistance marker (*hDHFR)* is used to select for transfectants that carry the plasmid and the second marker (neomycin phosphotransferase) allows the selection of transfected parasites that have integrated the modified locus (Birnbaum et al., 2017) (4.4.9).

The application of CRISPR/Cas in *P. falciparum* since 2014 has additionally improved the speed and scale of genome editing and can also be used to generate cell lines containing the previously described knockout or knockdown systems (Ghorbal et al., 2014; Zhang et al., 2014; Lee et al., 2019). Originally, CRISPR/Cas is part of the adaptive immune system of bacteria that causes site-specific double-strand breaks in foreign DNA, like invading bacteriophages (Jinek et al., 2012). As *P. falciparum* lacks the ability to repair double-strand breaks using non-homologous end joining (NHEJ), it only uses homology-directed repair (HDR) and homologous donor templates. Three components are needed that can be coded on a single or multiple plasmids: site-specific guide RNA(s) that bind to the respective DNA sequence, the Cas9 endonuclease that is recruited by the guide RNA leading to a double-strand break and a donor template that contains the desired, modified gene sequence (Lee et al., 2019).

Every method has its advantages and disadvantages that need to be considered in the selection of a suitable method. While inducible ligands like glucosamine in the *glmS* system or shield in the DD system can affect the protein knockdown in a fast and concentration-dependent manner (*glmS*), the toxic effect cannot be neglected. Other systems rely on genetic modifications and fusion proteins that can also alter the structure and function of the POI. A common problem with knockdown systems is that the degree of knockdown might not be enough to see a phenotype, especially for enzymes (Kudyba et al., 2021). A ~80% downregulation of Plasmepsin V using the *glmS* system was not enough to obtain a growth defect (Sleebs et al., 2014). Only a conditional knockout using diCre and tetR-DOZI with a knockdown of >99% could demonstrate the essential function in blood stages (Boonyalai et al., 2018; Polino et al., 2020). Even though genetic manipulations in *P. falciparum* are not as easy as in other organisms, many systems have

been developed to study the function of essential genes which will help to better understand the biology of the parasite (Kudyba et al., 2021).

1.7 Aim of this study

Malaria is one of the most important infectious diseases worldwide and even with constant research scientists have not been able to develop an effective vaccine for the eradication of the disease and emerging resistances against antimalarial drugs show the importance to develop new therapies (Rocamora & Winzeler, 2020). In order to ensure its own survival, quickly after invasion the parasite starts to export hundreds of proteins to the host cell which leads to host cell modifications that are crucial for parasite survival and are the reason for most of the pathology associated with malaria (Maier et al., 2009; Bartoloni & Zammarchi, 2012; Jonsdottir et al., 2021). It is predicted that over 400 parasite-encoded proteins are transported to the host cell and that many of these are involved in host cell modification. In order to reach their destination, the proteins need to be transported across the parasite plasma membrane, the parasitophorous vacuole membrane (PVM), and through the cytosol of the host cell. This protein trafficking system is unique in *Plasmodium* species and has therefore been a main area of interest in research (Przyborski et al., 2016).

This project aims to characterize candidate exported proteins in blood stages of *P. falciparum* as the role of many exported proteins in parasite survival is still unknown. The candidate genes are predicted to be essential in *piggyBac* transposon insertional mutagenesis (Zhang et al., 2018) and selection-linked integration targeted gene disruption (SLI-TGD) (Ouayoue Noutong, 2021). In this study, the four PEXEL proteins PF3D7_0113300, PF3D7_0220300, PF3D7_0220600, and PF3D7_0301600 were further characterized using the *glmS* ribozyme method, a conditional knockdown system on mRNA level that can be activated via glucosamine-6-phosphate. A special interest was in parasite growth, morphology, protein localization, and host cell modifications such as cytoadherence. This way, I want to contribute to a better understanding of protein export and the function of some exported proteins in host cell modification and growth of the parasite in asexual blood stages *in vitro*.

2. Results

2.1 Selection of gene candidates

P. falciparum exports hundreds of proteins to the host cell which leads to host cell modifications that are crucial for parasite survival and are the reason for most of the pathology associated with malaria (1.3 and 1.4) (Hiller et al., 2004; Marti et al., 2004; Maier et al., 2009).

It is predicted that over 400 parasite-encoded proteins are transported to the host cell (Matthews et al., 2018), and by using bioinformatics, a list of 15 gene candidates, that fulfill the following criteria, was generated:

1) Predicted exported proteins (according to *PlasmoDB*).
2) Not part of the *stevor*, *var,* or *rif* multigene families as their expression is mutually exclusive.
3) Not previously knocked out.
4) High transcript levels at 0-16 or 44-48 hpi as most proteins that are involved in host cell modification are expressed during that time.
5) Coding sequence of at least 600 bp due to cloning reasons.

A high-throughput screening using *piggyBac* transposon insertional mutagenesis generated around 38,000 mutants and predicted 10 out of these 15 gene candidates to be essential for blood stage development *in vitro* (Zhang et al., 2018). To further investigate the essentiality of the gene candidates, a PhD student in our working group applied the SLI-TGD method and was able to generate one knockout cell line of a gene that was predicted to be essential by Zhang et al. The other 14 genes turned out to be refractory to genetic manipulation using this knockout approach and are therefore likely essential (Ouayoue Noutong, 2021) (Table 1). However, many genes are known to be essential that have been classified as non-essential in the high-throughput screening and vice versa which shows that the results of the *piggyBac* transposon insertional mutagenesis are just a hint of a gene's essentiality in blood stages and it always needs to be further investigated using other methods.

Tab. 1: Classification of gene candidates. The predicted essentiality of target genes by *piggyBac* transposon insertional mutagenesis and SLI-TGD.

Gene ID	*piggyBac* prediction (Zhang et al., 2018)	SLI-TGD prediction (Ouayoue Noutong, 2021)
PF3D7_0113300	essential	essential
PF3D7_0113900	essential	essential
PF3D7_0220300	non-essential	essential
PF3D7_0220600	essential	essential
PF3D7_0220700	essential	essential
PF3D7_0301600	non-essential	essential
PF3D7_0301800	essential	essential
PF3D7_0310400	essential	essential
PF3D7_0701900	non-essential	essential
PF3D7_1001900	non-essential	non-essential
PF3D7_1038600	essential	essential
PF3D7_1102600	essential	essential
PF3D7_1149200	non-essential	essential
PF3D7_1301200	essential	essential
PF3D7_1401200	essential	essential

2.2 Generation of *glmS* cell lines using selection-linked integration (SLI)

In this study, the SLI-*glmS* approach was used to generate inducible knockdown cell lines of 11 genes that could not be knocked out before (1.6). In order to generate the constructs, about 750-1000 bp of the GOI were amplified via PCR and cloned into the pSLI-glmS/M9-HA vectors using the restriction enzymes NotI and MluI. After ligation, the plasmids were transformed into competent *E. coli* cells (*Top10* or *XL1Blue*) and correct integration was verified via colony PCR, test digest, and sequencing (4.2) (plasmid maps in Supplement 1). The vector contains hDHFR and the second selectable marker neomycin phosphotransferase (NeoR) which confers resistance to G418 and is only expressed when the parasites have integrated the modified sequence into the genome via single crossover homologous recombination. A skip-peptide (S) between the GOI and NeoR leads to the expression of two separate proteins (Figure 12) (Prommana et al., 2013). Moreover, an HA-tag and the *glmS* sequence are inserted after the 3' end of the GOI. The constructs were transfected into the *P. falciparum* CS2 cell line, which mainly expresses the PfEMP1 variant VAR2CSA after selection on CSA and is known to be a slow switcher (Reeder et al., 1999). Those characteristics are important for analyses of CSA-binding efficiency in the downregulated cell lines. Additionally, an inactivated version of the *glmS* ribozyme, called M9, was generated and used as a control parasite line in all experiments. As CS2 was the parental cell line in this study, the respective orthologous gene sequences were used for cloning and transfection (4.1.2).

After transfection (4.4.8), the parasites were cultivated with WR99210 until they grew back (~30 days) to select transfectants that have taken up the plasmid and expressed hDHFR. To further select for integrants, the culture was split into three parts and cultivated with 400, 600, and 800 µg/ml G418 until viable parasites were seen (~14-30 days). If no parasites grew back after 10 weeks (three tries), the integration failed (4.4.9). Genomic DNA (gDNA) of those parasites that could grow in the highest G418 concentration was used to verify correct integration via PCR (4.2.1 and 4.2.2). The episome (pARL_fw and HA_rev), wildtype genomic locus (5'fw and 3'rev), 5' integration locus (5'fw and HA_rev), and 3' integration locus (pARL_fw and 3'rev) were amplified using the respective primers (Figure 12). Additional PCR controls were hDHFR to verify the presence of the plasmid, EMP3 as a gDNA control, and water instead of a DNA template to reveal any possible contaminations in the PCR sample.

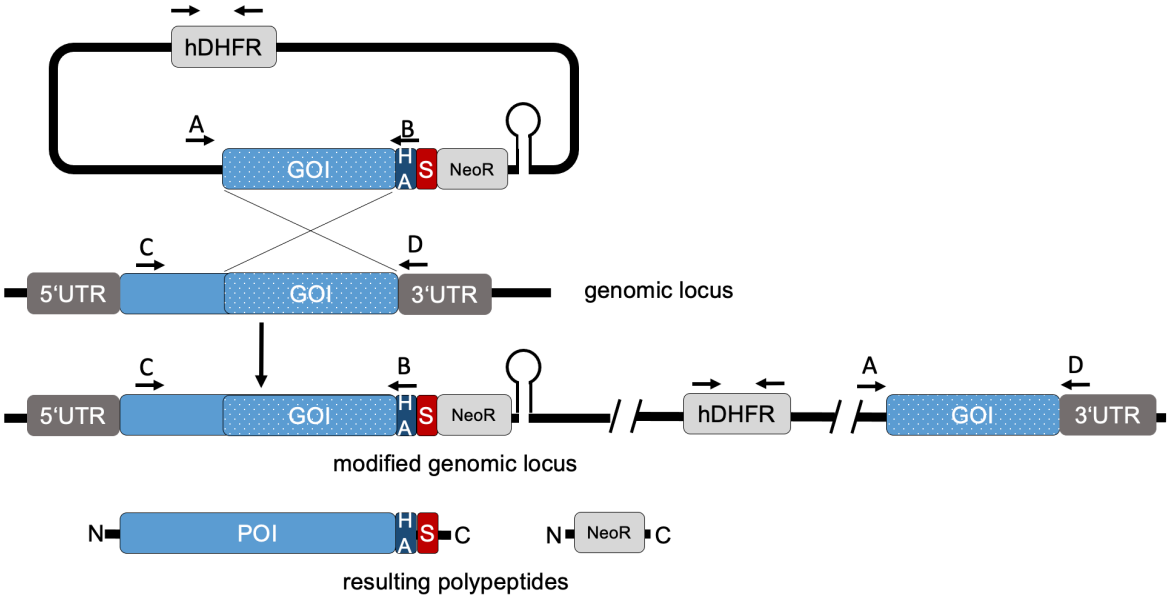

Fig. 12: Strategy to generate the *glmS* knockdown cell lines. Genetic modification via homologous recombination and selection-linked integration (SLI). Arrows indicate the primers for the integration PCR (A: pARL_fw; B: HA_rev; C: 5'fw; D: 3'rev). The Skip-peptide (S) between the HA-tagged gene of interest (GOI) and the neomycin resistance cassette (NeoR) causes the expression of two separate proteins that allows for the selection of integrants. UTR: untranslated region; POI: protein of interest.

All transfectants grew back after ~30 days under WR99210 selection and were then cultivated with different concentrations of G418 to select for parasites that have integrated the modified genomic locus. Six *glmS* knockdown cell lines could be verified while five transfectants did not grow back after selection with G418 for 10 weeks. After three negative selection trials, the integration was considered to be failed. The cell lines CS2PF3D7_0220600$^{glmS/M9}$, CS2PF3D7_0113300$^{glmS/M9}$, CS2PF3D7_0220300$^{glmS/M9}$ and CS2PF3D7_0301600$^{glmS/M9}$ are further characterized in this study (Table 2).

Tab. 2: Gene candidates modified with SLI-*glmS*. Transfectants and integrants with the modified genes. Selection with G418 was performed for up to 10 weeks * Cell lines analyzed in this study.

Gene ID	Transfectant	Integrant
PF3D7_0113300*	Yes	Yes
PF3D7_0220300*	Yes	Yes
PF3D7_0220600*	Yes	Yes
PF3D7_0220700	Yes	Yes (double bands)
PF3D7_0301600*	Yes	Yes
PF3D7_0310400	Yes	No (3x G418 selection)
PF3D7_0701900	Yes	No (3x G418 selection)
PF3D7_1038600	Yes	No (3x G418 selection)
PF3D7_1149200	Yes	No (3x G418 selection)
PF3D7_1301200	Yes	No (3x G418 selection)
PF3D7_1401200	Yes	Yes (Jonsdottir et al., 2021)

2.3 Phenotypic characterization of PF3D7_0113300

The *P. falciparum* gene PF3D7_0113300 codes for an exported PEXEL protein of 71 kDa with unknown function (PlasmoDB). *In silico* analyses show no predicted transmembrane domains and a predicted protein structure of coiled-coil motifs and disordered regions (UniProt) (Figure 13E).

After cloning and transfecting the respective plasmid into *P. falciparum* CS2 and selecting first with WR99210 and then with G418 to get parasites that have integrated the modified genomic locus, gDNA was used to verify correct integration via PCR (2.2). *GlmS* and M9 cell lines selected with 800 µg/ml G418 showed 5' and 3' integration without any remaining wildtype locus. Remnant plasmids (episome) and hDHFR were detectable and the EMP3 control demonstrated gDNA integrity (Table 3, Figure 13AB).

Tab. 3: Primer combinations and expected sizes for integration PCR of CS2PF3D7_0113300$^{glmS/M9}$.

	Primers	Expected size
5' Integration	5'fw_0113300 HA_rev	1386 bp
3' Integration	pARL_fw 3'rev_0113300	1270 bp
Wildtype locus	5'fw_0113300 3'rev_0113300	1515 bp
Episome	pARL_fw HA_rev	1141 bp
hDHFR	hDHFR_fw hDHFR_rev	531 bp
EMP3 (gDNA control)	EMP3_fw EMP3_rev	792 bp

Expression of the HA-tagged POI was verified via Western Blot analysis of enriched trophozoite-stage infected erythrocytes using α-HA (expected size ~66 kDa) and α-Aldolase (expected size ~40 kDa) as a loading control (4.3.2). The HA-tagged POI could be detected in the *glmS* and M9 cell lines with an additional higher band that likely constitutes a non-skipped fusion protein, with no detection in the CS2 parental cell line (Figure 13C, full-size WB in Supplement 2A). In theory, the expression of the POI can be downregulated on mRNA level by adding glucosamine (GlcN) to the cell culture. This activates the *glmS* ribozyme leading to self-cleavage and ultimately degradation of the mRNA and reduced protein abundance (Prommana et al., 2013). To verify downregulation, synchronized *glmS* and M9 cell lines were cultivated with 0, 1.25, 2.5, and 5 mM GlcN for 72 h and analyzed in a Western Blot as described above (4.4.10). The band intensities corresponding to the HA-tagged POI appeared weaker the more GlcN was being used. However, a quantification of the downregulation was not possible due to the high background signal and overall low protein abundance (Figure 13D, full-size WB in Supplement 2B).

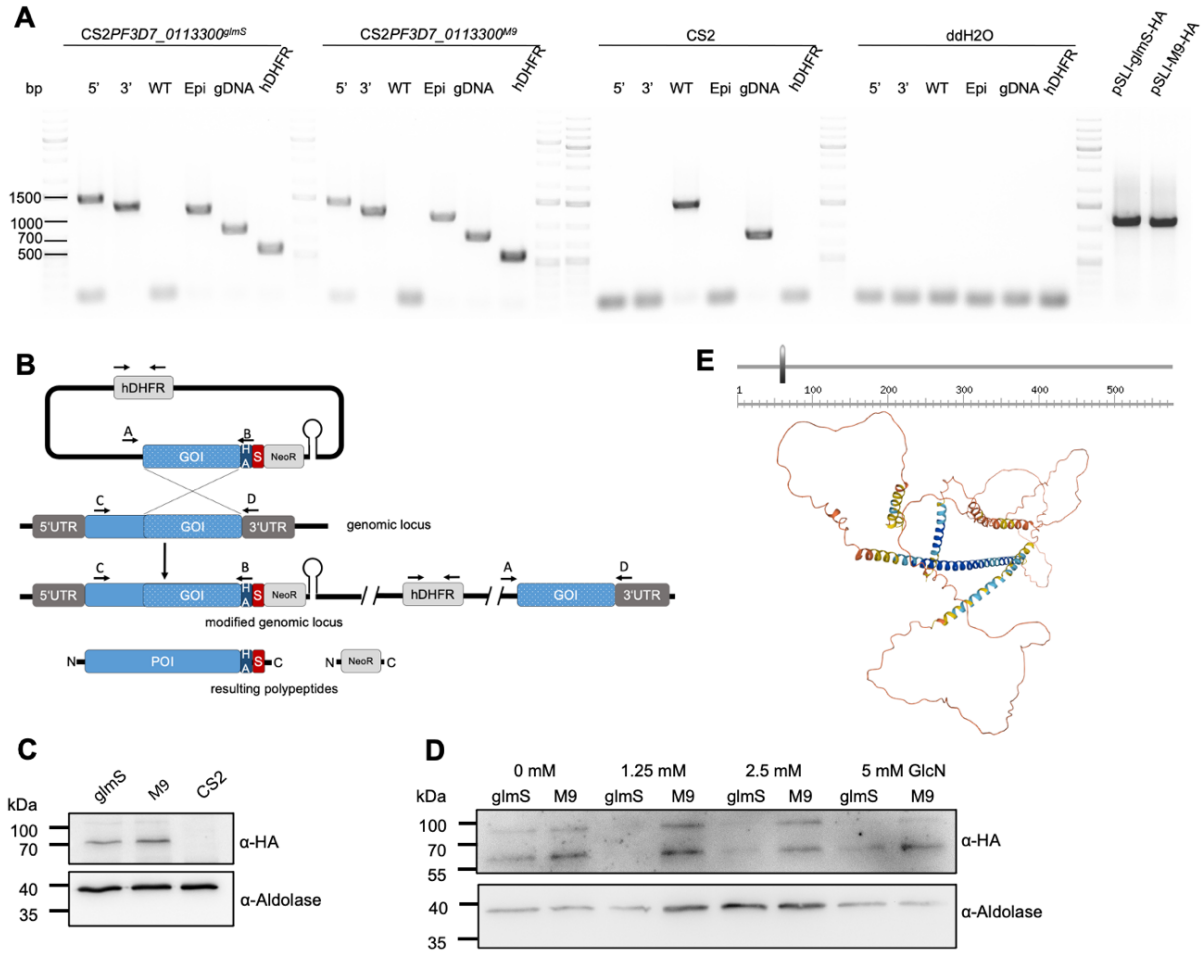

Fig. 13: Verification of CS2PF3D7_0113300$^{glmS/M9}$ and efficiency of knockdown. A) Integration PCR using genomic DNA (gDNA) of CS2PF3D7_0113300$^{glmS/M9}$ and the parental strain CS2 verifies wildtype-free integrants. *GlmS* and M9 cell lines show 3' (primers A and D: 1270 bp) and 5' (primers C and B: 1386 bp) integration, hDHFR (531 bp) and

episomal bands (Epi primers A and B: 1141 bp). The wildtype locus (WT primers C and D: 1515 bp) is only amplified from gDNA of the wildtype CS2 cell line. EMP3 serves as a positive control for the gDNA (792 bp). **B)** Strategy to generate the *glmS* knockdown cell line via homologous recombination and using selection-linked integration (SLI). Arrows indicate the primers for the integration PCR (see A). The Skip-peptide (S) between the HA-tagged gene of interest (GOI) and the neomycin resistance cassette (NeoR) causes the expression of two separate proteins that allows for the selection of integrants. UTR: untranslated region; POI: protein of interest. **C)** Western blot analysis of enriched trophozoites shows the expression of the HA-tagged POI using α-HA (expected size ~66 kDa) and α-Aldolase (expected size ~40 kDa) as a loading control. The higher HA-band is an unskipped version of the HA-tagged POI bound to neomycin phosphotransferase (~30 kDa) **D)** Downregulation in asexual blood stages after cultivation with 0, 1.25, 2.5, and 5 mM glucosamine (GlcN) for 72 h. Western blot analysis of enriched trophozoites using α-HA (expected size ~66 kDa) and α-Aldolase (expected size ~40 kDa) as a loading control. Representative of three independent experiments. **E)** PF3D7_0113300 is a PEXEL protein (grey bar: PEXEL signal sequence) that contains no transmembrane (TM) domains (PlasmoDB). A computational model predicts a structure made of coiled-coil motifs and disordered regions (UniProt). Scale: amino acids.

To analyze the growth of the *glmS*/M9 cell lines, a SybrGreen-based growth assay over 72 h with a starting parasitemia of 0.2% (ring stages) and 0-5 mM GlcN was performed (4.4.11). This did not show a growth defect that is due to a protein knockdown. The end parasitemia significantly decreased for both cell lines, *glmS* and M9, with increasing GlcN concentrations, likely due to the cytotoxic effect of GlcN itself (Figure 14A). In all further experiments, 2.5 mM GlcN was used for downregulation. Giemsa-stained blood smears over the period of the growth assay did not show any visible morphological differences in the developmental stages of the *glmS* and M9 cell lines (Figure 14CD). After the 72 h growth assay, the parasites were cultured for 4-6 h longer and 20 images of Giemsa-stained blood smears of mature schizonts were analyzed by counting the individual merozoites per schizont. The number per schizont (~16) did not differ between the *glmS* and M9 cell lines culturerd without and with 2.5 mM GlcN (Figure 14B).

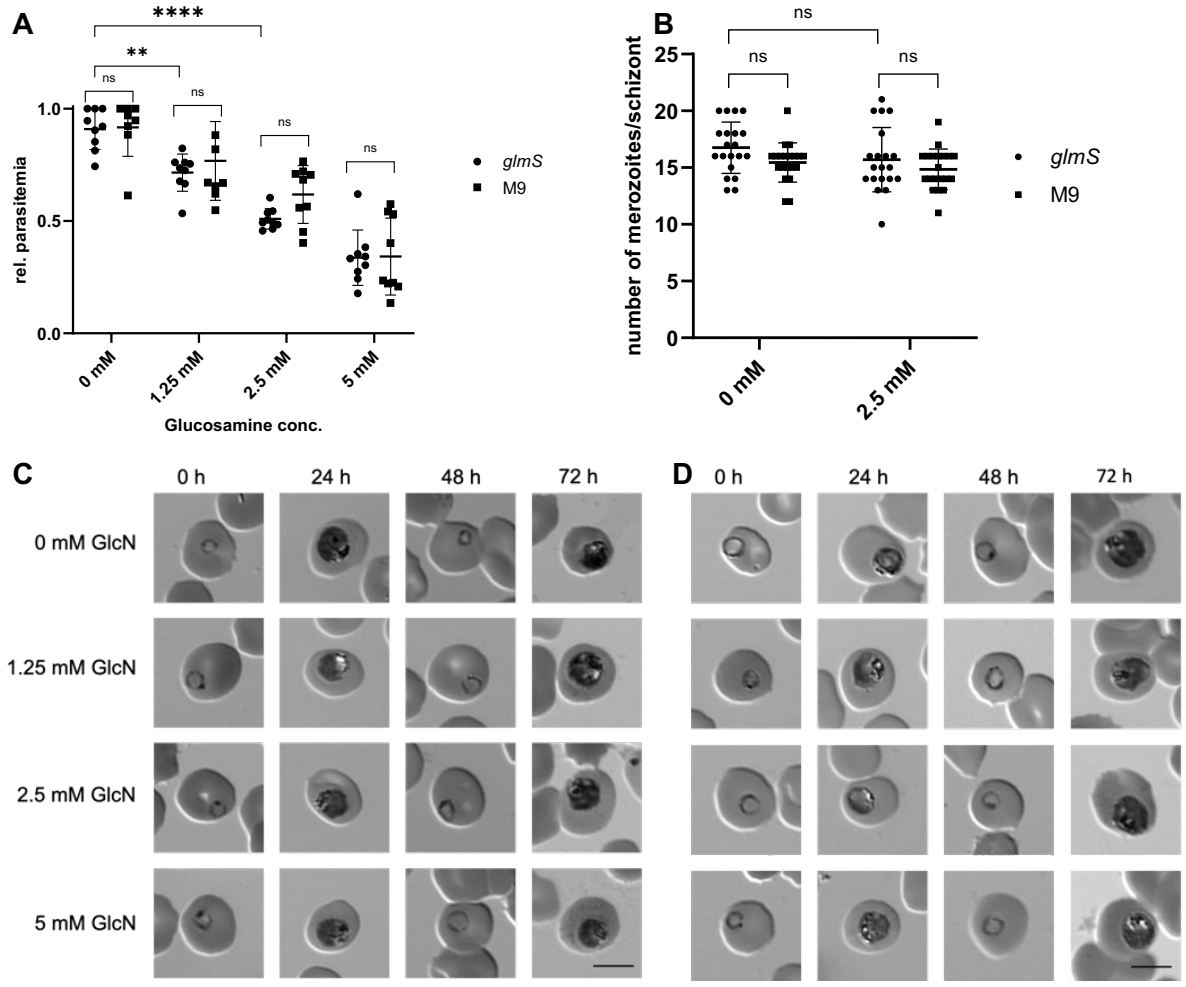

Fig. 14: Knockdown of PF3D7_0113300 does not impair parasite growth. A) SybrGreen-based growth assay over 72 h shows the toxic effect of glucosamine (GlcN) in *glmS* and M9 cell lines. Emission of SybrGreen at 530 nm was measured with a Clariostar plate reader, normalized to the highest value at 0 mM GlcN (set to 1), and statistically analyzed using GraphPad Prism 8.3.1. n=3; ns: not significant; ** p<0.01; **** p<0.0001 (Student's t-test). **B)** The number of merozoites per schizont is not affected by a knockdown with 2.5 mM GlcN after 72 h. Merozoites were counted in images of schizonts in Giemsa-stained blood smears. n=20; ns: not significant (Student's t-test). C+D) Morphology of parasites is not affected by a knockdown in *glmS* **(C)** and M9 **(D)** cell lines. Images of Giemsa-stained parasites at 0 h, 24 h, 48 h, and 72 h after starting the knockdown using 0-5 mM GlcN were edited in ImageJ 2.3.0. Scale bar 5 µm.

In order to get more information about the localization and distribution of PF3D7_0113300, several immunofluorescence assays (IFA) with different fixation methods (Acetone/10%Methanol on slides and PFA/0.0075% GA in solution) and different α-HA antibodies were performed (4.5.1). However, probably due to the low expression, it was not possible to take low background images with a specific HA signal. As the knockdown of an exported protein can have an effect on the distribution of other exported proteins by interfering with the export system, the localization of SBP1, KAHRP, EMP3, and REX1 was analyzed via IFAs using specific primary antibodies (Maier et al., 2008). SBP1 is an integral membrane protein that resides in the MCs and plays a crucial

role in PfEMP1 export as KO parasites are not able to transport PfEMP1 to the erythrocyte surface (Maier et al., 2007). The peripheral membrane protein REX1 is also a MC maker protein that is localized at the cytoplasmic side and is important for the correct structure of MCs (Hanssen et al., 2008b, McHugh et al., 2015). EMP3 and KAHRP localize to MCs during their export to the erythrocyte membrane, where they are major components of knobs and have an influence on cytoadherence (Crabb et al., 1997, Waterkeyn et al., 2000, Maier et al., 2009).

Synchronized *glmS* and M9 parasites were cultivated without and with 2.5 mM GlcN for 72 h before trophozoite-stage cell cultures were fixed for IFAs. Neither did a downregulation of PF3D7_0113300 affect the distribution of the respective proteins nor the cultivation with GlcN in the M9 control (Supplement 9, 10).

It is known that prolonged *in vitro* cultivation of *P. falciparum* can lead to a knobless phenotype and highly reduced cytoadherence due to deletions in the subtelomeric region of chromosome 2. A potential breaking point is in the *kahrp* gene which also leads to a loss of *emp3* and *kahsp40* which are located at the telomeric side of *kahrp* (Figure 15A) (Pologe & Ravetch, 1986, Culvenor et al., 1987, Pasloske et al., 1993). To verify an intact subtelomeric region, *kahrp, emp3* and *kahsp40* were amplified from gDNA via PCR followed by digestion. All three genes could be detected in CS2PF3D7_0113300^{glmS} and CS2PF3D7_0113300^{M9} (Figure 15BC).

As there were no deletions in the subtelomeric end of chromosome 2 that would lead to reduced cytoadherence, the effect of the downregulation of PF3D7_0113300 on binding to CSA could be studied in a static binding assay. The exact principle is explained in more detail in chapter 1.5. Briefly, a synchronized *glmS* culture was cultivated for 72 h without and with 2.5 mM GlcN, trophozoites were enriched via gelatine flotation and the infected erythrocytes were incubated on a CSA-covered plate to allow binding. To ensure that the binding was specific, a control group was incubated with soluble CSA prior to being pipetted onto the CSA-covered plate. Bound cells were counted by analyzing images of Giemsa-stained cells via Ilastik 1.4 and ImageJ 2.3.0 (4.4.13). As expected, the specificity control group (CSA SOL) that was incubated with soluble CSA showed highly reduced binding to CSA. Downregulation of the POI with 2.5 mM GlcN led to a slightly reduced binding that was however not statistically significant (p=0.074113) (Figure 15D). As the parasite frequently switches between different *var* genes, the cultures were selected three times for VAR2CSA on CSA-covered flasks prior to any cytoadherence experiments (4.4.12).

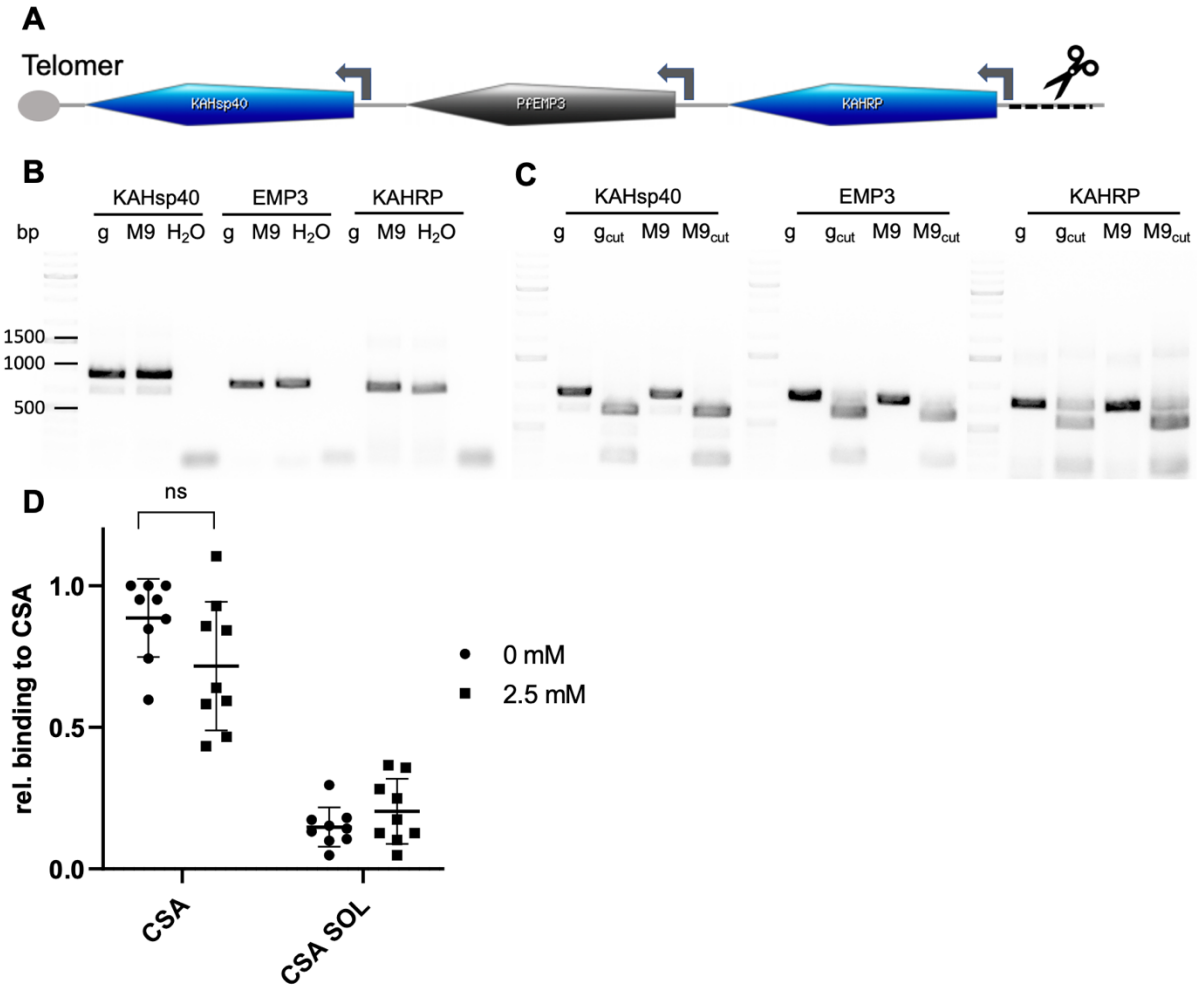

Fig.15: Knockdown of PF3D7_0113300 does not significantly reduce binding to CSA. A) The subtelomeric region of one arm of chromosome 2 codes for KAHsp40, EMP3, and KAHRP. A loss of KAHRP due to a stochastic break at a potential breaking point (scissors) also leads to the loss of KAHsp40 and EMP3 and results in a knobless phenotype. **B)** PCR of genomic DNA verifies intact *kahsp40* (900 bp), *emp3* (792 bp), and *kahrp* (717 bp) in the *glmS*(g) and M9 cell lines. **C)** A test digest of the amplified genes from B with HindIII (KAHsp40: 670 + 230 bp), AluI (EMP3: 602 + 190 bp) and NdeI (KAHRP: 526 + 191 bp) verifies PCR results. **D)** A knockdown with 2.5 mM GlcN for 72 h does not lead to significantly reduced binding to CSA in a static binding assay. Incubation of infected erythrocytes with soluble CSA (CSA SOL) prior to the assay prevents binding to CSA-covered plates. Microscopic images of Giemsa-stained cells were analyzed with Ilastik 1.4 and ImageJ 2.3.0, the number of cells was normalized (highest number at 0 mM CS2 set to 1) and statistically analyzed with GraphPad Prism 8.3.1. n=3; ns: not significant p=0.074113 (Student's t-test).

2.4 Phenotypic characterization of PF3D7_0220300

The second gene analyzed in this study is PF3D7_0220300 which codes for an exported PEXEL protein of 25.3 kDa with unknown function (PlasmoDB). PCR analysis of the *glmS* and M9 cell lines after selection with 800 µg/ml G418 showed 5' and 3' integration without any remaining wildtype locus. Remnant plasmids (episome) and hDHFR were detectable and the EMP3 control demonstrated gDNA integrity (Table 4, Figure 16AB).

Tab. 4: Primer combinations and expected sizes for integration PCR of CS2PF3D7_0220300$^{glmS/M9}$.

	Primers	Expected size
5‘ Integration	5’fw_0220300 HA_rev	1007 bp
3‘ Integration	pARL_fw 3’rev_0220300	1031 bp
Wildtype locus	5’fw_0220300 3’rev_0220300	1055 bp
Episome	pARL_fw HA_rev	983 bp
hDHFR	hDHFR_fw hDHFR_rev	531 bp
EMP3 (gDNA control)	EMP3_fw EMP3_rev	792 bp

Expression of the HA-tagged POI was verified via Western Blot analysis of enriched trophozoite-stage infected erythrocytes using α-HA (expected size ~22 kDa) and α-Aldolase (expected size ~40 kDa) as a loading control (4.3.2). The HA-tagged POI could be detected in the *glmS* and M9 cell lines with no detection in the CS2 parental cell line (Figure 16C, full-size WB in Supplement 3A).

In order to demonstrate that the *glmS* ribozyme system is working effectively, CS2PF3D7_0220300$^{glmS/M9}$ were cultivated with 0-5 mM GlcN for 72 h with subsequent Western Blot analysis. This showed weaker HA-bands in the *glmS* sample the more GlcN was used while the HA-band intensity in the M9 control did not change (Figure 16D, full-size WB in Supplement 3B). The protein abundance was quantified by measuring the band intensities in Western Blots of three independent experiments via ImageJ 2.3.0 and normalizing the HA-band intensities to the respective band intensities of Aldolase. Quantification verified that there was no significant difference in the abundance of the POI in CS2PF3D7_0220300^{M9}. However, the *glmS* cell line showed a significant reduction of protein abundance with 2.5 mM GlcN to 36% (p=0.0087) and 5 mM GlcN to 18% (p=0.0014) while cultivation with 1.25 mM GlcN did not lead to a statistically significant downregulation (p=0.1629) (Figure 16E). In all further experiments, the downregulation was performed with 2.5 mM GlcN.

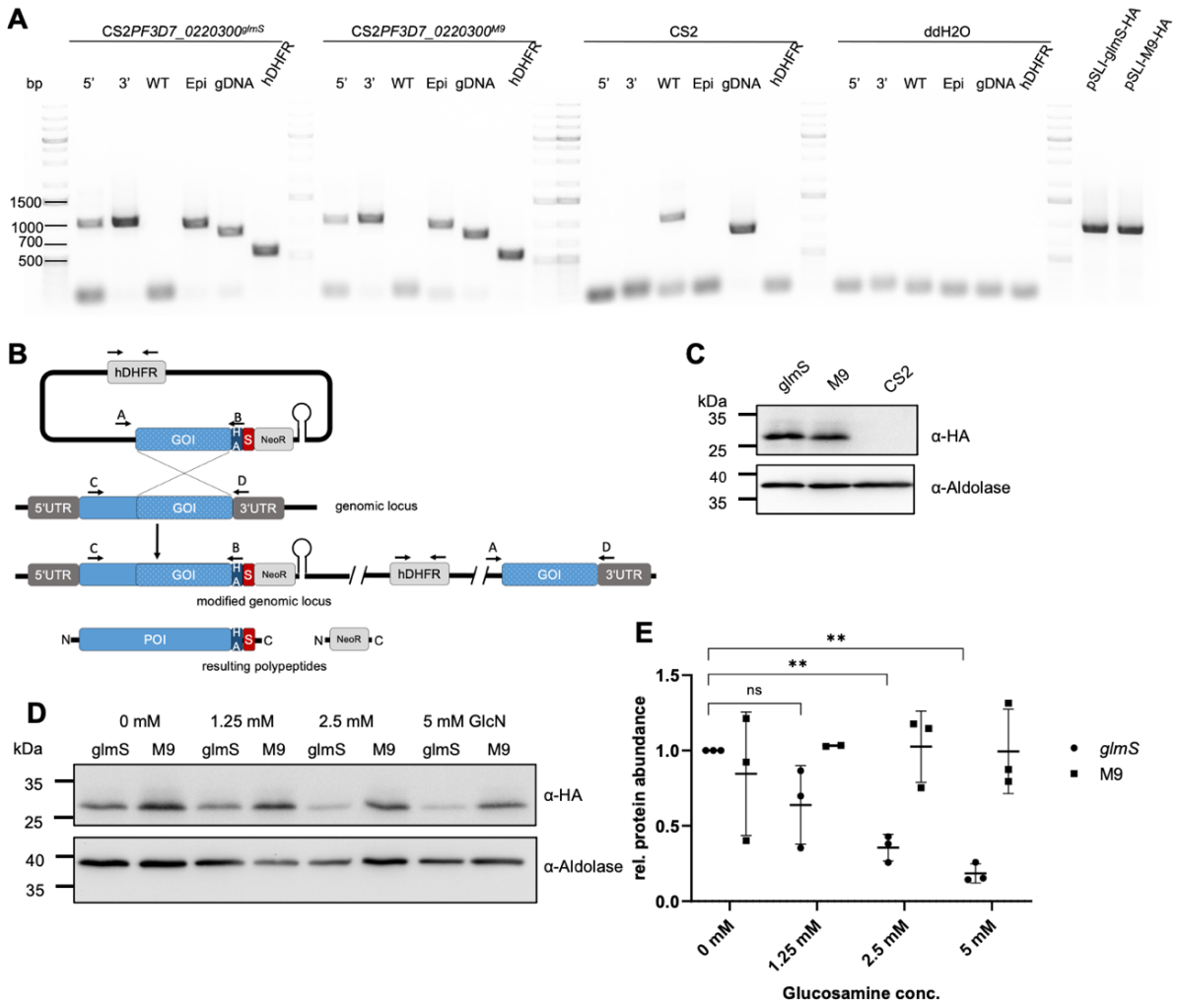

Fig. 16: Verification of CS2PF3D7_0220300$^{glmS/M9}$ and efficiency of knockdown. A) Integration PCR using genomic DNA (gDNA) of CS2PF3D7_0220300$^{glmS/M9}$ and the parental strain CS2 verifies wildtype-free integrants. *GlmS* and M9 cell lines show 3' (primers A and D: 1031 bp) and 5' (primers C and B: 1007 bp) integration, hDHFR (531 bp) and episomal bands (Epi primers A and B: 983 bp). The wildtype locus (WT primers C and D: 1055 bp) is only amplified from gDNA of the wildtype CS2 cell line. EMP3 serves as a positive control for the gDNA (792 bp). **B)** Strategy to generate the *glmS* knockdown cell line via homologous recombination and using selection-linked integration (SLI). Arrows indicate the primers for the integration PCR (see A). The Skip-peptide (S) between the HA-tagged gene of interest (GOI) and the neomycin resistance cassette (NeoR) causes the expression of two separate proteins that allows for the selection of integrants. UTR: untranslated region; POI: protein of interest. **C)** Western blot analysis of enriched trophozoites shows the expression of the HA-tagged POI using α-HA (expected size ~22 kDa) and α-Aldolase (expected size ~40 kDa) as a loading control. **D)** Downregulation in asexual blood stages after cultivation with 0, 1.25, 2.5, and 5 mM glucosamine (GlcN) for 72 h. Western blot analysis of enriched trophozoites using α-HA (expected size ~22 kDa) and α-Aldolase (expected size ~40 kDa) as a loading control. Representative of three independent experiments. **E)** Quantification of protein abundance of three independent Western blot experiments (see D). Band intensities of HA were measured using ImageJ 2.3.0, normalized to the respective band intensity of aldolase (*glmS* 0 mM GlcN set to 1), and statistically analyzed using GraphPad Prism 8.3.1. n=3, ns: not significant; ** p<0.01 (Student's t-test).

A downregulation of PF3D7_0220300 did not lead to a significant growth defect after 72 h (4.4.11). However, the end parasitemia in the growth assay did decrease the more GlcN was used, once again showing the cytotoxic effect of GlcN itself (Figure 17A). Giemsa-stained blood

smears over the period of the growth assay did not show any visible morphological differences in the developmental stages of the *glmS* and M9 cell lines (Figure 17CD). Moreover, the number of merozoites per schizont (~16) did not differ between the *glmS* and M9 cell lines cultured without and with 2.5 mM GlcN (Figure 17B).

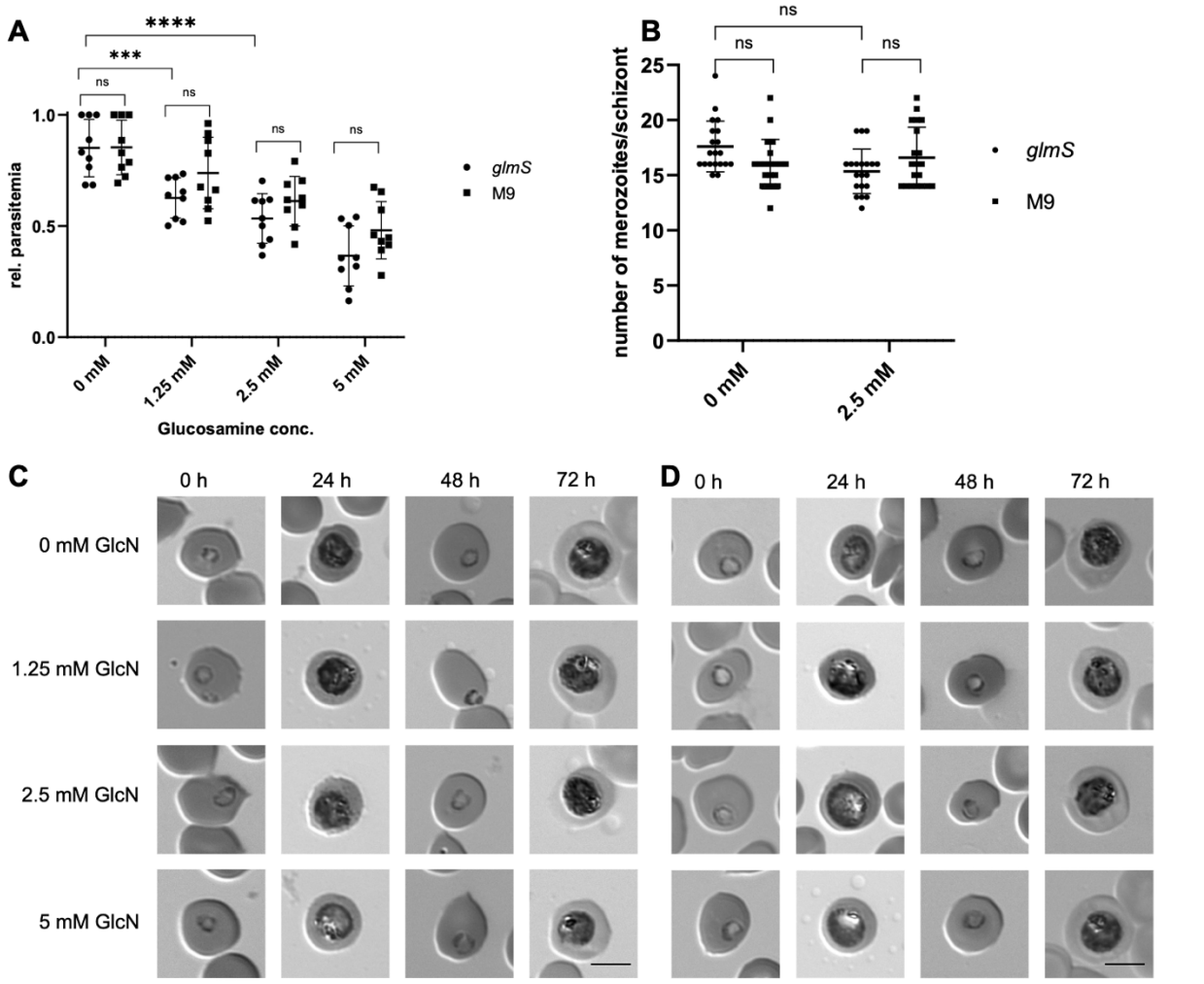

Fig. 17: Knockdown of PF3D7_0220300 does not impair parasite growth. A) SybrGreen-based growth assay over 72 h shows the toxic effect of glucosamine (GlcN) in *glmS* and M9 cell lines. Emission of SybrGreen at 530 nm was measured with a Clariostar plate reader, normalized to the highest value at 0 mM GlcN (set to 1), and statistically analyzed using GraphPad Prism 8.3.1. n=3; ns: not significant; *** p<0.001; **** p<0.0001 (Student's t-test). **B)** The number of merozoites per schizont is not affected by a knockdown with 2.5 mM GlcN after 72 h. Merozoites were counted in images of schizonts in Giemsa-stained blood smears. n=20; ns: not significant (Student's t-test). C+D) Morphology of parasites is not affected by a knockdown in *glmS* **(C)** and M9 **(D)** cell lines. Images of Giemsa-stained parasites at 0 h, 24 h, 48 h, and 72 h after starting the knockdown using 0-5 mM GlcN were edited in ImageJ 2.3.0. Scale bar 5 µm.

In order to get more information about the localization of PF3D7_0220300, erythrocytes infected with trophozoite-stage parasites were enriched via MACS (4.4.7) and subsequent hypotonic lysis separated the sample in pellet and supernatant fractions before performing a Western Blot (4.3.2).

The pellet fraction contains the membrane-bound proteins with PfEMP1 being a control and the supernatant contains soluble proteins like the control protein Aldolase. Interestingly, the HA-tagged POI could be detected in the pellet fraction and slightly in the supernatant fraction, while all controls were as expected. There was no HA-signal in the CS2 control and whole *glmS* and CS2 samples showed bands corresponding to Aldolase and EXP1 (Figure 18A full-size WB in Supplement 4).

Moreover, IFAs with SBP1, REX1, EMP3, and KAHRP did not show a different protein distribution upon downregulation with 2.5 mM GlcN (Supplement 9, 10).

In silico analyses show a predicted protein structure of α-folds and two predicted transmembrane domains matching the described results of the hypotonic lysis Western Blot above (UniProt) (Figure 18B).

Next, the distribution of the HA-tagged POI was studied via IFAs in solution using α-HA (mouse) and the secondary antibody α-mouse Cy3. The nuclei were highlighted with DAPI (4.5.1). Fluorescent microscopy images of a trophozoite-infected erythrocyte show a dot-like distribution of the exported, HA-tagged POI in the erythrocyte cytosol, indicating a localization at the MCs (Figure 18C). Based on these results, a co-localization study with the MC-resident protein SBP1 was performed, using α-HA (mouse), α-SBP1 (rabbit), and suitable secondary antibodies. Immunolabelling with SBP1 showed a distinct MC-like distribution in the erythrocyte cytosol and only a partly co-localization with PF3D7_0220300-HA.

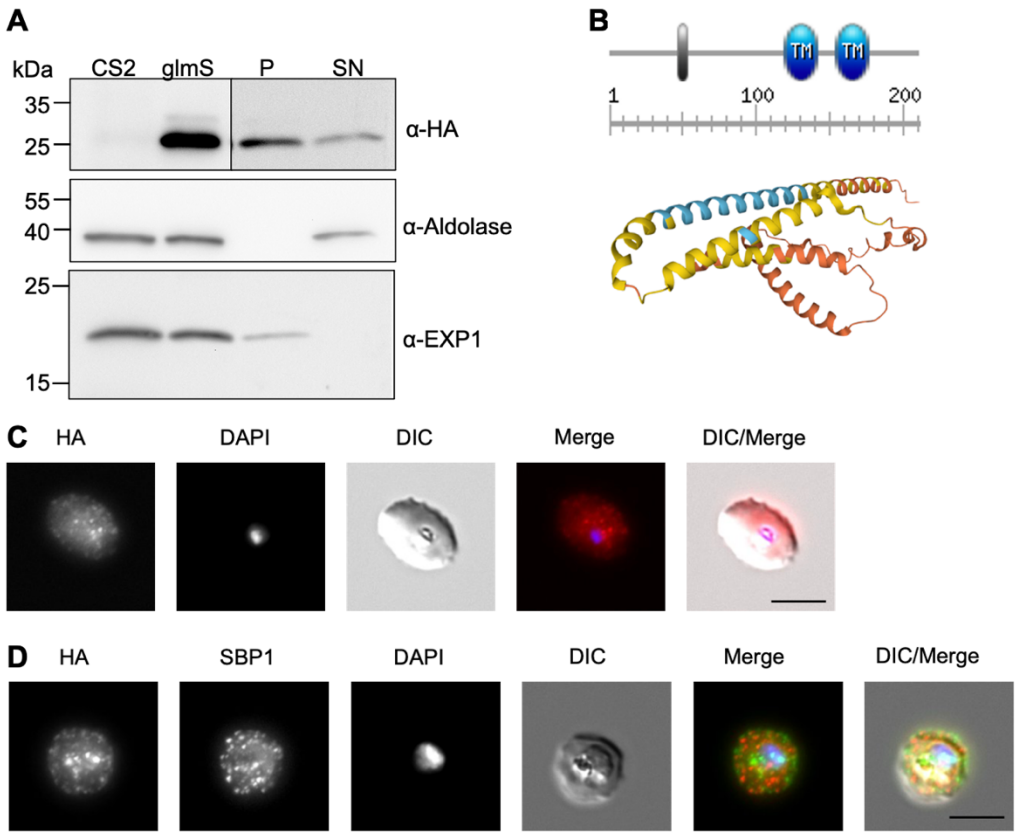

Fig.18: PF3D7_0220300 is a membrane-bound, exported protein. A) Enriched trophozoite-stage parasites were hypotonically lysed and analyzed in a Western blot. The HA-tagged POI was detected in the pellet (P) and supernatant (SN) fraction using α-HA (expected size ~22 kDa). Aldolase (expected size ~40 kDa) and EXP1 (expected size ~16 kDa) served as a control for soluble and membrane-bound proteins, respectively. **B)** PF3D7_0220300 is a PEXEL protein (grey bar: PEXEL signal sequence) that contains two transmembrane (TM) domains (PlasmoDB). A computational model predicts a structure made of α-folds (UniProt). **C)** Immunolabelling of the HA-tagged POI using α-HA (mouse) and α-mouse Cy3 (red). The nucleus was highlighted with DAPI (blue). Erythrocytes infected with trophozoites were fixed in 4% PFA and 0.0075% GA. Images were edited in ImageJ 2.3.0. Scale bar 5 µm. **D)** Co-immunolabelling of the HA-tagged POI (green) and the Maurer's cleft protein SBP1 using α-SBP1 (rabbit) (red). The nucleus was highlighted with DAPI (blue). Erythrocytes infected with trophozoites were fixed in 4% PFA and 0.0075% GA. Images were edited in ImageJ 2.3.0. Scale bar 5 µm.

In the next step, the effect of a downregulated POI on cytoadherence was analyzed. But before that, the subtelomeric region of chromosome 2 needed to be examined via PCR and digestion to exclude any possible gene deletions that could lead to a knobless phenotype and reduced cytoadherence. PCR analysis detected *kahsp40, emp3,* and *kahrp* in the *glmS* and M9 cell lines, which was further verified with the digestion of the respective bands (Figure 19ABC).

Interestingly, a static CSA-binding assay after selection on CSA showed significantly reduced binding upon downregulation of PF3D7_0220300 with 2.5 mM GlcN (p=0.000561). The specificity control group (CSA SOL) that was incubated with soluble CSA showed highly reduced binding to CSA, as expected (Figure 19D). As cytoadherence is mainly mediated by PfEMP1 presented on top of knobs, PfEMP1 VAR2CSA was quantified by flow cytometry using α-

VAR2CSA P11 (rabbit) and α-rabbit Cy3. The mean fluorescence intensity (MFI) of PfEMP1 VAR2CSA in DAPI-positive cells significantly decreased upon downregulation with 2.5 mM in the *glmS* cell line ($p<0.000001$) while it stayed the same in the M9 control group. However, the MFI in CS2PF3D7_0220300$^{glmS/M9}$ was significantly lower than in the parental CS2 cell line ($p<0.000001$). As an additional control, the *P. falciparum* wildtype strain 3D7 was used, which was not selected on CSA and switches faster between PfEMP1 variants than CS2 (Maier et al., 2007). Therefore, it was expected that significantly less PfEMP1 VAR2CSA is expressed ($p<0.000001$), leading to less cytoadherence to CSA. This could also be seen in the flow cytometry experiment (Figure 19E). In summary, a downregulation of PF3D7_0220300 has a significant effect on cytoadherence as it led to reduced binding in static CSA-binding assays and reduced PfEMP1 fluorescence in flow cytometry experiments.

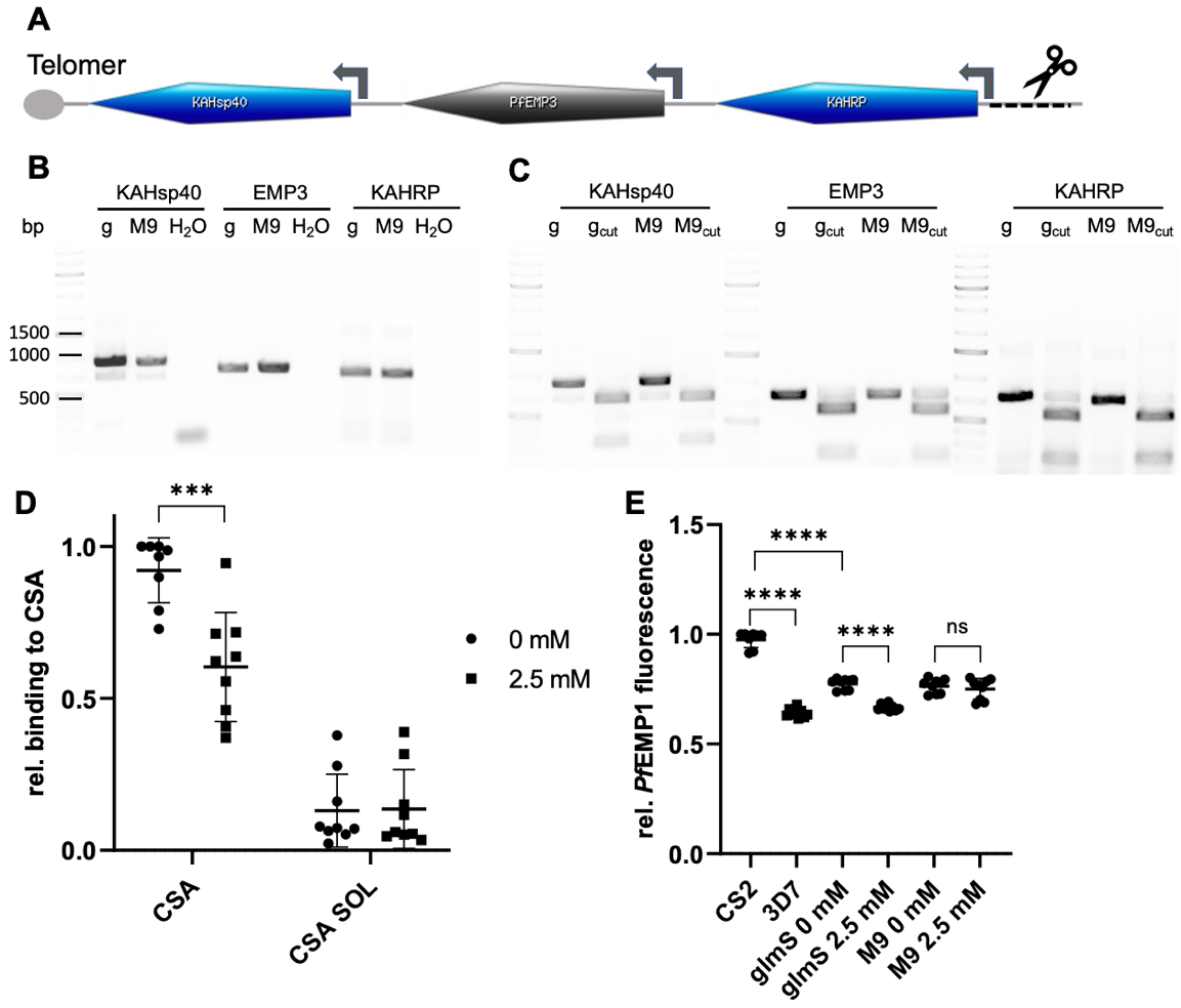

Fig.19: Knockdown of PF3D7_0220300 significantly reduces binding to CSA and PfEMP1 abundance on the surface of infected erythrocytes. A) The subtelomeric region of one arm of chromosome 2 codes for KAHsp40, EMP3, and KAHRP. A loss of KAHRP due to a stochastic break at a potential breaking point (scissors) also leads to the loss of KAHsp40 and EMP3 and results in a knobless phenotype. **B)** PCR of genomic DNA verifies intact *kahsp40*

(900 bp), *emp3* (792 bp), and *kahrp* (717 bp) in the *glmS* and M9 cell lines. **C)** A test digest of the amplified genes from B with HindIII (KAHsp40: 670 + 230 bp), AluI (EMP3: 602 + 190 bp) and NdeI (KAHRP: 526 + 191 bp) verifies PCR results. **D)** A knockdown with 2.5 mM GlcN for 72 h leads to significantly reduced binding to CSA in a static binding assay. Incubation of infected erythrocytes with soluble CSA (CSA SOL) prior to the assay prevents binding to CSA-covered plates. Microscopic images of Giemsa-stained cells were analyzed with Ilastik 1.4 and ImageJ 2.3.0, the number of cells was normalized (highest number at 0 mM CS2 set to 1) and statistically analyzed with GraphPad Prism 8.3.1. n=3; *** p=0.000561 (Student's t-test). **E)** The mean fluorescence intensity of *Pf*EMP1 VAR2CSA was measured with a CytoflexS, normalized to the highest value in CS2 (set to 1), and statistically analyzed with GraphPad Prism 8.3.1. Cells were cultivated ±2.5 mM GlcN for 72 h prior to preparation for flow cytometry with α-*Pf*EMP1 VAR2CSA P11 (rabbit) and α-rabbit Cy3. Nuclei were labeled with DAPI. n=3; ns: not significant; **** p<0.0001 (Dunnett's test).

2.5 Phenotypic characterization of PF3D7_0220600

The third gene analyzed in this study is PF3D7_0220600 which codes for an exported PEXEL protein of 25.9 kDa with unknown function (PlasmoDB). PCR analysis of the *glmS* and M9 cell lines after selection with 800 µg/ml G418 also showed 5' and 3' integration without any remaining wildtype locus. Remnant plasmids (episome) and hDHFR were detectable and the EMP3 control demonstrated gDNA integrity (Table 5, Figure 20AB).

Tab. 5: Primer combinations and expected sizes for integration PCR of CS2PF3D7_0220600$^{glmS/M9}$.

	Primers	Expected size
5' Integration	5'fw_0220600 HA_rev	1136 bp
3' Integration	pARL_fw 3'rev_0220600	929 bp
Wildtype locus	5'fw_0220600 3'rev_0220600	1130 bp
Episome	pARL_fw HA_rev	939 bp
hDHFR	hDHFR_fw hDHFR_rev	531 bp
EMP3 (gDNA control)	EMP3_fw EMP3_rev	792 bp

Expression of the HA-tagged POI was verified via Western Blot analysis of enriched trophozoite-stage infected erythrocytes using α-HA (expected size ~24 kDa) and α-Aldolase (expected size ~40 kDa) as a loading control (4.3.2). The HA-tagged POI could be detected in the *glmS* and M9 cell lines with no detection in the CS2 parental cell line (Figure 20C, full-size WB in Supplement 5A).

In order to demonstrate that the *glmS* ribozyme system is working effectively, CS2PF3D7_0220600$^{glmS/M9}$ were cultivated with 0-5 mM GlcN for 72 h with subsequent Western Blot analysis. This showed weaker HA-bands in the *glmS* sample the more GlcN was used while the HA-band intensity in the M9 control did not change. Moreover, very weak HA-bands corresponding to a molecular weight of around 50 kDa could be detected in some samples which

likely represent a non-skipped version of the HA-tagged POI (Figure 20D, full-size WB in Supplement 5B). The protein abundance was quantified by measuring the band intensities in Western Blots of three independent experiments via ImageJ 2.3.0 and normalizing the HA-band intensities to the respective band intensities of Aldolase. Quantification verified that there was no significant reduction in the abundance of the POI in CS2PF3D7_0220600^{M9}, but cultivation with GlcN did lead to a significantly higher protein abundance (0 mM vs. 1.25 mM p=0.0030). However, the *glmS* cell line showed a highly significant reduction of protein abundance with 1.25 mM GlcN to 39% (p<0.0001), 2.5 mM GlcN to 19% (p<0.0001), and 5 mM GlcN to 11% (p<0.0001) (Figure 20E). In all further experiments, the downregulation was performed with 2.5 mM GlcN.

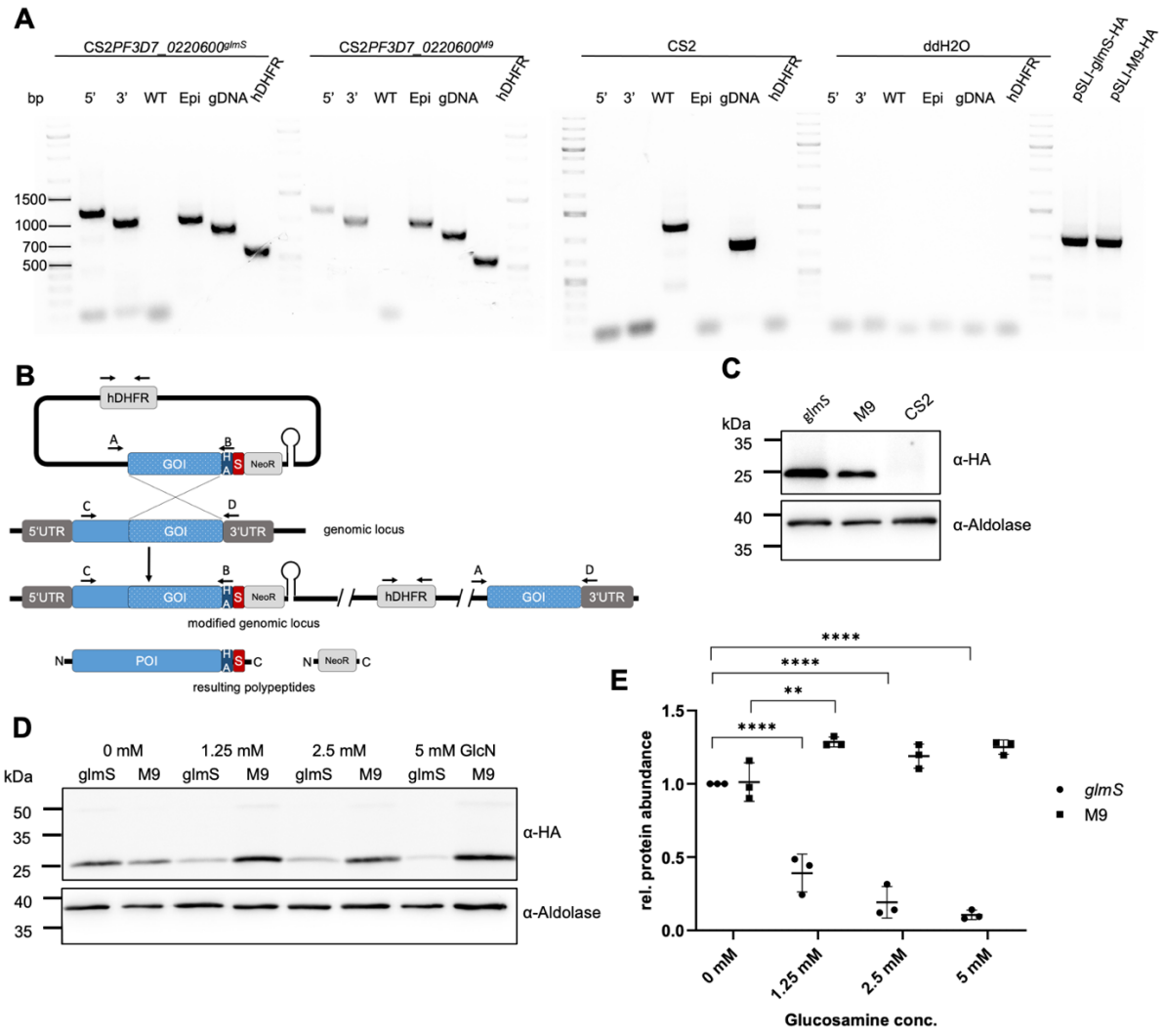

Fig. 20: Verification of CS2PF3D7_0220600$^{glmS/M9}$ and efficiency of knockdown. A) Integration PCR using genomic DNA (gDNA) of CS2PF3D7_0220600$^{glmS/M9}$ and the parental strain CS2 verifies wildtype-free integrants. *GlmS* and M9 cell lines show 3' (primers A and D: 929 bp) and 5' (primers C and B: 1136 bp) integration, hDHFR (531 bp) and episomal bands (Epi primers A and B: 939 bp). The wildtype locus (WT primers C and D: 1130 bp) is only amplified from gDNA of the wildtype CS2 cell line. EMP3 serves as a positive control for the gDNA (792 bp). **B)** Strategy to generate the *glmS* knockdown cell line via homologous recombination and using selection-linked integration (SLI).

Arrows indicate the primers for the integration PCR (see A). The Skip-peptide (S) between the HA-tagged gene of interest (GOI) and the neomycin resistance cassette (NeoR) causes the expression of two separate proteins that allows for the selection of integrants. UTR: untranslated region; POI: protein of interest. **C)** Western blot analysis of enriched trophozoites shows the expression of the HA-tagged POI using α-HA (expected size ~24 kDa) and α-Aldolase (expected size ~40 kDa) as a loading control. **D)** Downregulation in asexual blood stages after cultivation with 0, 1.25, 2.5, and 5 mM glucosamine (GlcN) for 72 h. Western blot analysis of enriched trophozoites using α-HA (expected size ~24 kDa) and α-Aldolase (expected size ~40 kDa) as a loading control. Representative of three independent experiments. **E)** Quantification of protein abundance of three independent Western blot experiments (see D). Band intensities of HA were measured using ImageJ 2.3.0, normalized to the respective band intensity of aldolase (*glmS* 0 mM GlcN set to 1), and statistically analyzed using GraphPad Prism 8.3.1. n=3, ** p<0.01, **** p<0.0001 (Student's t-test).

Similar to the other studied proteins, a downregulation of PF3D7_0220600 did not lead to a significant growth defect after 72 h (4.4.11). However, the end parasitemia in the growth assay did decrease the more GlcN was used, once again showing the cytotoxic effect of GlcN itself (Figure 21A). Giemsa-stained blood smears over the period of the growth assay did not show any visible morphological differences in the developmental stages of the *glmS* and M9 cell lines (Figure 21CD). Moreover, the number of merozoites per schizont (~15) did not differ between the *glmS* and M9 cell lines cultured without and with 2.5 mM GlcN (Figure 21B).

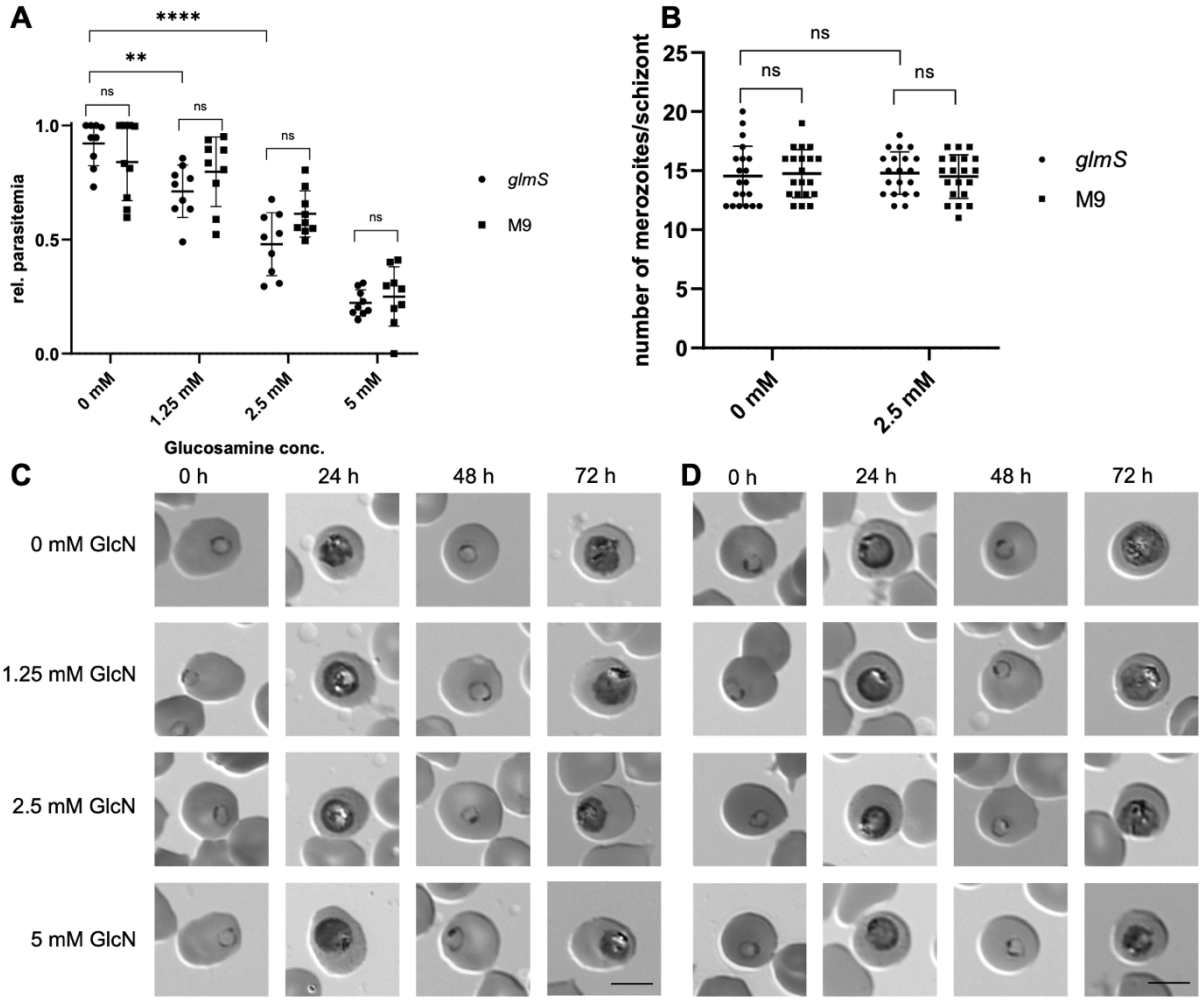

Fig. 21: Knockdown of PF3D7_0220600 does not impair parasite growth. A) SybrGreen-based growth assay over 72 h shows the toxic effect of glucosamine (GlcN) in *glmS* and M9 cell lines. Emission of SybrGreen at 530 nm was measured with a Clariostar plate reader, normalized to the highest value at 0 mM GlcN (set to 1), and statistically analyzed using GraphPad Prism 8.3.1. n=3; ns: not significant; ** p<0.01; **** p<0.0001 (Student's t-test). **B)** The number of merozoites per schizont is not affected by a knockdown with 2.5 mM GlcN after 72 h. Merozoites were counted in images of schizonts in Giemsa-stained blood smears. n=20; ns: not significant (Student's t-test). C+D) Morphology of parasites is not affected by a knockdown in *glmS* **(C)** and M9 **(D)** cell lines. Images of Giemsa-stained parasites at 0 h, 24 h, 48 h, and 72 h after starting the knockdown using 0-5 mM GlcN were edited in ImageJ 2.3.0. Scale bar 5 µm.

In order to get more information about the localization of PF3D7_0220600, a Western Blot after hypotonic lysis of magnetically enriched trophozoite-stage parasites was performed (4.3.2, 4.4.7). Interestingly, the HA-tagged POI could be detected in the pellet fraction and slightly in the supernatant fraction, while all controls were as expected. There was no HA-signal in the CS2 control and whole *glmS* and CS2 samples showed bands corresponding to Aldolase and EXP1 (Figure 22A full-size WB in Supplement 6).

Moreover, IFAs with SBP1, REX1, EMP3, and KAHRP did not show a different protein distribution upon downregulation with 2.5 mM GlcN (Supplement 9,10).

In silico analyses show a predicted protein structure of α-folds and one predicted transmembrane domain matching the described results of the hypotonic lysis Western Blot above (UniProt) (Figure 22B).

Next, the distribution of the HA-tagged POI was studied via IFA in solution using α-HA (mouse) and the secondary antibody α-mouse Cy3. The nuclei were highlighted with DAPI (4.5.1). Fluorescent microscopy images of a trophozoite-infected erythrocyte show that the HA-tagged POI is located at the erythrocyte membrane. Z-stacks further show an even distribution under or above the surface of the infected erythrocyte (Figure 22C).

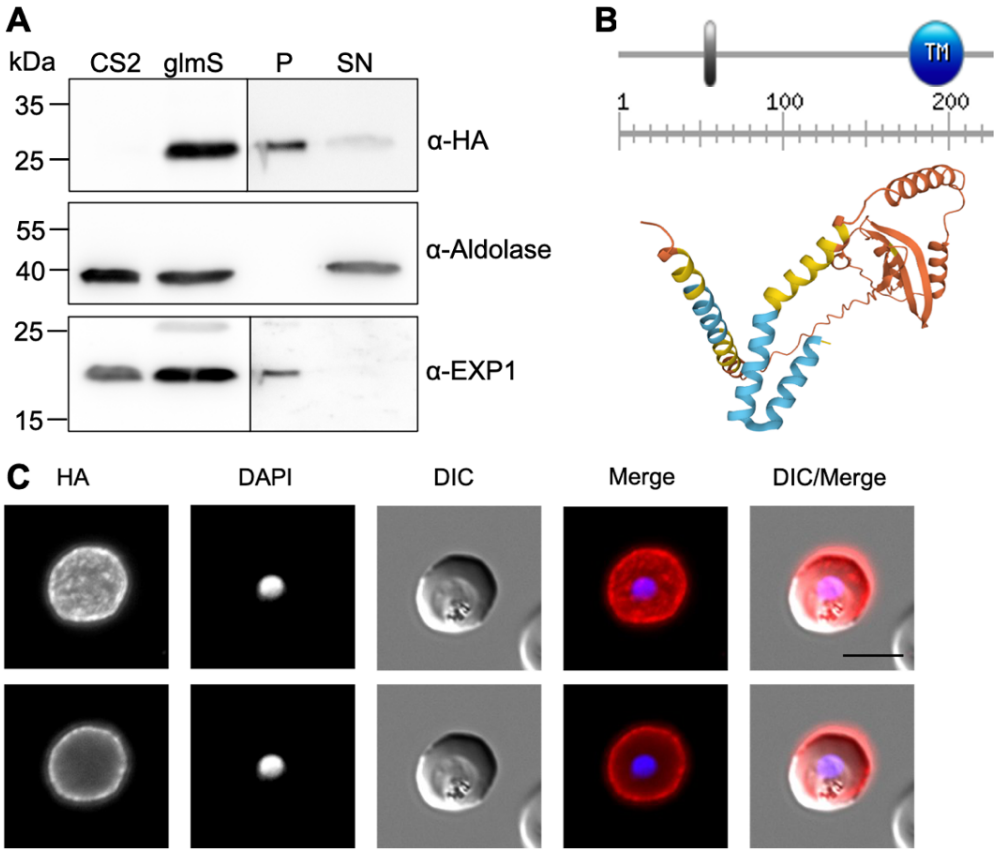

Fig. 22: PF3D7_0220600 is a membrane-bound protein that is localized at the erythrocyte membrane. A) Enriched trophozoite-stage parasites were hypotonically lysed and analyzed in a Western blot. The HA-tagged POI was detected in the pellet (P) and supernatant (SN) fraction using α-HA (expected size ~24 kDa), Aldolase (expected size ~40 kDa) and EXP1 (expected size ~16 kDa) served as a control for soluble and membrane-bound proteins, respectively. **B)** PF3D7_0220600 is a PEXEL protein (grey bar: PEXEL signal sequence) that contains one transmembrane (TM) domain (PlasmoDB). A computational model predicts a structure made of α-folds (UniProt). Scale: amino acids. **C)** Immunolabelling of the HA-tagged POI using α-HA (mouse) and α-mouse Cy3 (red). The nucleus was highlighted with DAPI (blue). Erythrocytes infected with trophozoites were fixed in 4% PFA and 0.0075% GA. A Z-stack of the HA signal (upper) and a slice (lower) through the erythrocyte infected with a trophozoite-stage parasite shows a localization at the erythrocyte membrane. Images were edited in ImageJ 2.3.0. Scale bar 5 µm.

After the subtelomeric region of chromosome 2 was examined via PCR and digestion of *kahsp40, emp3,* and *kahrp*, a static CSA-binding assay with CSA-selected CS2PF3D7_0220600^{glmS}

parasites was performed (Figure 23AB). Downregulation of the POI with 2.5 mM GlcN led to significantly reduced binding to CSA (p=0.008241) (Figure 23D). One outlier was excluded from the analysis of *glmS* 2.5 mM GlcN (CSA) using the 2 sigma rule. The specificity control group (CSA SOL) that was incubated with soluble CSA showed highly reduced binding to CSA, as expected (Figure 23D).

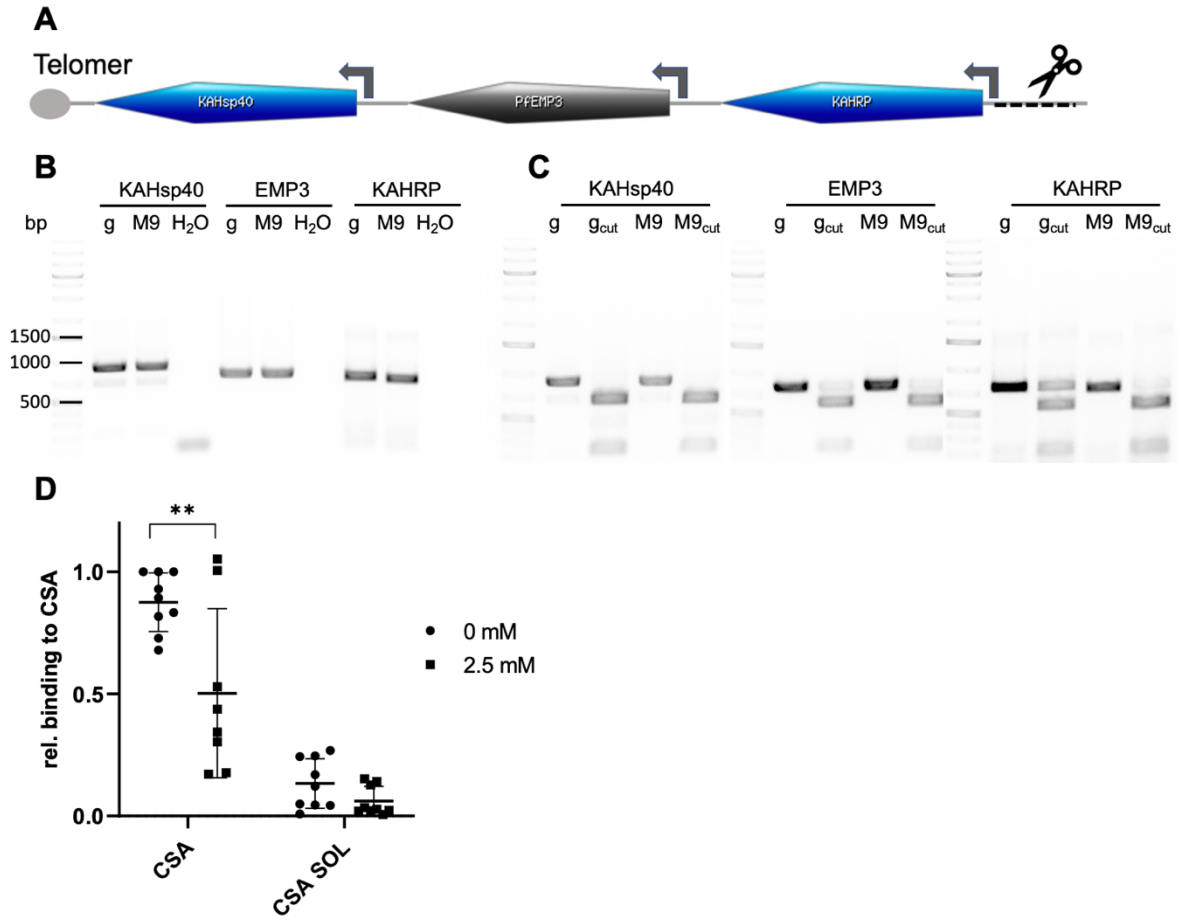

Fig. 23: Knockdown of PF3D7_0220600 does not significantly reduce binding to CSA. A) The subtelomeric region of one arm of chromosome 2 codes for KAHsp40, EMP3, and KAHRP. A loss of KAHRP due to a stochastic break at a potential breaking point (scissors) also leads to the loss of KAHsp40 and EMP3 and results in a knobless phenotype. **B)** PCR of genomic DNA verifies intact *kahsp40* (900 bp), *emp3* (792 bp), and *kahrp* (717 bp) in the *glmS* and M9 cell lines. **C)** A test digest of the amplified genes from B with HindIII (KAHsp40: 670 + 230 bp), AluI (EMP3: 602 + 190 bp) and NdeI (KAHRP: 526 + 191 bp) verifies PCR results. **D)** A knockdown with 2.5 mM GlcN for 72 h significantly reduces binding to CSA in a static binding assay. Incubation of infected erythrocytes with soluble CSA (CSA SOL) prior to the assay prevents binding to CSA-covered plates. Microscopic images of Giemsa-stained cells were analyzed with Ilastik 1.4 and ImageJ 2.3.0, the number of cells was normalized (highest number at 0 mM CS2 set to 1) and statistically analyzed with GraphPad Prism 8.3.1. n=3; ** p=0.008241 (Student's t-test).

2.6 Phenotypic characterization of PF3D7_0301600

The last gene analyzed in this study is PF3D7_0301600 (GEXP21: gametocyte exported protein 21) which codes for an exported PEXEL protein of 87.5 kDa with unknown function (PlasmoDB). PCR analysis of the *glmS* and M9 cell lines after selection with 800 µg/ml G418 also showed 5'

and 3' integration without any remaining wildtype locus. Remnant plasmids (episome) and hDHFR were detectable and the EMP3 control demonstrated gDNA integrity (Table 6, Figure 24AB).

Tab. 6: Primer combinations and expected sizes for integration PCR of CS2PF3D7_0301600$^{glmS/M9}$.

	Primers	Expected size
5' Integration	5'fw_0301600 HA_rev	2022 bp
3' Integration	pARL_fw 3'rev_0301600	1310 bp
Wildtype locus	5'fw_0301600 3'rev_0301600	2053 bp
Episome	pARL_fw HA_rev	1279 bp
hDHFR	hDHFR_fw hDHFR_rev	531 bp
EMP3 (gDNA control)	EMP3_fw EMP3_rev	792 bp

Expression of the HA-tagged POI was verified via Western Blot analysis of enriched trophozoite-stage infected erythrocytes using α-HA (expected size ~82 kDa) and α-Aldolase (expected size ~40 kDa) as a loading control (4.3.2). The HA-tagged POI could be detected in the *glmS* and M9 cell lines with no detection in the CS2 parental cell line. However, the HA-band ran higher than expected, at around 110 kDa. Moreover, additional HA-bands corresponding to a molecular weight of around 130 kDa could be detected in some samples which likely represent a non-skipped version of the HA-tagged POI (Figure 24C, full-size WB in Supplement 7A).

In order to demonstrate that the *glmS* ribozyme system is working effectively, CS2PF3D7_0301600$^{glmS/M9}$ were cultivated with 0-5 mM GlcN for 72 h with subsequent Western Blot analysis. This showed weaker HA-bands in the *glmS* sample the more GlcN was used while the HA-band intensity in the M9 stayed similar (Figure 24D, full-size WB in Supplement 7B).

Quantification verified that there was no significant difference in the abundance of the POI in CS2PF3D7_0301600^{M9}. However, the *glmS* cell line showed a highly significant reduction of protein abundance with 1.25 mM GlcN to 42% (p=0.0017), 2.5 mM GlcN to 39% (p=0.0012) and 5 mM GlcN to 24% (p=0.0002) (Figure 24E). In all further experiments, the downregulation was performed with 2.5 mM GlcN.

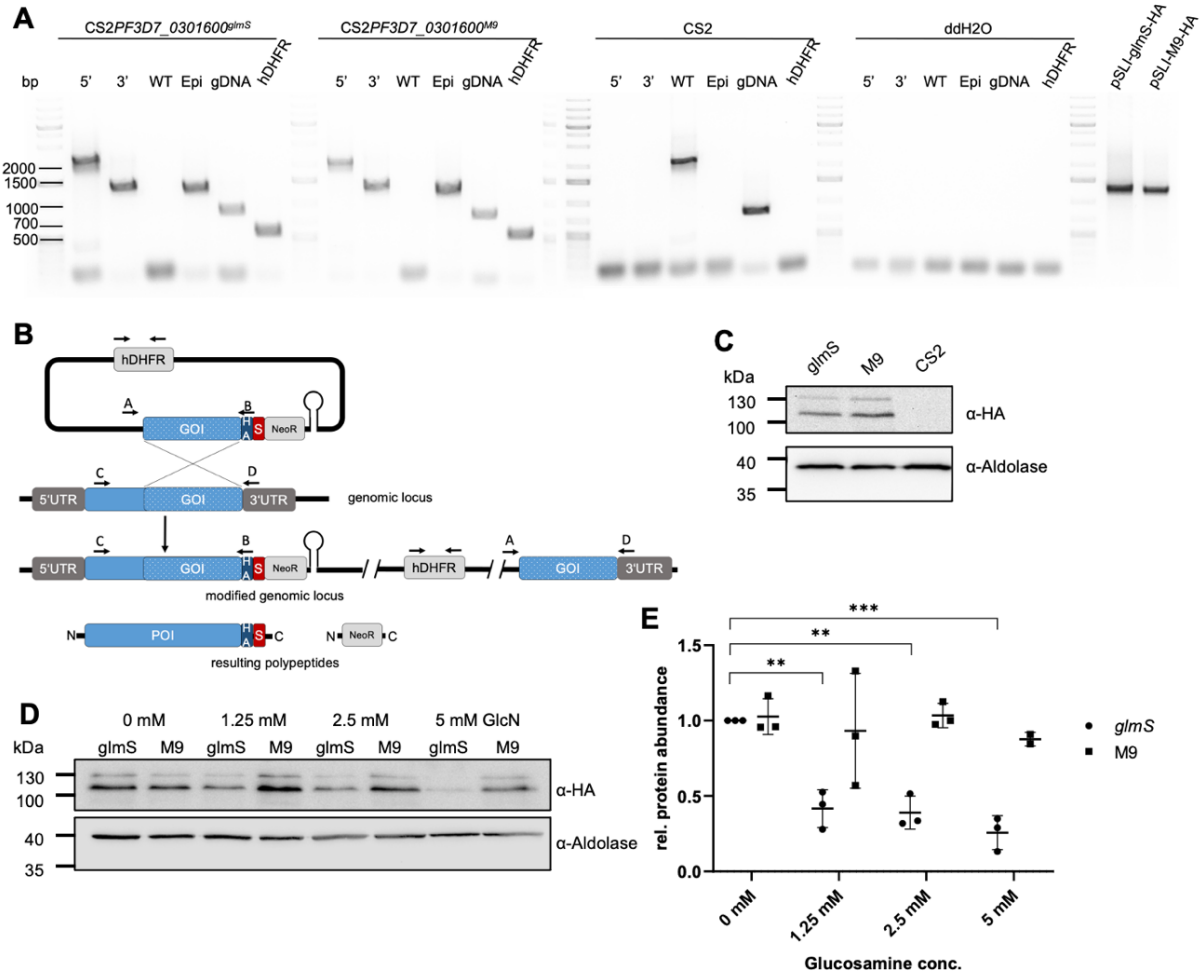

Fig. 24: Verification of CS2PF3D7_0301600$^{glmS/M9}$ and efficiency of knockdown. A) Integration PCR using genomic DNA (gDNA) of CS2PF3D7_0301600$^{glmS/M9}$ and the parental strain CS2 verifies wildtype-free integrants. *GlmS* and M9 cell lines show 3' (primers A and D: 1310 bp) and 5' (primers C and B: 2022 bp) integration, hDHFR (531 bp), and episomal bands (Epi primers A and B: 1279 bp). The wildtype locus (WT primers C and D: 2053 bp) is only amplified from gDNA of the wildtype CS2 cell line. EMP3 serves as a positive control for the gDNA (792 bp). **B)** Strategy to generate the *glmS* knockdown cell line via homologous recombination and using selection-linked integration (SLI). Arrows indicate the primers for the integration PCR (see A). The Skip-peptide (S) between the HA-tagged gene of interest (GOI) and the neomycin resistance cassette (NeoR) causes the expression of two separate proteins that allows for the selection of integrants. UTR: untranslated region; POI: protein of interest. **C)** Western blot analysis of enriched trophozoites shows the expression of the HA-tagged POI using α-HA (expected size ~82 kDa) and α-Aldolase (expected size ~40 kDa) as a loading control. The higher HA-band is an unskipped version of the HA-tagged POI bound to neomycin phosphotransferase (~30 kDa) **D)** Downregulation in asexual blood stages after cultivation with 0, 1.25, 2.5, and 5 mM glucosamine (GlcN) for 72 h. Western blot analysis of enriched trophozoites using α-HA (expected size ~82 kDa) and α-Aldolase (expected size ~40 kDa) as a loading control. Representative of three independent experiments. **E)** Quantification of protein abundance of three independent Western blot experiments (see D). Band intensities of HA were measured using ImageJ 2.3.0, normalized to the respective band intensity of aldolase (*glmS* 0 mM GlcN set to 1), and statistically analyzed using GraphPad Prism 8.3.1. n=3, ** p<0.01; ** p<0.001 (Student's t-test).

Just like the other studied proteins, a downregulation of PF3D7_0301600 did not lead to a significant growth defect after 72 h (4.4.11). However, the end parasitemia in the growth assay did decrease the more GlcN was used, once again showing the cytotoxic effect of GlcN itself

(Figure 25A). Giemsa-stained blood smears over the period of the growth assay did not show any visible morphological differences in the developmental stages of the *glmS* and M9 cell lines (Figure 25CD). Moreover, the number of merozoites per schizont (~17) did not significantly differ between the *glmS* and M9 cell lines cultured without and with 2.5 mM GlcN (Figure 25B).

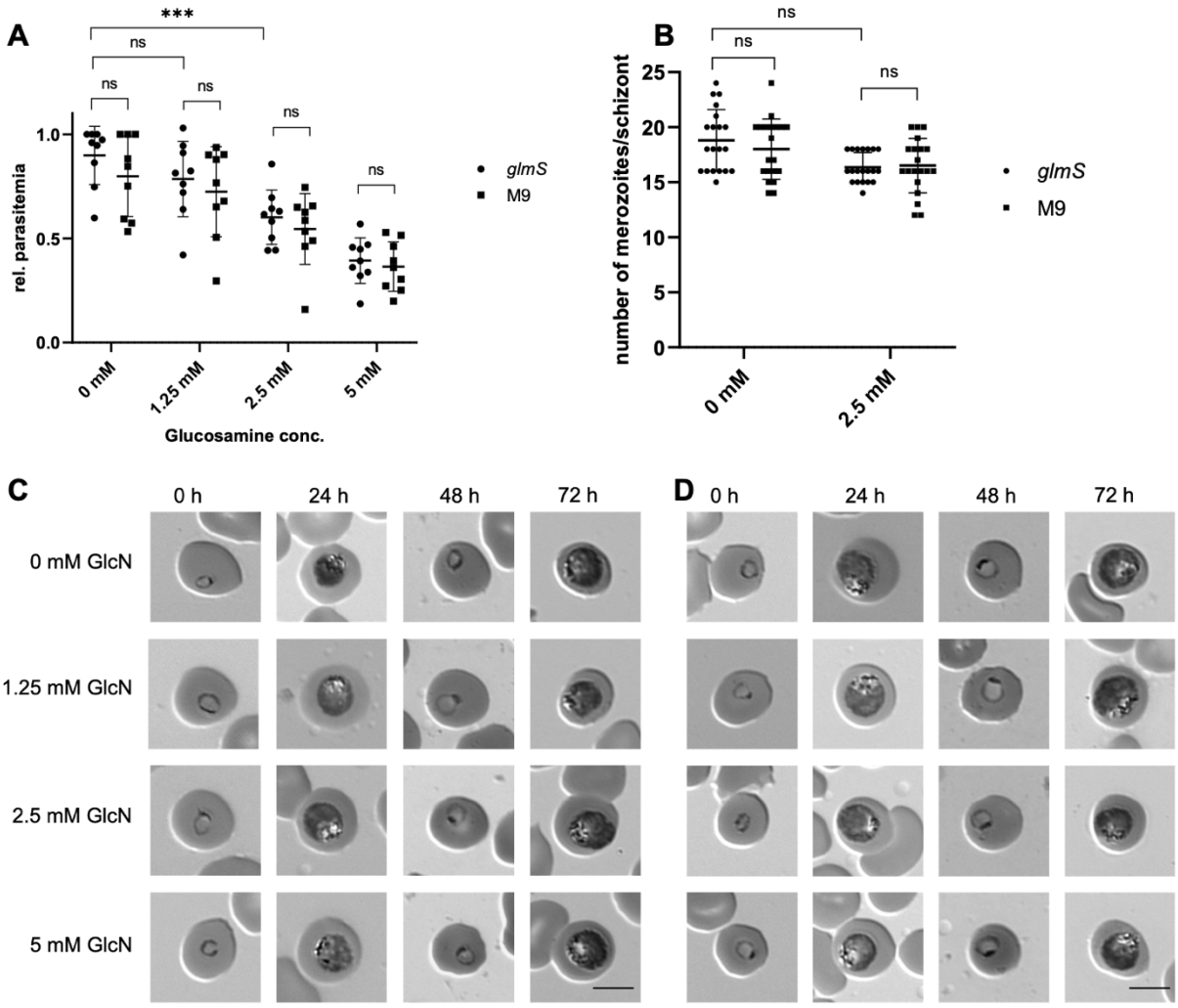

Fig. 25: Knockdown of PF3D7_0301600 does not impair parasite growth. A) SybrGreen-based growth assay over 72 h shows the toxic effect of glucosamine (GlcN) in *glmS* and M9 cell lines. Emission of SybrGreen at 530 nm was measured with a Clariostar plate reader, normalized to the highest value at 0 mM GlcN (set to 1), and statistically analyzed using GraphPad Prism 8.3.1. n=3; ns: not significant; *** p<0.001 (Student's t-test). **B)** The number of merozoites per schizont is not affected by a knockdown with 2.5 mM GlcN after 72 h. Merozoites were counted in images of schizonts in Giemsa-stained blood smears. n=20; ns: not significant (Student's t-test). C+D) Morphology of parasites is not affected by a knockdown in *glmS* **(C)** and M9 **(D)** cell lines. Images of Giemsa-stained parasites at 0 h, 24 h, 48 h, and 72 h after starting the knockdown using 0-5 mM GlcN were edited in ImageJ 2.3.0. Scale bar 5 µm.

In order to get more information about the localization of PF3D7_0301600, a Western Blot after hypotonic lysis of magnetically enriched trophozoite-stage parasites was performed (4.3.2, 4.4.7).

Interestingly, the HA-tagged POI could only be detected in the supernatant fraction, while all controls were as expected. However, several distinct HA-bands with a lower molecular weight could be detected after hypotonic lysis, likely due to proteolytic degradation of the POI. There was no HA-signal in the CS2 control and whole *glmS* and CS2 samples showed bands corresponding to Aldolase and EXP1 (Figure 26A full-size WB in Supplement 8). Moreover, IFAs with SBP1, REX1, EMP3, and KAHRP did not show a different protein distribution upon downregulation with 2.5 mM GlcN (Supplement 9,10).

In silico analyses show a predicted protein structure of coiled coils, disordered regions, a stretch of polar residues (20 amino acids), and no predicted transmembrane domain matching the described results of the hypotonic lysis Western Blot above (UniProt) (Figure 26B). Moreover, 9 P2.4EST motifs were found, that are potential proteolytic cleavage sites (epestfind EMBOSS). Next, the distribution of the HA-tagged POI was studied via IFA in solution using α-HA (mouse) and the secondary antibody α-mouse Cy3. The nuclei were highlighted with DAPI (4.5.1). Fluorescent microscopy images of a trophozoite-infected erythrocyte show a dot-like distribution of the exported, HA-tagged POI in the erythrocyte cytosol, indicating a localization at the MCs (Figure 26C). Based on these results, a co-localization study with the MC-resident protein SBP1 was performed, using α-HA (mouse), α-SBP1 (rabbit), and suitable secondary antibodies. Immunolabelling with SBP1 showed a distinct MC-like distribution in the erythrocyte cytosol and only a partly co-localization with PF3D7_0301600-HA (Figure 26D).

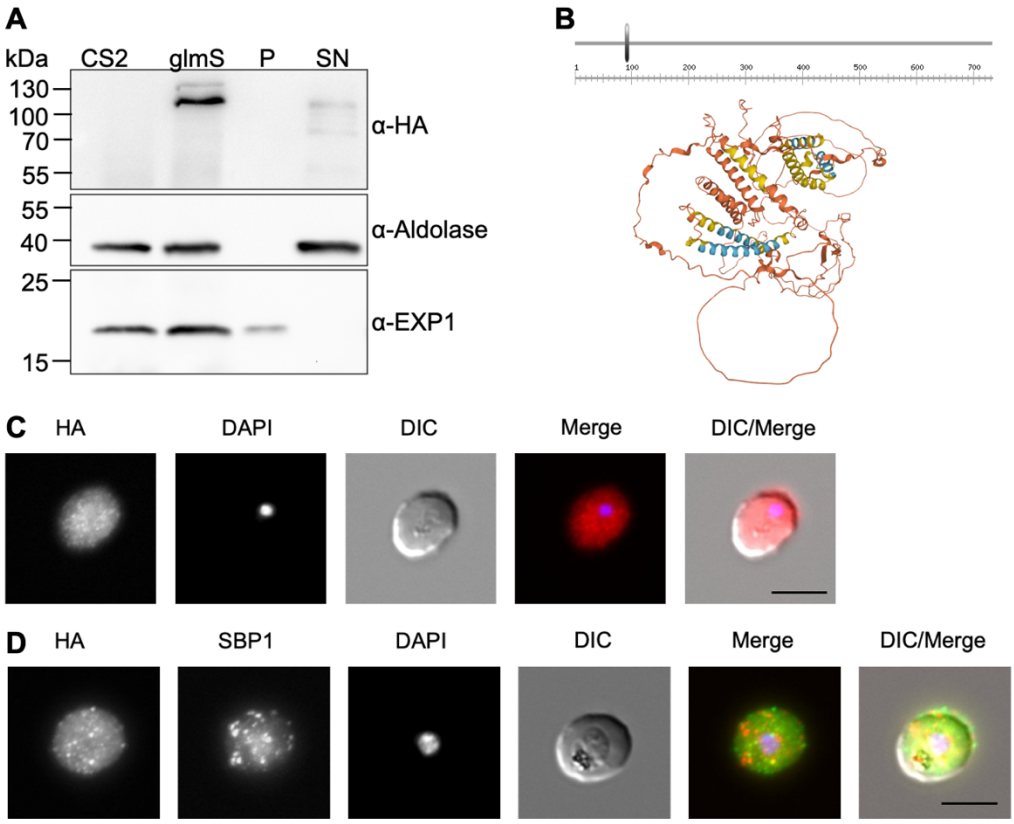

Fig. 26: PF3D7_0301600 is a soluble, exported protein. A) Enriched trophozoite-stage parasites were hypotonically lysed and analyzed in a Western blot. Fragments of the HA-tagged POI were detected in the supernatant (SN) fraction using α-HA (expected size ~82 kDa). Aldolase (expected size ~40 kDa) and EXP1 (expected size ~16 kDa) served as a control for soluble and membrane-bound proteins, respectively. The higher HA-band in the *glmS* sample is an unskipped version of the HA-tagged POI bound to neomycin phosphotransferase (~30 kDa). **B)** PF3D7_0301600 is a PEXEL protein (grey bar: PEXEL signal sequence) that contains no transmembrane (TM) domains (PlasmoDB). A computational model of PF3D7_0301600 predicts a structure made of α-folds and disordered regions (UniProt). Scale: amino acids. **C)** Immunolabelling of the HA-tagged POI using α-HA (mouse) and α-mouse Cy3 (red). The nucleus was highlighted with DAPI (blue). Erythrocytes infected with trophozoites were fixed in 4% PFA and 0.0075% GA. Images were edited in ImageJ 2.3.0. Scale bar 5 µm. **D)** Co-immunolabelling of the HA-tagged POI (green) and the Maurer's cleft protein SBP1 using α-SBP1 (rabbit) (red). The nucleus was highlighted with DAPI (blue). Erythrocytes infected with trophozoites were fixed in 4% PFA and 0.0075% GA. Images were edited in ImageJ 2.3.0. Scale bar 5 µm.

After the subtelomeric region of chromosome 2 was examined via PCR and digestion of *kahsp40, emp3,* and *kahrp*, a static CSA-binding assay with CSA-selected CS2PF3D7_0301600^{glmS} parasites was performed (Figure 27AB). Downregulation of the POI with 2.5 mM GlcN led to significantly reduced binding to CSA (p=0.000008). The specificity control group (CSA SOL) that was incubated with soluble CSA showed highly reduced binding to CSA, as expected (Figure 27D).

Due to the highly reduced cytoadherence to CSA upon downregulation of PF3D7_0301600, PfEMP1 VAR2CSA was analyzed via flow cytometry. The mean fluorescence intensity (MFI) of PfEMP1 VAR2CSA in DAPI-positive cells did not significantly change upon downregulation with 2.5 mM GlcN in the *glmS* and M9 cell lines (*glmS*: p=0.66; M9: p=0.28).

However, the MFI in CS2PF3D7_0220300$^{glmS/M9}$ was significantly lower than in the parental CS2 cell line (p=0.000066). The additional 3D7 control expressed significantly less PfEMP1 VAR2CSA than CS2 (p=0.000052) (Figure 27E). In summary, a downregulation of PF3D7_0301600 has a significant effect on cytoadherence as it led to reduced binding in static CSA-binding assays while the PfEMP1 VAR2CSA fluorescence in flow cytometry experiments did not change.

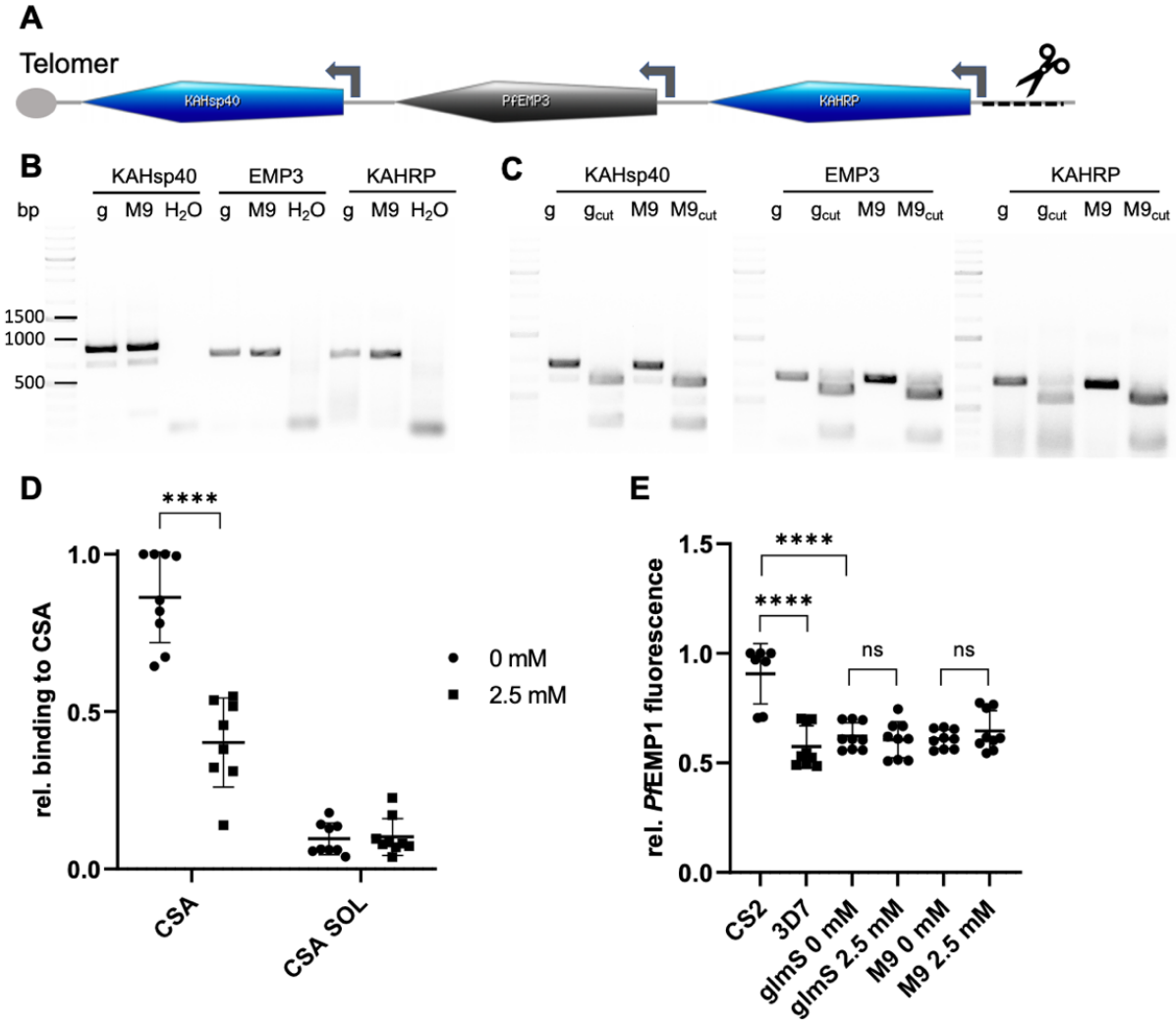

Fig. 27: Knockdown of PF3D7_0301600 significantly reduces binding to CSA. A) The subtelomeric region of one arm of chromosome 2 codes for KAHsp40, EMP3, and KAHRP. A loss of KAHRP due to a stochastic break at a potential breaking point (scissors) also leads to the loss of KAHsp40 and EMP3 and results in a knobless phenotype. **B)** PCR of genomic DNA verifies intact *kahsp40* (900 bp), *emp3* (792 bp), and *kahrp* (717 bp) in the *glmS* and M9 cell lines. **C)** A test digest of the amplified genes from B with HindIII (KAHsp40: 670 + 230 bp), AluI (EMP3: 602 + 190 bp) and NdeI (KAHRP: 526 + 191 bp) verifies PCR results. **D)** A knockdown with 2.5 mM GlcN for 72 h leads to significantly reduced binding to CSA in a static binding assay. Incubation of infected erythrocytes with soluble CSA (CSA SOL) prior to the assay prevents binding to CSA-covered plates. Microscopic images of Giemsa-stained cells were analyzed with Ilastik 1.4 and ImageJ 2.3.0, the number of cells was normalized (highest number at 0 mM CS2 set to 1) and statistically analyzed with GraphPad Prism 8.3.1. n=3; **** p=0.000008 (Student's t-test). **E)** The mean fluorescence intensity of *Pf*EMP1 VAR2CSA was measured with a CytoflexS, normalized to the highest value in CS2 (set to 1), and statistically analyzed with GraphPad Prism 8.3.1. Cells were cultivated ±2.5 mM GlcN for 72 h prior to preparation for flow cytometry with α-*Pf*EMP1 VAR2CSA P11 (rabbit) and α-rabbit Cy3. Nuclei were labeled with DAPI. n=3; ns: not significant; **** p<0.0001 (Dunnett's test)

2.7 Overview of all results and additional electron microscopy experiments

All four studied transgenic cell lines were verified via PCR and the expression of the HA-tagged POIs was demonstrated in Western Blots. Cultivation with 0-5 mM GlcN and subsequent Western Blot analysis showed an efficient *glmS* ribozyme system with statistically significant downregulation of the POIs. The subtelomeric region of chromosome 2, which codes for *kahsp40*, *emp3,* and *kahrp*, was analyzed via PCR and showed no deletions (2.3-2.6). All further experimental results are summarized in table 7 below (Table 7).

Based on the significant results of the CSA-binding assay and PfEMP1 VAR2CSA flow cytometry in some downregulated cell lines, the effect of a downregulation of the POIs was analyzed by comparing the morphology of knobs on the surface of infected erythrocytes and the morphology of knobs via electron microscopy. For this, synchronized *glmS* and M9 cell lines were cultivated ± 2.5 mM GlcN for 72 h, trophozoite-infected erythrocytes were enriched via MACS for scanning electron microscopy (SEM) or gelafundin flotation for transmission electron microscopy (TEM) and further prepared for imaging (4.5.2, 4.5.3). The surface of all infected erythrocytes in SEM images showed knob morphologies ranging from typical, small, and evenly distributed knobs (Figure 28, eg. *glmS* 0 mM top image) to enlarged and fewer knobs (Figure 28, eg. glmS 0 mM third image from top). However, these differences could not be linked to a downregulation of the POIs as various morphologies could be observed in all cell lines, *glmS* and M9 ± 2.5 mM GlcN (Figure 28 and Supplement 11-13).

The same knob distribution could be seen in TEM images. Moreover, Mauer's clefts were examined in more detail as there are several known exported proteins that are crucial for correct MC architecture and contribute to the export of PfEMP1 to the surface which affects the cytoadherence (1.4) (DeKoning-Ward et al., 2016). As a result, typical disc-like MCs with ~100-250 nm length could be observed close to the erythrocyte membrane in all cell lines (Figure 29 and Supplement 14-16). This suggests that PF3D7_0113300, PF3D7_0220300, PF3D7_0220600, and PF3D7_030160 are not important for the correct localization and formation of MCs *in vitro*.

Tab. 7: Summary of the results.

	PF3D7_0113300	PF3D7_0220300	PF3D7_0220600	PF3D7_0301600
***In silico* analyses**	-71 kDa -no predicted TM domain -predicted coiled coils, disordered regions	-25.3 kDa -predicted α-folds -2 predicted TM domains	-25.9 kDa -predicted α-folds -1 predicted TM domain	-87.5 kDa -predicted coiled coils, disordered regions, a stretch of polar residues -no predicted TM domain -9 predicted PEST motifs
Growth assay	-No growth defect due to downregulation of POI -Cytotoxic effect of glucosamine			
Merozoites/ schizont	-number of merozoites per schizont is not affected by downregulation of POI or glucosamine			
Development (Giemsa)	-downregulation of POI does not affect parasite development and morphology			
Localization (IFA, WB)	-no specific signal in IFA/WB after hypotonic lysis →low expression	-membrane-bound -partly co-localization with SBP1 (MC)	-membrane-bound -localized at RBCM	-soluble protein -partly co-localization with SBP1 (MC)
Static CSA binding assay	-not significant	-significantly less binding after KD (***p=0.000561)	-significantly less binding after KD (** p=0.008241)	-significantly less binding after KD (**** p=0.000008)
PfEMP1 flow cytometry		-significantly less PfEMP1 signal after KD (****p<0.000001)		-no stat. significant difference
SEM/TEM	-downregulation likely does not affect distribution and shape of knobs and Maurer's clefts -needs to be repeated			

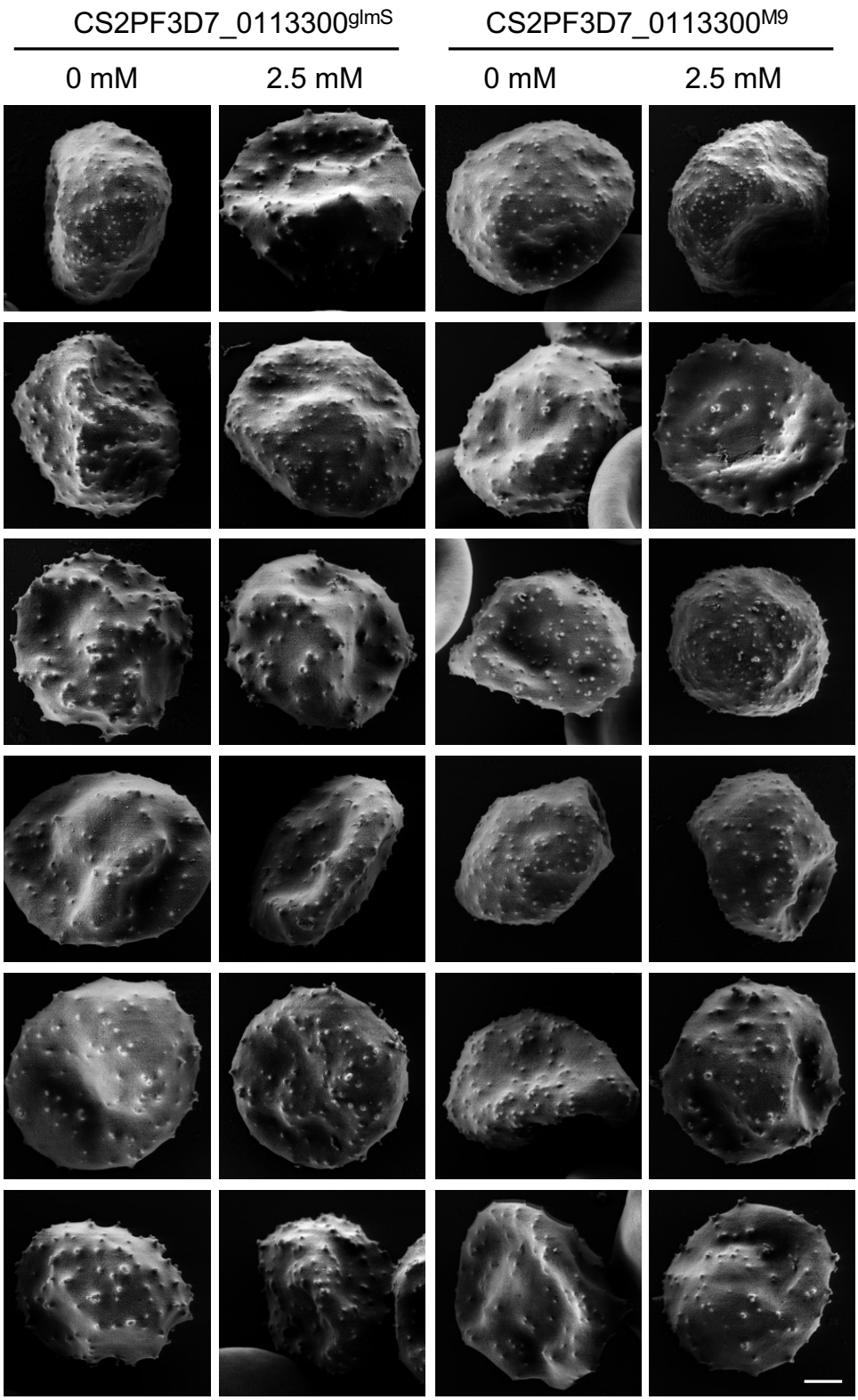

Fig. 28: Scanning electron microscopy (SEM) images of CS2PF3D7_0113300$^{glmS/M9}$. Parasite-infected erythrocytes cultivated ± 2.5 mM GlcN for 72 h. Scale bar 1 µm.

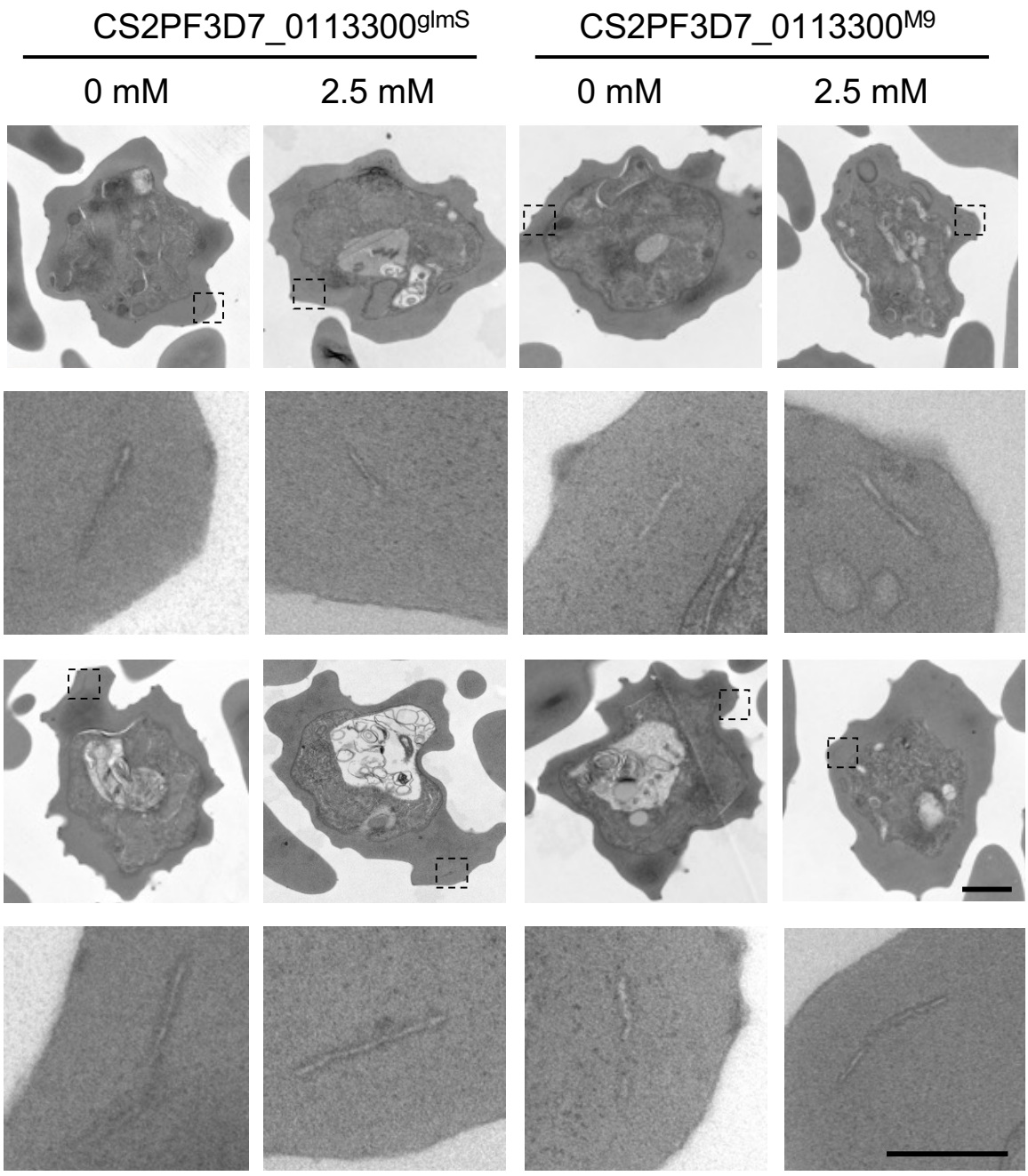
CS2PF3D7_0113300glmS
CS2PF3D7_0113300M9
0 mM
2.5 mM
0 mM
2.5 mM

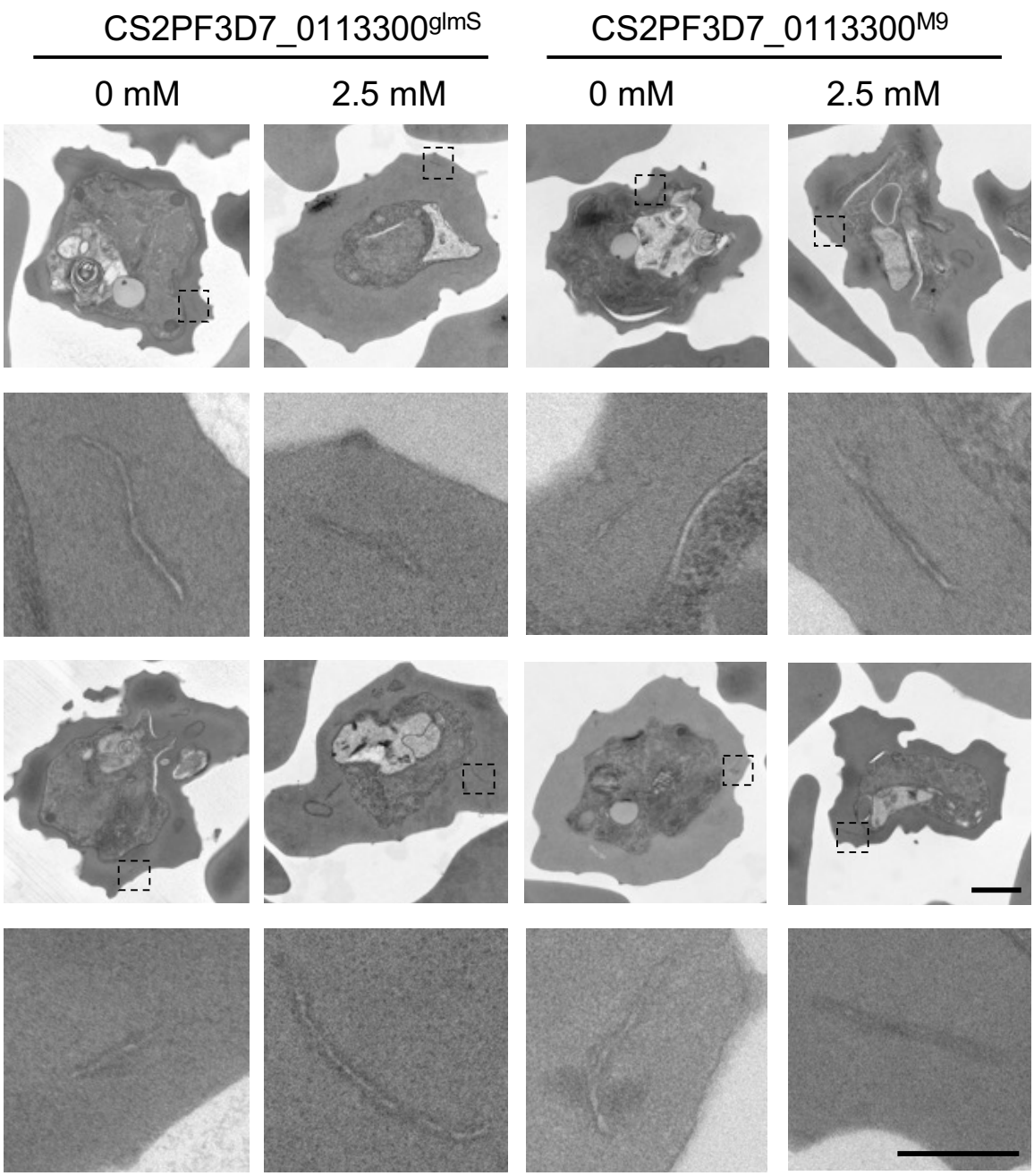

Fig. 29: Transmission electron microscopy (TEM) images of CS2PF3D7_0113300$^{glmS/M9}$. Parasite-infected erythrocytes cultivated ± 2.5 mM GlcN for 72 h. Detailed images of Maurer's clefts. Scale bar 1 µm (full size image), 0.2 µm (detail image).

3. Discussion

Quickly after invasion of erythrocytes, the malaria parasite *P. falciparum* starts to export hundreds of proteins in order to establish a new protein transport pathway and remodel its host cell for survival (Maier et al., 2009, Matthews et al., 2018). However, a lack of genetic systems to study essential genes that are involved in host cell modification has hampered extensive progress in this field over the last decades (Kudyba et al., 2021). Luckily among others, the *glmS* ribozyme system has been developed, which is an inducible knockdown system on mRNA level that can be activated via glucosamine-6-phosphate (Prommana et al., 2013). In this study, *glmS* and inactivated M9 control cell lines were generated to phenotypically characterize the four predicted essential, exported proteins PF3D7_01133300, PF3D7_0220300, PF3D7_0220600 and PF3D7_0301600.

3.1 Essentiality of selected genes and generation of *glmS* cell lines

The 15 gene candidates code for predicted exported proteins that fulfill several previously defined criteria and were selected using bioinformatics (2.1). A high-throughput screening via *piggyBac* transposon insertional mutagenesis predicted 10 out of these 15 gene candidates to be essential for blood stage development *in vitro* (Zhang et al., 2018). Interestingly, the only gene that could be knocked out using selection-linked integration targeted gene disruption (SLI-TGD) codes for Pfj23 (PF3D7_1001900) which was refractory to inactivation by Maier et al., but it was predicted to be non-essential by Zhang et al. (Maier et al., 2008; Zhang et al., 2018; Ouayoue Noutong, 2021). These contrasting results show that the essentiality of genes cannot be determined by only one method as every system has its flaws, potential for technical errors and its success could be gene-dependent.

In order to characterize those genes, that could not be knocked out via SLI-TGD, the SLI-*glmS* approach was used to generate inducible knockdown cell lines. First experiments in our lab added a GFP sequence at the 3' end of the GOIs in front of the *glmS* ribozyme sequence. As a result, only three genes could be modified like this including Pfj23 (data not published). I then took the rest of the gene candidates and tried to generate HA-tagged *glmS* knockdown cell lines using SLI and I successfully generated 6 wildtype-free *glmS*-HA cell lines (Table 2). One of them, PF3D7_1401200, was recently published in a paper and therefore not further investigated in this study (Jonsdottir et al., 2021). The smaller size of the HA-tag (3.5 kDa) in comparison to the GFP-tag (27 kDa) could be the reason why it was possible to generate those cell lines, as a big tag can interfere with protein folding and therefore rendering it unfunctional. However, the five genes PF3D7_0310400, PF3D7_0701900, PF3D7_1038600, PF3D7_1149200 and PF3D7_1401200

could not even be genetically manipulated by adding *glmS*-HA (Table 2). Three consecutive selections with G418 for 10 weeks each did not give rise to viable parasites and these genes are considered essential for blood stage development *in vitro*. The SLI system enables the selection of integrated clones with an additional selectable marker and therefore drastically decreases the time to generate modified cell lines, as it is normally integrated via passive homologous recombination events that are very time-consuming and quite inefficient in *P. falciparum* (Birnbaum et al., 2017). For the four studied genes, *glmS* and inactive M9 control cell lines were successfully generated using SLI and parasites selected with the highest G418 concentration (800 µg/ml) were used to verify integration. Previous selections showed that lower G418 concentrations can lead to a mixed culture with wildtype and modified loci, which would still have to be cloned out in a time-consuming process (data not shown).

3.2 Verification of transgenic cell lines

Integration PCRs of CS2PF3D7_0113300$^{glmS/M9}$ (2.3), CS2PF3D7_0220300$^{glmS/M9}$ (2.4), CS2PF3D7_0220600$^{glmS/M9}$ (2.5) and CS2PF3D7_0301600$^{glmS/M9}$ (2.6) showed successful integration, wildtype-free cultures as well as remaining episomal plasmids. This has also been observed by others in our working group using this method and could be explained by an uptake of multiple plasmids during transfection. However, as no transcription is possible from this plasmid, it should not have an effect on the parasite itself (O'Donnell et al., 2001). A fifth transgenic cell line (CS2PF3D7_0220700$^{glmS/M9}$) showed several double bands that could not be removed upon optimization of the PCR and was not further analyzed in this study (data not shown). In order to verify expression of the HA-tagged POIs, Western Blots were performed that showed successful expression of the studied proteins. Surprisingly, the detected band of PF3D7_0301600-HA corresponded to a molecular weight about 30 kDa higher than expected (2.6). This could be due to the intrinsic, disordered regions (IDR) that can affect the running behavior of the POI in an SDS gel. About 32.7% of the *P. falciparum* proteome is intrinsically disordered and the highly flexible IDR proteins are important in protein-ligand binding, binding to DNA/RNA and can act as flexible linkers. Apical and exported proteins show the highest rate of IDRs, further indicating its potential function in invasion and sequestration (Guy et al., 2015). Moreover, Western Blots detecting PF3D7_0113300-HA (2.3), PF3D7_0220600-HA (2.5) and PF3D7_0301600-HA (2.6) showed an additional band around 30 kDa higher than the HA-tagged POIs which likely represents a non-skipped version of the POIs . In theory, the Skip-peptide between the HA-tagged GOI and the gene coding for neomycin phosphotransferase should lead to an expression of two separate proteins. However, the skipping efficiency seems to be gene-

dependent. While CS2PF3D7_0220300$^{glmS/M9}$ (2.4) did not show any evidence of incomplete skipping, the other three cell lines showed significant differences in the amount of unskipped fusion protein. This could further impair the generation of integrated cell lines of genes with high skipping rates, as the resulting fusion protein is significantly larger. Interestingly, the paper introducing the SLI system did not report this problem (Birnbaum et al., 2017). However, other working groups did observe skipping which might be improved by discovering other skipping peptides in the future.

3.3 Localization of candidate proteins

The localization and distribution of the studied proteins was investigated via Western Blot of hypotonically lysed cell fractions and IFAs. PF3D7_0220300 and PF3D7_0220600 are proteins consisting of two and one predicted transmembrane domain, respectively. Western Blots show that the majority of these HA-tagged POIs is located in the pellet fraction, corresponding to a membrane-bound form (2.4, 2.5). Interestingly, a small amount can also be detected in the soluble supernatant fraction which could be the protein that has not yet reached its final destination and is transported in a soluble state. Therefore, the solubility state of some proteins can differ according to the stage of development (Matthews et al., 2018). PF3D7_0301600 does not have a predicted transmembrane domain and can only be detected in the supernatant fraction after hypotonic lysis of trophozoite-infected erythrocytes. Apart from running at a higher molecular weight than expected, the soluble protein seems to be proteolytically cleaved after lysis, as several specific bands can be detected in the Western Blot (2.6). A possible reason could be that the protein consists of many PEST motifs which are regions enriched with specific amino acids that are known to be potential proteolytic cleavage sites. In *P. falciparum,* these PEST motifs are mainly found in highly regulated proteins involved in metabolism and in surface exposed proteins like PfEMPs, MSPs, SERAs and RIFINs (Mitchell & Bell, 2003). A Western Blot of CS2PF3D7_0113300$^{glmS/M9}$ after hypotonic lysis and IFAs were not possible due to the low protein expression of the predicted soluble protein.

IFAs of CS2PF3D7_0220300^{glmS} and CS2PF3D7_0301600^{glmS} showed a punctuated distribution of the HA-tagged POIs in the host cell cytosol which indicates a localization at the MCs, where most exported proteins either go through on their way to the erythrocyte membrane or it is their final destination (Deponte et al., 2012; de Koning-Ward et al., 2016). A co-immunolabelling with the MC-resident protein SBP1 showed partly co-localization, further indicating a MC protein (2.4; 2.6). As PF3D7_0220300 consists of two predicted transmembrane domains and was proven to be a membrane-bound protein, it is likely integrated into the MC

membrane. Studies have shown that the C>T variant of this gene locus is associated with sickle hemoglobin (HbS) and confers a protective effect against severe malaria depending on the genotype (Band et al., 2022). Moreover, a previous knockdown study using the DHFR destabilization domain (DDD) and the stabilizing ligand trimethoprim showed that it plays a role in glucose uptake and interacts with host stomatin in double-membrane vesicles in the erythrocyte cytosol (Butler, 2014). Therefore, the protein distribution observed in IFAs in this study could also correspond to these double-membrane vesicles and play a role in protein transport, which should be further investigated. Interestingly, PF3D7_0301600 is a soluble protein without any transmembrane domains or GPI-anchor and still shows a MC-like distribution. Due to its stretch of polar residues, it could be able to bind to the outside of MCs. KAHRP and EMP3 are also known to transiently bind to the negatively charged outer membrane of MCs via their positively charged histidine-rich and lysine-rich regions (pKi 9.7) at the N-terminal end, respectively (Wickham et al., 2001; Knuepfer et al., 2005b). The exported proteins PF3D7_0113300 and PF3D7_0301600 consist of coiled-coil motifs that often confer specialized functions as structural proteins, motor proteins, transcription factors or in protein transport (Hawthorne et al., 2004). The second membrane-bound protein PF3D7_0220600 is localized at the erythrocyte membrane, where it is likely integrated with its predicted transmembrane domain (2.5). A protease protection assay could show whether the N- or C-terminus is exposed to the outside of the infected erythrocyte. A subsequent Western Blot would show a shortened HA-tagged POI in case the N-terminus was exposed and has been degraded by the protease and the HA-signal would disappear if the C-terminus would have been degraded by the protease. Moreover, sequential membrane extraction using urea could verify that the protein is integrated into the membrane as urea is able to extract peripheral membrane proteins.

3.4 Downregulation of target proteins via glucosamine

To investigate the knockdown efficiency of the *glmS* ribozyme upon treatment with GlcN, synchronized *glmS* and M9 parasite cultures were cultivated with 0, 1.25, 2.5 and 5. mM GlcN for 72 h. A Western Blot of purified trophozoite-infected erythrocytes was performed to detect the HA-tagged POIs and Aldolase, which was used as a loading control to normalize the respective HA-bands. All *glmS* cell lines showed efficient downregulation with 2.5 mM GlcN to 36% (PF3D7_0220300; 2.4), 19% (PF3D7_0220600; 2.5) and 39% (PF3D7_0301600; 2.6) and 5 mM GlcN reduced the protein abundance to 18%, 11% and 24%, respectively. A quantification of the band intensities of PF3D7_0113300 was not possible due to a high background signal that is likely caused by a low expression of the POI (2.3). In comparison to the other POIs,

PF3D7_0113300 is mainly expressed in the ring stages, which could explain the low protein abundance in trophozoite-infected erythrocytes (López-Barragán et al., 2011). However, the band intensities corresponding to the HA-tagged POI appeared weaker the more GlcN was being used verifying a working *glmS* ribozyme. Interestingly, the control cell line CS2PF3D7_0220600^{M9} showed higher protein abundance when cultivated with GlcN. This phenomenon has also been observed in a study with Pfj23 and could be a positive effect of GlcN itself as it is known that GlcN affects the gene expression of *P. falciparum* (Prommana et al., 2013; Diehl, 2019). However, this particular effect seems to be highly gene-dependent, as it was not observed in the other three studied proteins. Moreover it should be noted that any genetic modification such as performed here can affect the gene expression. Not only was a HA sequence inserted into the 3' UTR of the GOIs but also a second selection cassette (neomycin phosphotransferase; 795 bp) and the *glmS* ribozyme (166 bp) that was inserted after the *P. berghei* dihydrofolate reductase-thymidylate synthase 3'-transcription terminator sequence which could all be the reason why some genes were refractory to this genetic modification (Prommana et al., 2013).

3.5 Effect of downregulation on growth and selected parasite marker proteins

A SybrGreen-based assay was performed to investigate the parasites growth over 72 h (1.5 cycles) while Giemsa-stained blood smears over the period of the growth assay showed the morphology and development of the parasites after downregulation with 2.5 mM GlcN. As SybrGreen binds to double-stranded DNA, the measured emission signal correlates to the parasitemia. Interestingly, the end parasitemia significantly decreased in all cell lines, *glmS* and M9, the more GlcN was used. Giemsa-stained blood smears showed a slightly delayed development of parasites cultivated with 5 mM GlcN (2.3-2.6). These results demonstrate the cytotoxic effect of GlcN itself and not the effect of a downregulated POI. However, it could mask slight growth defects due to a downregulation. As 2.5 mM GlcN led to a significant downregulation of the POIs without strong cytotoxic effects, this concentration was used in all further experiments. A recent study showed that significant growth defects after downregulation of PF3D7_1401200 could only be seen after two cycles, which could also be the case for the proteins studied here (Jonsdottir et al., 2021). This exported protein was also part of the list of selected genes in this study, but it was set aside after the paper was published. Interestingly, a downregulation of PF3D7_0220300 using DDD also showed a significant growth defect after four days, which further indicates that longer assays could be able to reveal a growth phenotype in blood stage development *in vitro*. However, these results could also be due to the used knockdown method that works on protein level by removing a ligand that stabilizes the protein. The study showed that

the protein could still be detected after knockdown, but it was not exported anymore (Butler, 2014). Unlike that study, the residual protein after downregulation using the *glmS* system is still exported and doesn't lose its function. It should also be noted that PF3D7_0220600 has four predicted paralogous genes. One of them is PF3D7_0220700 which lies directly next to PF3D7_0220600 and could possibly have a similar function that could compensate for the downregulated gene. It would be interesting to investigate the phenotype of a double-knockdown cell line of these paralogous genes.

Due to the reduced end parasitemia observed in SybrGreen growth assays, the merozoites of 20 mature schizonts were counted in images of Giemsa-stained blood smears. A downregulation of the POIs using 2.5 mM GlcN did not show a significant difference in the number of merozoites per schizont, with an average of ~15-20 merozoites per schizont. This indicates that the reduced end parasitemia is not due to a reduced number of merozoites but likely due to more inefficient invasion or developmental problems in the early stages after invasion.

A downregulation of the exported POIs can also affect the localization of other exported proteins by interfering with their export, which is why I investigated the distribution of the selected marker proteins EMP3, SBP1, KAHRP and REX1 via IFA (Maier et al., 2008). No visible difference could be observed upon downregulation of the POIs, indicating that they are not crucial for the export and correct localization of the marker proteins. However, as there is still some residual protein left after downregulation via the *glmS* ribozyme, it is possible that the downregulation is not efficient enough to see a phenotype (3.7).

3.6 Investigation of cytoadhesion to chondroitin sulfate A

Before analyzing the cytoadhesion, the subtelomeric region of chromosome two was examined for deletions that can occur after prolonged cultivation *in vitro*. A potential breaking point is in the *kahrp* gene that also leads to a loss of *emp3* and *kahsp40* which are located at the telomeric side of *kahrp* and these deletions result in a knobless phenotype with highly reduced cytoadherence (Pologe & Ravetch, 1986, Culvenor et al., 1987, Pasloske et al., 1993). PCR verified an intact subtelomeric region in all cell lines. However, as this is a qualitative method, it is still possible that some parasites possess a deletion.

All cultures were selected at least three times on CSA prior to the experiments to select for parasites that express the PfEMP1 variant VAR2CSA (1.5). Moreover, frequent selection via gelatine flotation ensured that the infected erythrocytes show normal, evenly distributed knobs on the surface. Static binding assays showed a significant reduction of binding to CSA upon downregulation of PF3D7_0220300, PF3D7_0220600 and PF3D7_0301600 while

downregulation of PF3D7_0113300 only resulted in a slight reduction. Giemsa-stained blood smears demonstrated that the parasite cultures were in similar developmental stages when cultivated ±2.5 mM GlcN, as this could also affect the binding to CSA. A slight developmental delay could only be observed with 5 mM GlcN which is why I used 2.5 mM GlcN for downregulation in these experiments. In earlier stages, PfEMP1 might not be presented properly on the surface of the infected erythrocytes which would lead to highly reduced binding. However, it should be noted that these are not *in vivo* conditions and a binding assay under flow might give more information. Moreover, even though this static binding assay underwent a lot of optimization, there are still critical steps that can influence the outcome such as the timing and speed of pipetting and the fixation which is why additional experiments should be considered to verify those results.

In order to investigate whether the reduced binding to CSA upon downregulation of PF3D7_0220300 and PF3D7_0301600 is due to less presentation of PfEMP1 on the surface of infected erythrocytes, the MFI of PfEMP1 VAR2CSA was measured via flow cytometry. The significantly decreased signal in 3D7 compared to CS2 verified specific binding of the used antibody to PfEMP1 VAR2CSA which is significantly more expressed in *P. falciparum* CS2 (Maier et al., 2008). Only CS2PF3D7_0220300^{glmS} incubated with 2.5 mM GlcN showed significantly less PfEMP1 VAR2CSA signal which can explain the reduced binding to CSA (2.4). So far, I have only performed this experiment with cell lines, that have shown significantly reduced binding, but it should also be done with the other cell lines in the future.

Another recent knockout study of the exported protein GEXP07 has also shown a defective export of PfEMP1 which resulted in this cytoadhesion phenotype (McHugh et al., 2020). Interestingly, a downregulation of PF3D7_0301600 did not lead to reduced PfEMP1 VAR2CSA signal (2.6). In this case, the reduced binding to CSA could be due to deformed knobs that cannot present PfEMP1 properly which was also observed with PFA66 and Pfj23 by Diehl et al. and Ouayoue Noutong (Diehl et al., 2021; Ouayoue Noutong, 2021). This was investigated via scanning electron microscopy (SEM) and transmission electron microscopy (TEM) imaging. However, as all cell lines analyzed in this study showed normal, small, evenly distributed knobs as well as deformed and enlarged knobs, it was not possible to draw any conclusions from it (2.7; Supplements). As any technical issues can be ruled out in this reliably used method, it could be due to the used blood during this time (personal communication: Dr. Marek Cyrklaff, Heidelberg). To further investigate this hypothesis, it should definitely be repeated. TEM images also showed normal distribution and morphology of Maurer's clefts (MC) in all cell lines (2.7; Supplements). A knockout of exported proteins like Pfj23, REX1 or SBP1 have shown globular, stacked or

otherwise deformed MCs respectively, which is also associated with a disturbed protein export, especially of PfEMP1 (Ouayoue Noutong, 2021; McHugh et al., 2015; Cooke et al., 2006). All in all, three out of the four exported proteins have shown reduced binding to CSA in static assays with one presenting less PfEMP1 VAR2CSA on the surface of infected erythrocytes. The exact mechanism, how export and presentation of PfEMP1 is disturbed, needs to be further investigated for example via immunogold labelling in TEM or subcellular fractionation to find out the localization of PfEMP1 and where it could be stuck on the way to the surface.

3.7 Drawbacks of the *glmS* system

The *glmS* ribozyme system can be used to downregulate the expression of essential genes via GlcN in a concentration-dependent manner. However, the cytotoxicity of GlcN itself needs to be considered when optimizing and analyzing an experiment. A very necessary control is a cell line coding for the inactive version of the *glmS* ribozyme called M9, that will show the effect of GlcN without downregulating the POI. Another disadvantage is that the downregulation efficiency and skipping rate seems to be gene-dependent and residual protein could still be enough to fulfill its function. Several knockdown studies have demonstrated that no phenotype could be observed *in vitro* unless the protein abundance was drastically reduced or fully removed (Diehl, 2019). This goes to show that genetic deletions should be the preferred choice to investigate non-essential genes unless you want to observe the phenotype with different amounts of residual protein. However for essential genes, interesting results have also been found by others, showing that it is a good and fast way to selectively downregulate proteins.

Other systems for conditional protein knockout or knockdown studies that initially target DNA, RNA or protein levels are explained in more detail in chapter 1.6. However, it is important to note that even if no interesting phenotype can be observed upon deletion or downregulation of a POI *in vitro*, it can still be essential for survival *in vivo*. The inducible knockout method using DiCre can be activated by the addition of rapamycin and excises DNA sequences that are flanked by specific Cre-recombinase recognition sites called *loxP* sites. Coupled with CRISPR/Cas9, transgenic cell lines can be generated efficiently and faster than by using conventional integration methods (Knuepfer et al., 2017). I have already cloned several guide and rescue plasmids that can be used to generate conditional knockout DiCre cell lines of candidate exported proteins (plasmids were a kind gift of Dr. Ellen Knuepfer and Dr. Moritz Treeck, Crick Institute London). However, I was not able to generate a DiCre-expressing cell line in *P. falciparum* CS2, which is probably due to the new transfection method using AMAXA. With more experience and optimization, we hope to establish this promising method in our laboratory, generate transgenic

cell lines and interesting data that will broaden our knowledge of protein export and host cell modification in *P. falciparum*.

4 Material and Methods

4.1 Material

4.1.1 Organisms and cell lines

Strain /Cell line	Description	Source
E. coli Top10	Electrocompetent strain F-mcr ∆(mrr-hsdRMS-mcrBC) thi80lacZ∆M15 ∆lacX74 recA1 araD139 ∆(araleu)7697 galU galK rpsL (StrR) endA1 nup	Life Technologies, Carlsbad, USA
E.coli XL1Blue	chemically competent strain recA1 endA1 gyrA96 thi-1 hsdR17 supE44 relA1 lac [F proAB laclqZ∆M15 Tn10 (Tetr)]	Agilent Technologies, Waldbronn, Germany
P. falciparum 3D7	Parasite wildtype	Walliker et al., 1987
P. falciparum CS2	Parasite wildtype	Beeson et al., 2000
CS2*PF3D7_0220600*^{glmS}	pSLI-glmS-HA_PF3D7_0220600 integrated into *P. falciparum* CS2; for downregulation of *PF3D7_0220600*	Generated during this project
CS2*PF3D7_0220600*^{M9}	pSLI-glmS-HA_PF3D7_0220600 integrated into *P. falciparum* CS2; control cell line	Generated during this project
CS2*PF3D7_0220700*^{glmS}	pSLI-glmS-HA_PF3D7_0220700 integrated into *P. falciparum* CS2; for downregulation of *PF3D7_0220700*	Generated during this project
CS2*PF3D7_0220700*^{M9}	pSLI-glmS-HA_PF3D7_0220700 integrated into *P. falciparum* CS2; control cell line	Generated during this project
CS2*PF3D7_0113300*^{glmS}	pSLI-glmS-HA_PF3D7_0113300 integrated into *P. falciparum* CS2; for downregulation of *PF3D7_0113300*	Generated during this project
CS2*PF3D7_0113300*^{M9}	pSLI-glmS-HA_PF3D7_0113300 integrated into *P. falciparum* CS2; control cell line	Generated during this project

CS2*PF3D7_0220300*^{glmS}	pSLI-glmS-HA_PF3D7_0220300 integrated into *P. falciparum* CS2; for downregulation of *PF3D7_0220300*	Generated during this project
CS2*PF3D7_0220300*^{M9}	pSLI-glmS-HA_PF3D7_0220300 integrated into *P. falciparum* CS2; control cell line	Generated during this project
CS2*PF3D7_0301600*^{glmS}	pSLI-glmS-HA_PF3D7_0301600 integrated into *P. falciparum* CS2; for downregulation of *PF3D7_0301600*	Generated during this project
CS2*PF3D7_0301600*^{M9}	pSLI-glmS-HA_PF3D7_0301600 integrated into *P. falciparum* CS2, control cell line	Generated during this project

4.1.2 Gene IDs

No.	**Gene ID *P. falciparum 3D7***	**Gene ID *P. falciparum IT***	**Gene annotation**
1	PF3D7_0220600	PfIT_020025100	Plasmodium exported protein (hyp9), unknown function
2	PF3D7_0220700	PfIT_020025200	Plasmodium exported protein (hyp9), unknown function
3	PF3D7_1102600	PfIT_110007100	GEXP14 (gametocyte exported protein 14), Plasmodium exported protein, unknown function
4	PF3D7_1301200	PfIT_130006000	GBPH2 (glycophorin-binding protein homolog 2)
5	PF3D7_1038600	PfIT_100042300	Plasmodium exported protein, unknown function
6	PF3D7_0113300	PfIT_010016400	Plasmodium exported protein (hyp1), unknown function

7	PF3D7_0220300	PfIT_020024800	Plasmodium exported protein, unknown function
8	PF3D7_0701900	PfIT_070006800	Plasmodium exported protein, unknown function
9	PF3D7_1149200	PfIT_130076600	RESA3 (ring-infected erythrocyte surface protein)
10	PF3D7_0301600	PfIT_030006400	GEXP21 (gametocyte exported protein 21), Plasmodium exported protein (hyp1), unknown function

4.1.3 Plasmids

Plasmid	**Selection marker**		**Source**
	E. coli	***P. falciparum***	
pSLI-glmS-HA	AmpR	hDHFR, NeoR	Dr. Markus Ganter
pSLI-M9-HA	AmpR	hDHFR, NeoR	Dr. Markus Ganter
pSLI-glmS-HA_PF3D7_0220600	AmpR	hDHFR, NeoR	Generated during this project
pSLI-M9-HA_PF3D7_0220600	AmpR	hDHFR, NeoR	Generated during this project
pSLI-glmS-HA_PF3D7_0220700	AmpR	hDHFR, NeoR	Generated during this project
pSLI-M9-HA_PF3D7_0220700	AmpR	hDHFR, NeoR	Generated during this project
pSLI-glmS-HA_PF3D7_1301200	AmpR	hDHFR, NeoR	Generated during this project
pSLI-M9-HA_PF3D7_1301200	AmpR	hDHFR, NeoR	Generated during this project
pSLI-glmS-HA_PF3D7_1038600	AmpR	hDHFR, NeoR	Generated during this project
pSLI-M9-HA_PF3D7_1038600	AmpR	hDHFR, NeoR	Generated during this project
pSLI-glmS-HA_PF3D7_0113300	AmpR	hDHFR, NeoR	Generated during this project
pSLI-M9-HA_PF3D7_0113300	AmpR	hDHFR, NeoR	Generated during this project
pSLI-glmS-HA_PF3D7_0220300	AmpR	hDHFR, NeoR	Generated during this project
pSLI-M9-HA_PF3D7_0220300	AmpR	hDHFR, NeoR	Generated during this project
pSLI-glmS-HA_PF3D7_0701900	AmpR	hDHFR, NeoR	Generated during this project
pSLI-M9-HA_PF3D7_0701900	AmpR	hDHFR, NeoR	Generated during this project
pSLI-glmS-HA_PF3D7_1149200	AmpR	hDHFR, NeoR	Generated during this project

pSLI-M9-HA_PF3D7_1149200	AmpR	hDHFR, NeoR	Generated during this project
pSLI-glmS-HA_PF3D7_0301600	AmpR	hDHFR, NeoR	Generated during this project
pSLI-glmS-HA_PF3D7_0301600	AmpR	hDHFR, NeoR	Generated during this project

4.1.4 Oligonucleotides

Oligonucleotide	**Sequence (5'-3')**	**Use**
PF3D7_0220600_NotI_fw	CGGCGGCCGCGTATTTCATTCTTATAGTTACATTTACC	Cloning
PF3D7_0220600_MluI_rev	TCCGACGCGTAAAAAGCCATTTCTTAATTGTACTAAAATAATTTTTTGC	Cloning
PF3D7_0220700_NotI_fw	CGGCGGCCGCCGGATAAATCTATGTATAATGAGAATGTTC	Cloning
PF3D7_0220700_MluI_rev	TCCGACGCGTAAACAGTGCATTCCATACAGATATAAAATAATTTTTACC	Cloning
PF3D7_1102600_NotI_fw	CGGCGGCCGCGAGAAGTTTAGTAATTTACATGTTGG	Cloning
PF3D7_1102600_MluI_rev	TCCGACGCGTTTGGTATACCACATAAGATTCCTC	Cloning
PF3D7_1301200_NotI_fw	CGGCGGCCGCGTGGAGACAAATACCAACAAGATGC	Cloning
PF3D7_1301200_MluI_rev	TCCGACGCGTGGAACTTTCATCATTTGGATCTGTG	Cloning
PF3D7_1038600_NotI_fw	CGGCGGCCGCGGAAAGACGCCATGATATAC	Cloning
PF3D7_1038600_MluI_rev	TCCGACGCGTATGTGAGGGGAGAAATACTGC	Cloning
PF3D7_0113300_NotI_fw	CGGCGGCCGCGACACATATCATACGTGCTATGGACC	Cloning
PF3D7_0113300_MuI_rev	TCCGACGCGTAAAATGGCGCTCTAAAAAGTTGGTTACAGG	Cloning
PF3D7_0220300_NotI_fw	CGGCGGCCGCCACTATAAACCTTAAATTAACTAATAG	Cloning

PF3D7_0220300_MluI_rev	TCCGACGCGTTGCTTCGGGTTTGTATATTTTAACC	Cloning
PF3D7_0701900_NotI_fw	CGGCGGCCGCGACACCTATGTTTAAGGATTTTATGG	Cloning
PF3D7_0701900_MluI_rev	TCCGACGCGTTCTTAATGTTTGTGCTACATGTC	Cloning
PF3D7_1149200_NotI_fw	CGGCGGCCGCGGATGGACATTACAATATGTTTCTATGAG	Cloning
PF3D7_1149200_MluI_rev	TCCGACGCGTTTCATCATATTCTTCGTTGTGTTCC	Cloning
PF3D7_0301600_NotI_fw	CGGCGGCCGCCATGATGGATTTCCATCAGGATGG	Cloning
PF3D7_0301600_MluI_rev	TCCGACGCGTATATATATCATATATATTACTGCCTACACG	Cloning
HA_rev	GGTACATCGTATGGATAAGAACC	Integration PCR/ Colony PCR
pARL_fw	GGAATTGTGAGCGGATAACAATTTCACACAGG	Integration PCR
hDHFR_fw	CATGGTTCGCTAAACTGCATCG	PCR control
hDHFR_rev	GTACTTAATGCCTTTCTCCTCC	PCR control
EMP3_fw	AGTAAGGGATCCTAGAACTAAGG	PCR control (gDNA)
EMP3_rev	CCAAGTGCATTTTCTCTCATACC	PCR control (gDNA)
KAHsp40_fw	GGATCATCTCCGTTTAGTGG	PCR control
KAHsp40_rev	CCATTTCCTCCTAATGCTTC	PCR control
KAHRP_fw	GTAAATCACCAAGCACCACAGG	PCR control
KAHRP_rev	CTGAATAGCCTGCACCATGG	PCR control
5'fw_0220600	ATCTACATAAATTAGTTCTTGTTTGG	Integration PCR
3'rev_0220600	CAGAATATCTTATGATTATAATTCCTC	Integration PCR
5'fw_0220700	CATGAATTAATAAAGATATTGAAAATAAGG	Integration PCR
3'rev_0220700	GACCGTTTCCATATCCGATAC	Integration PCR
5'fw_0113300	GGACAATAAATATGAAGAAACG	Integration PCR

3'rev_0113300	GAGAAATGTATGTGATAATGTATAATATG	Integration PCR
5'fw_0220300	TCTACAAGGTGTGTATGTGG	Integration PCR
3'rev_0220300	CGGTATCAAATTTAGGTATGG	Integration PCR
5'fw_0301600	GCAAGATGAAGAGAAAGCATCC	Integration PCR
3'rev_0301600	GCACGTTCTAATGTTATAATAAC	Integration PCR

4.1.5 Chemicals

Chemical	**Supplier**
Acetate	Merck, Darmstadt, Germany
Acetone	Merck, Darmstadt, Germany
Agar-Agar	Roth, Karlsruhe, Germany
Agarose	Peqlab (VWR), Radnor, USA
AlbuMAX II	Gibco (Thermo Fisher Scientific), Waltham, USA
APS	Roth, Karlsruhe, Germany
Bromophenol blue	Sigma-Aldrich, Taufkirchen, Germany
BSA (Albumin Fraction V)	Roth, Karlsruhe, Germany
Cacodylate sodium salt	Roth, Karlsruhe, Germany
$CaCl_2$	Roth, Karlsruhe, Germany
Carbenicillin	Roth, Karlsruhe, Germany
CSA	Sigma-Aldrich, Taufkirchen, Germany
DAPI	Thermo Fisher Scientific
DMSO	Roth, Karlsruhe, Germany
DNA-Dye NonTox	Applichem, Darmstadt, Germany
DTT	Roth, Karlsruhe, Germany
EDTA	Roth, Karlsruhe, Germany
EGTA	Roth, Karlsruhe, Germany
Ethanol	Roth, Karlsruhe, Germany
Fluoromount-G	SouthernBiotech, Birmingham, USA
Geneticin (G418)	Gibco (Thermo Fisher Scientific), Waltham, USA
Gelafundin ISO 40 mg/ml	B Braun, Melsungen, Germany
Giemsa	Sigma-Aldrich, Taufkirchen, Germany
Glucose	Merck, Darmstadt, Germany

Glucosamine	Sigma-Aldrich, Taufkirchen, Germany
Glutaraldehyde	Roth, Karlsruhe, Germany
Glycerol	Roth, Karlsruhe, Germany
Glycine	Roth, Karlsruhe, Germany
H_2O_2 (25%)	Merck, Darmstadt, Germany
HCl	Roth, Karlsruhe, Germany
HEPES	Roth, Karlsruhe, Germany
Hypoxanthine	Cc pro, Oberdorla, Germany
Immersion oil	Sigma-Aldrich, St. Louis, USA
K_2HPO_4	Roth, Karlsruhe, Germany
KCl	Roth, Karlsruhe, Germany
KH_2PO_4	Roth, Karlsruhe, Germany
KOH	Roth, Karlsruhe, Germany
Luminol	Applichem, Darmstadt, Germany
Methanol	Roth, Karlsruhe, Germany
$MgCl_2$	Roth, Karlsruhe, Germany
Milk powder	Roth, Karlsruhe, Germany
NaCl	Roth, Karlsruhe, Germany
Na_2HPO_4	Roth, Karlsruhe, Germany
NaOH	Roth, Karlsruhe, Germany
Neomycin	Sigma-Aldrich, Taufkirchen, Germany
Osmium tetroxide	Sigma-Aldrich, Taufkirchen, Germany
PBS (pH 7.2)	Gibco (Thermo Fisher Scientific), Waltham, USA
Paraformaldehyde	Roth, Karlsruhe, Germany
P-coumaric acid	Sigma-Aldrich, Taufkirchen, Germany
Peptone/Tryptone	Roth, Karlsruhe, Germany
PIC	Calbiochem (Merck), Darmstadt, Germany
PMSF	Merck, Darmstadt, Germany
Poly-L-lysine solution (0.01%)	Sigma-Aldrich, Taufkirchen, Germany
Ponceau S	Roth, Karlsruhe, Germany
RPMI 1640 (+HEPES,+L-Glutamine)	Gibco (Thermo Fisher Scientific), Waltham, USA
RPMI powder	Sigma-Aldrich, Taufkirchen, Germany
Rotiphorese Gel30 (37;5:1)	Roth, Karlsruhe, Germany

Saponin	Roth, Karlsruhe, Germany
SDS	Roth, Karlsruhe, Germany
SOB Broth	Roth, Karlsruhe, Germany
Sorbitol	Roth, Karlsruhe, Germany
SybrGreenI	Life technologies
TCA	Sigma-Aldrich, Taufkirchen, Germany
TEMED	Roth, Karlsruhe, Germany
Tris	Roth, Karlsruhe, Germany
Triton-X-100	Sigma-Aldrich, Taufkirchen, Germany
WR99210	Jacobus Pharmaceutical, Princeton, USA
Yeast extract	Oxioid (Thermo Fisher Scientific), Waltham, USA

4.1.6 Buffer and solutions

Buffer/Solution	**Composition**
Albumax solution	500 ml RPMI1640 (+HEPES+L-glutamine) 5% (w/v) AlbuMAXII
Blocking solution IFA	3% (w/v) BSA in PBS (pH 7.4)
Carbenicillin solution	50 mg/ml Carbenicillin in 50% ethanol
Cytomix solution	120 mM KCl 0.15 mM $CaCl_2$ 1 ml Stock solution I pH 7.6 (fc: 10 mM) 10 ml Stock solution II pH 7.6 (fc: 25 mM HEPES, 2 mM EGTA) 5 mM $MgCl_2$ Ad 100 ml ddH_2O
Cytomix Stock solution I (1 M Phosphate buffer)	86.6 mM K_2HPO_4 13.4 mM KH_2PO_4 pH 7.6 in ddH_2O
Cytomix Stock solution II (HEPES, EGTA)	250 mM $C_8H_{12}N_2O_4S$ (HEPES) 20 mM $C_{14}H_{24}N_2O_{10}$ (EGTA) pH 7.6 (with KOH) in ddH_2O

ECL solution	160 ml ddH_2O 32 ml 1 M Tris/HCl (pH 8.5) 3.2 ml 250 mM Luminol (in DMSO) 1.424 ml 90 mM P-coumaric acid (in DMSO)
Fixation solution IFA	4% (w/v) PFA 0.0075% GA in PBS (pH 7.4)
Freezing solution	28% (v/v) Glycerol 3% (w/v) D-sorbitol 0.65% (w/v) NaCl in ddH_2O
10x PBS (pH 7.4)	80 g NaCl (fc: ~1.37 M) 2 g KCl (fc: ~27 mM) 14.4 g Na_2HPO_4 (fc: ~88 mM) 2.4 g KH_2PO_4 (fc: ~18 mM) Ad 1 l ddH_2O
Permeabilisation solution IFA	0.1% Triton-X-100 (v/v) 125 mM Glycine in PBS (pH 7.4)
100 mM PMSF	0.174 g PMSF Ad 10 ml Isoprapanol
Ponceau S solution	0.2% Ponceau S 0.3% TCA in ddH_2O
2x SDS loading buffer (pH 6.8)	100 mM Tris 0.2% (w/v) Bomophenol blue 20% (v/v) Gylcerol 4% SDS 200 mM DTT in ddH_2O
Separation gel buffer	1.5 M Tris pH 8.8 in ddH_2O
5% Sorbitol solution	5% (w/v) D-sorbitol

	in ddH_2O
Stacking gel buffer	0.5 M Tris pH 6.8 in ddH_2O
SybrGreen buffer	0.16 g Saponin 5 ml 1 M Tris-HCl 1 ml 0.5 M EDTA 1.5 ml Triton-X-100 Ad 100 ml ddH_2O pH 7.4
50x TAE buffer	2 M Tris 50 mM EDTA (pH 8) in ddH_2O
10x Taq-buffer	200 mM Tris-HCl 100 mM KCl 100 mM $(NH_4)_2SO_4$ 20 mM $MgSO_4$ 1% (w/v) Triton-X-100 in ddH_2O
Taq reaction mix	600 µl Taq-buffer (10x) 120 µl dNTP Mix (10 mM each) Ad 6 ml ddH_2O
TE buffer	10 mM Tris (pH 8) 1 mM EDTA (pH 8) in ddH_2O
Thawing solution	I: 12% (w/v) NaCl II: 1.6% (w/v) NaCl III: 0.9% (w/v) NaCl + 0.2% (w/v) glucose in ddH_2O
10x Transfer buffer	250 mM Tris 1.92 M Glycine pH 8.3 in ddH_2O

4.1.7 Media

Media	**Composition**
Cell culture medium	500 ml RPMI1640 (+HEPES+L-glutamine) Supernatant of 50 ml human plasma (A^+) 10 ml 10 mM Hypoxanthin (fc: 0.2 mM) 5 ml 10 mg/ml Neomycin (fc: 0.1 mg/ml)
Transfection medium	500 ml RPMI1640 (+HEPES+L-glutamine) 25 ml supernatant of human plasma (A^+) 25 ml Albumax solution 10 ml 10 mM Hypoxanthin (fc: 0.2 mM) 5 ml 10 mg/ml Neomycin (fc: 0.1 mg/ml)
Cytoadhesion medium	8 g RPMI powder Ad 500 ml ddH_2O pH 7.2
LB_{Carb} medium	1% (w/v) Pepton/Trypton 0.5% (w/v) Yeast extract 170 mM NaCl Ad 1 l ddH_2O +50 µg/ml Carbenicillin
LB_{Carb} agar	1% (w/v) Pepton/Trypton 0.5% (w/v) Yeast extract 170 mM NaCl 15 g Agar Ad 1 l ddH_2O +100 µg/ml Carbenicillin
SOC medium	20 mM glucose in SOB medium
SOB medium	10.66 g SOB 400 ml ddH_2O

4.1.8. Antibodies

Antibody	**Origin**	**Dilution IFA**	**Dilution WB**	**Supplier**
α-HA (12CA5)	mouse	1:200	1:1000	Roche, Basel, Switzerland
α-Aldolase	rabbit	—	1:5000	Prof. Jude Przyborski

α-Exp1	rabbit	—	1:500	Prof. Jude Przyborski
α-SBP1	rabbit	1:500	—	Prof. Jude Przyborski
α-Rex1	rabbit	1:1000	—	Prof. Jude Przyborski
α-KAHRP	mouse	1:1000	—	Prof. Jude Przyborski
α-EMP3	rabbit	1:500	—	Prof. Jude Przyborski
A-EMP1 (P11)	rabbit	1:100 for flow cytometry		Benoit Gamain, Paris, France
α-mouse-HRP	goat	—	1:2000	Dako, Glostrup, Danmark
α-rabbit-HRP	goat	—	1:2000	Dako, Glostrup, Danmark
α-mouse-Cy3	goat	1:1000	—	Jackson ImmunoResearch, West Grove, USA
α-rabbit-Cy3	goat	1:1000 (1:2000 for flow cytometry)	—	Jackson ImmunoResearch, West Grove, USA
α-rabbit-Cy2	goat	1:1000	—	Jackson ImmunoResearch, West Grove, USA

4.1.9 Enzymes

Enzyme	**Supplier**
Taq-Polymerase	Self-made
KOD Hot Start Polymerase	Merck, Darmstadt, Germany
Antarctic Phosphatase	NEB, Ipswich, USA
T4 DNA Ligase	Thermo Fisher Scientific, Waltham, USA
Restriction enzymes (HindIII, NdeI, AluI, NotI, MluI)	NEB, Ipswich, USA

4.1.10 Marker

In an SDS gel for Western Blots, 4 µl of PageRuler^{TM} Prestained Protein Ladder were used as a molecular weight marker for proteins with 10-180 kDa. 5 µl of 1 kb Plus DNA Ladder were used on an agarose gel as a marker for DNA fragments (Figure 30).

A **B**

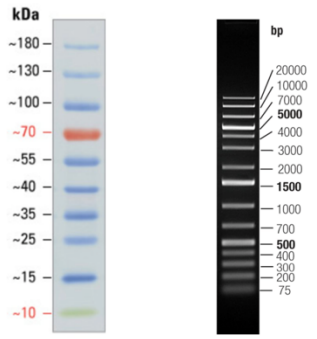

Fig. 30: DNA marker and protein molecular weight marker. A) *PageRuler™ Prestained Protein Ladder* (Thermo Fisher Scientific, Waltham, USA). **B)** *1 kb Plus DNA Ladder* (Thermo Fisher Scientifc, Waltham, USA).

4.1.11 Kits

Kit	**Supplier**
QIAquick® PCR Purification Kit	Qiagen, Venlo, Netherlands
QIAquick® Gel Extraction Kit	Qiagen, Venlo, Netherlands
QIAprep® Spin Miniprep Kit	Qiagen, Venlo, Netherlands
QIAGEN® Plasmid Maxi Kit	Qiagen, Venlo, Netherlands
QIAamp® DNA Blood Mini Kit	Qiagen Venlo, Netherlands

4.1.12 Equipment

Equipment	**Model**
Agarose gel electrophoresis: Power supply Agarose gel electrophoresis chambers Gel imaging system	 Amersham EPS 301 Owl separation systems B1A and B2 FastGene FAS-DIGI Compact with camera Pentax MX-1
Biospectrometer Cuvette	Eppendorf BioSpectrometer basic Eppendorf µCuvette G1.0
Centrifuges	Sorvall LYNX 4000 centrifuge Hettich Centrifuge Mikro 220R Megafuge 1.0R centrifuge Eppendorf centrifuge 5415R
Flow cytometer	Cytoflex S, Beckman coulter
Heat bath	PolyScience heat bath

Heat block, mixer	IKA Dry Block Heater 2 Neolab neoBlock II Eppendorf Thermomixer comfort
Ice machine	Icematic F80C
Incubator shaker *(E. coli)*	Innova 44 Incubator shaker series Max Q 6000 (Thermo Fisher Scientifc)
Incubator *(P. falciparum)*	Labotect C200
Magnetic cell sorter stand	Miltenyi Biotec Magnetic cell sorter
Microscopes: Light microscope Inverse microscope Fluorescence microscope Scanning electron microscope Transmission electron microscope	 Zeiss Axio Lab.A1 microscope Kern Inverted microscope OCM 161 with microscope camera ODC 832 Zeiss Axio Observer Z1 fluorescence microscope Zeiss Leo15030 scanning electron microscope Jeol JEM-1400 electron microscope
Orbital shaker Roller Vortexer	Heidolph unimax 2010 orbital shaker CAT RM5 roller Phoenix RS-VA10
PCR machines	FastGene FG-TC01 Eppendorf Mastercycler® nexus gradient
pH meter	Knick pH-Meter 766 Calimatic
Pipettes: Single channel pipettes Multipipette Electric Pipette 12-channel pipette	 Eppendorf Research, Gilson Pipetman Eppendorf M4 Brand AccuJet pro Eppendorf Research plus
Plate reader	Clariostar plate reader
Scales	Kern ABT 120-5DM Kern 474 Kern 440-47N

	Mettler AJ100
Sterile work bench	HERAsafe HS
Transfection: Electroporation system	 BioRad Capacitance Extender II BioRad Pulse Controller Plus BioRad Gene Pulser II
Ultra pure water system	membraPure Astacus
Vacuum pump	MAGV
Western Blot: SDS Gel system Power supply Transfer machine Developing machine	 BioRad Mini-PROTEAN Tetra cell system BioRad Power Pac 300 BioRad TransBlot Turbo Intas ECL Chemostar

4.1.13 Consumables

Consumables	**Supplier**
Steritop 0.22 µm	Merck, Darmstadt, Germany
15 ml and 50 ml tube	Greiner, Kremsmünster, Austria
2 ml, 5 ml, 10 ml, 25 ml pipette	Sarstedt, Nümbrecht, Germany Greiner, Kremsmünster, Austria
20 µl, 200 µl, 1000 µl filter tips	Nerbe plus, Winsen, Germany
TC Petri dish for cell culture	Sarstedt, Nümbrecht, Germany
Petri dish (100x 15 mm) for binding assay	Falcon (Corning, Corning, USA)
Cellstar cell culture flask T74	Greiner, Kremsmünster, Austria
TC 6-well und 12-well plate	Sarstedt, Nümbrecht, Germany
96-well plate (black; T bottom)	Greiner, Kremsmünster, Austria
1.5 ml, 2 ml SafeSeal tubes	Sarstedt, Nümbrecht, Germany
Cryo.S tubes	Greiner, Kremsmünster, Austria
PCR tube strips	Nippon Genetics, Düren, Germany
Gene Pulser Cuvette (0.2 cm)	BioRad, Hercules, USA
Three-way stopcock	B Braun, Melsungen, Germany
20 ml syringe	BD, Franclin Lakes, USA
Blunt cannula (0.8 x 22 mm)	B Braun, Melsungen, Germany

CS column	Miltenyi Biotec, Bergisch Gladbach, Germany
Nitrocellulose membrane 0.22 µm	Neolab, Heidelberg, Germany
Microscope slides ISO 8037/1	Epredia (Thermo Fisher Scientific, Waltham, USA)

4.1.14 Software and online tools

Software/Online tool	**Supplier**
GraphPad Prism 8.3.1	GraphPad Software Inc., La Jolla, USA
Ilastik 1.4	Ilastik team; Berg et al., 2019
ImageJ 2.3.0	Wayne Rasband, National Institute of Health, USA
PlasmoDB	www.plasmodb.org; Aurrecoechea et al., 2009
SnapGene Premium	GSL Biotech, Chicago, USA
UniProt	www.uniprot.org (The UniProt Consortium, 2017)
Intas software	Intas, Göttingen, Germany
ZEN 3.1	Zeiss, Wetzlar, Germany
MicrsocopeVIS	Kern & Sohn, Balingen, Germany
Clariostar software	BMG Labtech, Ortenberg, Germany

4.2 Molecular methods

4.2.1 Isolation of genomic DNA from *P. falciparum*

Genomic DNA served as a template for PCRs to amplify the respective inserts for cloning the *glmS* constructs and to verify the correct integration of transfectants. It was isolated from 200 µl blood of a well-grown parasite culture by following the protocol of the QIAamp DNA Blood Kit (Qiagen, Venlo, Netherlands) and eluting it in 100 µl of ddH_20.

4.2.2 Polymerase chain reaction (PCR)

The polymerase chain reaction (PCR) is a method for targeted amplification of DNA fragments by using a thermostable DNA polymerase and specific oligonucleotides (primer). A PCR program consists of three steps with different temperatures that are repeated up to 35 cycles. In the first step, the double-stranded DNA is denatured to single strands at 92-98 °C. Then, the temperature is reduced to 50-60 °C to allow the annealing of specific oligonucleotides to complementary sequences of the single-stranded DNA. The annealing temperature depends on the melting

temperature of the used oligonucleotides. In the following elongation step, the DNA polymerase elongates the DNA strand between the oligonucleotides by using the complementary template DNA. The optimal temperature for DNA polymerases is 72 °C, but as DNA from *P. falciparum* is very AT-rich with many repetitive sequences, the temperature was reduced to 68 °C to slow down the DNA polymerase and therefore optimize the elongation.

The self-made Taq-polymerase was used for colony PCRs to screen for positively transformed and ligated *E. coli* colonies and to verify the correct integration of transfected parasite lines. The proofreading KOD hot start DNA polymerase (Merck, Darmstadt, Germany) was used to amplify the inserts for cloning all *glmS* and M9 constructs and in case the PCR using Taq-polymerase did not give specific bands.

KOD reaction:

34 µl ddH2O
5 µl 10x KOD buffer
5 µl 2 mM dNTPs
3 µl 25 mM MgSO4
1 µl template DNA
25 pmol forward/reverse primer
1 µl KOD polymerase

KOD PCR program:

1) Initial denaturation: 95 °C, 10 min
2) Denaturation step: 95 °C, 1 min
3) Annealing step: 50-60 °C, 1 min
4) Elongation step: 68 °C, 30 s/kb + 10 sec
- repeat steps 2-4 for 35 cycles
5) Final elongation: 68 °C, 10 min
6) Hold at 4 °C

Taq reaction:

25 µl Taq reaction mix
25 pmol forward/reverse primer
0.5 µl Taq polymerase

Taq PCR program:

1) Initial denaturation: 95 °C, 10 min
2) Denaturation step: 95 °C, 1 min
3) Annealing step: 50-60 °C, 1 min
4) Elongation step: 68 °C, 1 min/kb +10 sec
- repeat steps 2-4 for 35 cycles
5) Final elongation: 68 °C, 1 min
6) Hold at 4 °C

4.2.3 Agarose gel electrophoresis

Agarose gel electrophoresis is a method to separate linear DNA fragments according to their size. Due to the negatively charged phosphate backbone of DNA, it can be separated in an electromagnetic field. As smaller DNA fragments run faster through the agarose mesh than bigger fragments, different concentrations of agarose can improve the separation in the gel. Depending

on the expected fragment sizes, a 0.8 or 1% agarose gel was poured. All samples were mixed with 6x DNA dye non-tox (AppliChem GmbH, Darmstadt, Germany) that binds to double-stranded DNA and can be visualized in a LED chamber at 470 nm (blue light). In comparison to the toxic ethidium bromide, DNA dye non-tox is a non-hazardous alternative, does not intercalate, and does not need UV light for visualization which can cause mutations (AppliChem GmbH, Darmstadt, Germany). To later assess the fragment size, the 1kb plus marker (Thermo Fisher Scientific, Waltham, USA) was loaded onto the gel. The samples were separated at 100-120 V for 30-40 min in TAE buffer and visualized at 470 nm.

4.2.4 Purification of DNA

During the cloning process, the intermediate products were purified to remove any substances that could disturb the following reactions. The QIAquick PCR Purification Kit (Qiagen, Venlo, Netherlands) was used to purify PCR products and restriction digests and it was eluted in 30 µl ddH_2O. To purify restricted vector DNA from an agarose gel, the QIAquick Gel Extraction Kit (Qiagen, Venlo, Netherlands) was used according to instructions and eluted in 30 µl ddH_2O.

4.2.5 Photometric measurements of DNA

The Eppendorf BioSpectrometer was used to determine the concentration of DNA by measuring the extinction at 260 nm as it is the absorption maximum of nucleic acids. This was important to set up correct ligation reactions (4.2.7), prepare the samples for sequencing (4.2.10), and prepare the plasmids for transfection (4.4.8). The ratio of absorption at 260 nm and 280 nm gives an impression of the purity and potential contamination with proteins.

4.2.6 Restriction digest of vectors and DNA fragments

Before ligating the PCR products into the pSLI-glmS-HA and pSLI-M9-HA vectors, they were digested with the respective restriction enzymes from New England Biolabs (NEB, Ipswich, USA) according to instructions. This was already considered while designing the primers for cloning. The used restriction enzymes NotI and MluI create sticky ends whereby complementary overhangs are formed that enable a ligation. PCR products were incubated for 2 h, vectors for 6 h, and test digestions were incubated for 1 h at 37 °C.

Insert restriction digest/ test digest:	Vector digest:
2 µl 10x CutSmart buffer	5 µl 10x CutSmart buffer
2.5 U per restriction enzyme	5 U per restriction enzyme
~1 µg insert / ~300 µg vector for test digestion	~2-5 µg vector
Ad 20 µl ddH_2O	Ad 50 µl ddH_2O

To prevent a re-ligation of the vector, it was dephosphorylated using the Antarctic Phosphatase (NEB, Ipswich, USA) by incubating it for 1 h before continuing with the purification (4.2.4) and ligation (4.2.7) process.

4.2.7 Ligation of DNA fragments

After restriction digestion of the respective inserts and vectors (4.2.6), the DNA fragments were ligated overnight at 16 °C by using the T4 DNA ligase (Invitrogen, Waltham, USA) according to instructions. DNA ligases link free 3' hydroxyl and 5' phosphate ends of nucleic acids. 100 ng vector DNA was ligated with insert DNA whose amount was calculated by using the following formula to ensure a three times excess of insert over vector. The DNA amount was double-checked on an agarose gel (4.2.3).

$$\text{ng InsertDNA} = \frac{\text{Vektor DNA (ng)} * \text{Insert DNA (bp)}}{\text{Vektor DNA (bp)}} * \frac{3}{1}$$

Ligation reaction:

100 ng Vector DNA
x ng Insert DNA
2 µl 5x Ligase buffer
1 U T4 DNA Ligase
Ad 10 µl ddH_2O

4.2.8 Transformation of competent *E. coli* cells

Electrocompetent *E.coli Top10* cells and chemically competent *E.coli XL1Blue* cells were used for transformation.

For the transformation of *XL1Blue* cells, 5 µl of the ligation was added to 50 µl competent cells and kept on ice for 30 min. Then, it was incubated at 42 °C for 90 s and immediately placed back

on ice for 2 min. After adding 300 µl SOC medium, it was incubated at 37 °C for 1 h. The cells were plated on agar plates containing 100 µg/ml carbenicillin and incubated overnight at 37 °C.
Before electroporation, the ligated DNA needed to be precipitated to remove salts and to resuspend it in ddH_2O. 20 µl of 100% ethanol (-20 °C) and 1 µl 3 M sodium acetate (pH 5.3) were added to the ligation (10 µl) and mixed. It was centrifuged (13,000 xg, 15 min, 4 °C), the supernatant was removed and the DNA was washed with 700 µl 70% ethanol. Then, the supernatant was removed and the precipitated DNA was dried at 50 °C to remove the remaining ethanol. It was resuspended with 10 µl ddH_2O by vortexing and incubation at 50 °C for 10 min. Before the transformation, the ligation was cooled down on ice.
Electrocompetent *TOP10* cells were transformed by adding 5 µl ligation to 50 µl competent cells. The mixture was transferred to cuvettes (0.2 cm gap) and electroporated at 2 kV, 25 µF, and 200 Ω. Then, 1 ml SOC media was added to the cells and it was incubated at 37 °C for 1 h before it was plated on agar plates containing 100 µg/ml carbenicillin and incubated overnight at 37 °C.

4.2.9 Isolation of plasmid DNA from *E. coli*

Plasmid DNA was isolated and purified from a 5 ml or 400 ml *E.coli* culture (LB medium) that was grown overnight (37 °C, 140 rpm) by using the QIAprep Spin Miniprep Kit (Qiagen, Venlo, Netherlands) or the QIAGEN Plasmid Maxi Kit (Qiagen, Venlo, Netherlands) according to instructions. For the plasmid preparation from 5 ml (Miniprep), the cells were first lysed in an alkaline solution to release the plasmids. The plasmids were bound to a silica membrane, washed, and eluted in 30 µl ddH_2O.
The protocol for the QIAGEN Plasmid Maxi Kit was slightly modified and used to isolate plasmids from a 400 ml culture. The cells were harvested (3000 xg, 15 min, 4 °C) and resuspended in 20 ml of resuspension buffer. Then, it was lysed with 20 ml of alkaline lysis buffer for 5 min and immediately neutralized with 20 ml neutralization buffer for 20 min on ice. The lysed cells were pelleted (3600 xg, 30 min, 4 °C) and the supernatant was poured through a filter onto the column. The bound plasmid DNA was washed, eluted, and precipitated according to instructions and resuspended in 1.5 ml TE-buffer for storage at -20 °C.

4.2.10 DNA sequencing

To verify correct integration and to exclude that mutations have developed during cloning, the isolated plasmids (4.2.9) were sequenced via Sanger sequencing. 10 µl of plasmid DNA (100 ng/µl) was mixed with 4 µl primer (5 µM) and sent to LGC genomics (Berlin, Germany).

4.3 Biochemical methods

4.3.1 Sodium dodecylsulfate polyacrylamide gel electrophoresis (SDS-PAGE)

A SDS-PAGE is used to separate proteins in an electrical field according to their molecular weight while smaller proteins run faster than bigger proteins. The anionic detergent SDS covers the native charge of the protein and leads to a negative charge that depends on the molecular weight of the protein. First of all, 2x SDS loading buffer with 100 mM DTT is added to the protein samples and it is denatured at 95 °C for 10 min. The reducing agent DTT breaks disulfide bonds in a protein promoting the denaturation of the proteins. The SDS gel consists of a 4% stacking gel and a 12% separation gel. A volume corresponding to $1x10^7$ cells and 6 µl of pre-stained protein molecular weight marker (Thermo Fisher Scientific, Waltham, USA) are loaded onto a prepared 12% SDS gel. The gel is run in a chamber filled with SDS buffer at 90 V for the first 10 min to ensure an even entry into the separation gel. Then, the voltage is turned up to 120 V for the remaining time. The SDS gel was then used to perform a Western Blot (4.3.2).

4% Stacking gel	12% Separation gel
5 ml 4% Stacking gel solution	10 ml 12% Separation gel solution
5 µl TEMED	5 µl TEMED
25 µl 10% APS	50 µl 10% APS

4% Stacking gel solution	12% Separation gel solution
61 ml ddH2O	34 ml ddH2O
25 ml Stacking gel buffer (pH 6.8)	25 ml Separation gel buffer (pH 8.8)
13 ml 30% Acrylamide	40 ml 30% Acrylamide
1 ml 10% SDS	1 ml 10% SDS

4.3.2 Semi-dry Western-Blot

A Western Blot is a biochemical method to detect proteins using specific antibodies. Firstly, the proteins are separated in an SDS gel (4.3.1) and transferred onto a nitrocellulose membrane. For this, a gel, a nitrocellulose membrane, and 12 blotting papers are soaked in transfer buffer before they were stacked in a Trans-Blot Turbo cassette (Bio-Rad, Hercules, USA) in the following order: 6 blotting papers, nitrocellulose membrane, gel, 6 blotting papers. The transfer was executed at 25 V and 1 A for 30 min in a Trans-Blot Turbo system (Bio-Rad, Hercules, USA) while the negatively charged proteins migrate to the anode and bind to the nitrocellulose membrane. Then, the membrane was soaked in Ponceau S solution for 30 s, followed by 1% acetate to visualize

protein bands and verify a correct transfer. The protein staining was removed by washing the membrane with PBS (pH 7.4). When using samples that contain a lot of hemoglobin eg. MACS-purified parasites (4.4.7), the membrane was incubated in ECL solution with 1:1000 30% H_2O_2 for 20-30 min to reduce disturbing hemoglobin signals. In the next step, the membrane was blocked with 5% milk powder in PBS (pH 7.4) for 1 h to prevent the unspecific binding of antibodies. Then, the first antibody directed against the protein of interest was diluted in 5% milk powder in PBS (pH 7.4) and incubated overnight at 4 °C while shaking. The next day, the membrane was washed three times with PBS (pH 7.4) for 10 min and incubated with the respective HRP-conjugated secondary antibody (Dako, Glostrup, Denmark) diluted 1:2000 in 5% milk powder in PBS (pH 7.4) for 2 h. After 2 h, the membrane was washed three times for 10 min with PBS (pH 7.4), soaked in ECL-solution with 1:1000 30% H2O2, and immediately developed with an Intas ECL ChemoStar device.

4.4 Cell biology methods

4.4.1 *In vitro* cultivation of *P. falciparum*

The parasites were cultivated in Petri dishes with cell culture medium and A^+ red blood cells from the blood bank of the university hospital in Heidelberg or Giessen at 4% hematocrit. They were incubated at 37 °C with a gas atmosphere of 90% N_2, 3-5% CO_2, and 5% O_2 (Trager and Jensen, 1976). The cell culture media consisted of 500 ml RPMI 1640 with HEPES and L-glutamine, 10 ml hypoxanthine solution (fc: 0.2 mM), 5 ml neomycin solution (fc: 0.1 mg/mL), and the supernatant of 50 ml human plasma (A^+). For transfectants, 500 ml RPMI 1640 with HEPES and L-glutamine, hypoxanthine (fc: 0.2 mM), neomycin (fc: 0.1 mg/mL), 25 ml of human plasma (A+), and 25 ml of sterile-filtered Albumax solution was used until parasites grew back. Albumax solution was prepared with 25 g of AlbuMAXII in 500 ml RPMI 1640 with HEPES and L-glutamine. Human plasma ($A^{+)}$ was obtained from the blood bank in Heidelberg or Giessen and stored at -4 °C. Four bags were thawed, pooled, aliquoted into 50 ml tubes, and heat-inactivated at 56 °C for two hours. Before adding the supernatant to the media, the plasma was pelleted (1600 xg, 10 min).

4.4.2 Giemsa staining of blood smears

To observe cultivated parasites and avoid stress caused by high parasitemia, blood smears were prepared at least three times a week. 5 µl of a parasite culture were spread evenly on a microscopy slide and air dried. The cells were fixed with methanol for a few seconds and stained in Giemsa solution for about 10 min. Afterwards, the microscopy slides were rinsed with water

and analyzed by light microscopy at a 1000x magnification using an oil immersion lens. The continuous culture was diluted according to the observed parasitemia.

4.4.3 Cryopreservation of parasites

For cryopreservation 0.5 ml of *P. falciparum* ring-stage infected red blood cells were resuspended in 0.5 ml of freezing solution and transferred into cryotubes. After snap freezing in liquid nitrogen for 10 min, they were stored in liquid nitrogen tanks at -80 °C until needed.

4.4.4 Thawing of parasites

To return cryopreserved *P. falciparum* cultures into continuous cell culture, cryotubes were thawed for a few minutes at 37 °C. Afterwards, 200 µl of 12% NaCl solution was added drop-wise and the diluted cell solution was transferred into a 15 ml tube. After 3 minutes, 5 ml of 1.2% NaCl solution was added drop-wise while agitating the tube. The same was done with 5 ml of 0.9% NaCl with 0.2% glucose before pelleting the cells (1600 xg, 2 min) and washing them once with media. The washed cells were reseeded with 0.5 ml A^+ blood and media and cultivated as described in 4.4.1.

4.4.5 Synchronization of asexual *P. falciparum* cultures via D-sorbitol

Infected red blood cells (RBCs) acquire an increased membrane permeability to solutes due to new permeability pathways generated by the parasite (Ginsburg and Stein., 1985). Therefore, treatment with d-sorbitol leads to osmotic lysis of RBCs infected with mature parasite stages (trophozoites and schizonts) while earlier ring stage parasites survive (Lambros and Vanderberg, 1979). Temporarily, this causes a more synchronous development of the parasite culture which can be improved by using d-sorbitol twice a day within 4-6 hours. A small parasite culture plate (500 µl blood) was pelleted via centrifugation (1600 xg, 2 min), resuspended in 5 ml 5% sorbitol solution, and incubated for 10-15 min at room temperature. The cell pellet was washed once with 10 ml of complete media and re-seeded for further cultivation.

4.4.6 Gelatine flotation selection

Due to host cell modifications, red blood cells infected with mature *P. falciparum* stages (trophozoites and schizonts) exhibit protrusions on the cell surface called knobs that play a pivotal role in cytoadherence (Luse and Miller, 1971). This leads to altered sedimentation properties in gelatine solutions allowing the enrichment of knob-forming infected red blood cells (iRBCs) (Goodyer et al., 1994). 500 µl iRBCs with trophozoites (parasitemia > 5%) were resuspended in

3 ml pre-warmed gelafundin solution and incubated for 10-20 min at 37°C. Uninfected and ring-infected RBCs are in the pellet while trophozoites and schizonts that form knobs stay in the supernatant. The supernatant was transferred to a new tube, pelleted (1600 xg, 2 min), washed once with 10 ml cell culture medium, and reseeded. Gelafundin solution was prepared with 25 ml Gelafundin® ISO 40 mg/ml (B. Braun Melsungen AG, Germany) and 15 ml RPMI 1640 with HEPES and L-glutamine.

4.4.7 Enrichment of trophozoites via magnetic cell separation (MACS)

P. falciparum uses hemoglobin as a main nutrient and degrades it into hemozoin that accumulates in mature parasite stages (trophozoites and schizonts) (Francis et al., 1997). The paramagnetic property of hemozoin can be utilized to enrich hemozoin-containing infected red blood cells (iRBCs) via MACS A CS-column, a cannula, and a 20 ml syringe were attached to a three-way stopcock and mounted onto the VarioMACS separator. The column was washed with ~20 ml PBS (pH 7.4) before starting the cell separation. A synchronized parasite culture with 5-10% trophozoites was pipetted onto the column with a flow rate of 1-2 drops per second. The first flowthrough was added onto the column once more to improve the yield. Afterwards, the column was washed with PBS (pH 7.4) and an increased flow rate to remove uninfected RBCs and ring stages that did not bind to the magnet. As soon as the flowthrough was clear, the column was removed from the VarioMACS separator and the hemozoin-containing iRBCs were eluted with PBS (pH 7.4). When the membrane-bound proteins should be separated from the soluble proteins, $2x10^8$ infected cells were resuspended in 180 µl 1 mM Tris, hypotonically lysed, and incubated in liquid nitrogen (à 30 sec) for three freezing/thawing cycles. After centrifugation (13,000 xg, 20 min, 4 °C), the soluble fraction was removed and centrifuged again to remove possible remaining membrane components. The pellet fraction was washed 5 times in PBS (pH 7.4) with 1 mM PMSF and PIC (1:200, Calbiochem), before preparing both fraction samples for Western Blot.

4.4.8 Transfection of *P. falciparum*

Transgenic *glms* knockdown cell lines were generated via electroporation (Wu et al., 1995). Firstly, 150 µg plasmid DNA (4.2.9) was precipitated by adding two volumes of 100% ethanol (-20 °C) and 1/10 volume of 3 M sodium acetate solution (pH 5.3). After centrifugation (13,000 xg, 15 min, 4 °C), the supernatant was carefully removed and the DNA pellet was stored in 70% ethanol at -20 °C until further use. On the day of transfection, the DNA was pelleted (13,000 xg, 15 min, 4 °C) and air dried under sterile conditions. 30 µl of TE-buffer was added and the DNA

was resuspended while shaking at 50 °C. Right before electroporation, 370 µl cytomix was added and vigorously mixed by vortexing. Meanwhile, a synchronized parasite culture (4.4.5) with 5-10% ring stages was pelleted (1600 xg, 2 min), 200 µl per transfection were mixed with the DNA-cytomix-solution and transferred to the electroporation cuvette (0.2 cm gap). The electroporation was conducted at 950 µF (Fidock and Willems, 1997) and 310 V. After electroporation, the parasites were immediately transferred to prepared Petri dishes with pre-warmed transfection media and 400 µl erythrocytes. After six hours, the respective selective agent was added to the culture (2.5 nM WR99210). The media was changed daily and 20 µl of fresh blood was added until no more living parasites were seen in Giemsa blood smears (4.4.2). Until transgenic parasites grew back, the media was changed twice a week.

4.4.9 Selection-linked integration (SLI)

The SLI system is a fast method to select clones that have integrated the modified sequence (Birnbaum et al., 2017). A SLI-based vector contains two resistance markers. The first selection gene codes for the human dihydrofolate reductase (*hDHFR*) that confers resistance to WR99210 and selects for parasites that have taken up the plasmid (transfectants). The second selection gene codes for neomycin phosphotransferase that confers resistance to *G418*. It is expressed under the promotor of the protein of interest but it is joined through a skip-peptide resulting in the expression of two separate proteins: the protein of interest and the neomycin phosphotransferase. Therefore, *G418* selects transfected parasites that have integrated the modified locus (integrants). All *glmS* and M9 constructs are based on the pSLI vector allowing for a fast and easy selection of integrants. The transfectants were selected with 400, 600, and 800 µg/ml *G418* in a 6-well plate and the media was changed daily until no more living parasites were seen. The media was changed twice a week until they grew back and the integration was verified by PCR (4.2.2) using genomic DNA of the culture with the highest G418 concentration as a template. If no parasites grew back after 10 weeks (three tries), the integration failed.

4.4.10 *glmS* knockdown assay

To determine the knockdown efficiency of the *glmS* cell lines a synchronized *glmS* and M9 control culture (see 4.3.5) with 1% starting parasitemia (ring stages) was cultivated with 0, 1.25, 2.5, and 5 mM glucosamine (GlcN) for 72 h. The media with and without GlcN was changed daily and the trophozoite-infected red blood cells were enriched via magnetic cell separation (MACS) after 72 h. The purified parasites were resuspended in PBS (pH 7.4) with 1 mM PMSF, protease inhibitor cocktail (PIC, 1:200, Calbiochem), and SDS loading buffer and incubated at 95 °C for 10 min. The

samples were either stored at -20 °C or an equivalent of $1x10^7$ infected cells were directly run on an SDS-Gel (4.3.1) and analyzed via Western Blot (4.3.2). An α-HA (mouse) primary antibody and α-mouse-HRP secondary antibody were used to detect the HA-tagged protein of interest and the evenly expressed parasite protein aldolase served as a loading control (α-Aldolase (rabbit) and α-rabbit-HRP). The band intensities correspond to the respective protein abundance. Three independent experiments were measured via ImageJ, normalized to the aldolase control bands, and statistically analyzed in GraphPad Prism. Every day, a Giemsa blood smear was prepared to observe the development of the parasites (4.4.2).

4.4.11 SybrGreen-based growth assay

In order to analyze the growth of transgenic parasites, synchronized (4.4.5) *glmS* and M9 control cell lines were set up with a starting parasitemia of 0.2% ring stages, a hematocrit of 1.25%, and cultivated in triplicates with 0, 1.25, 2.5 and 5 mM glucosamine (GlcN) for 72 h. This assay was performed in a black U-bottom 96-well plate with 200 µl per well. Non-infected red blood cells were used as a negative control. After 72 h, the plate was placed in an -80 °C freezer for one day resulting in the lysis of the cells. On the next day, the plate was thawed at room temperature for 2 h. 50 µl SybrGreenI solution (1:10,000) was pipetted to each well and after 1 h of incubation in the dark at room temperature, it was measured at a Clariostar plate reader (excitation: 482±16 nm, emission: 530±40 nm, 10 flashes per well). As SybrGreenI binds to double-stranded DNA, the emission corresponds to the parasitemia allowing rapid analysis of the parasite development (Bennett et al., 2004). The mean value of the negative control was subtracted from each measurement and the measurements were normalized to the highest reading at 0 mM GlcN. Statistic analysis was performed using GraphPad Prism.

4.4.12 Chondroitin-sulphate A (CSA) binding selection

Due to host cell modifications, red blood cells infected with *P. falciparum* (trophozoites and schizonts) bind with different binding abilities to endothelial host cell receptors. This is facilitated by PfEMP1 which is presented on top of the knobs. PfEMP1 belongs to the *var* multigene family that consists of about 60 copies while only one copy is expressed at once and the parasite undergoes regular switching between different variants to evade the human immune system. The PfEMP1 variant VAR2CSA binds specifically to CSA (Biggs et al., 1991; Biggs et al., 1992; Beeson et al., 1998). All generated transfectants are based on the *P. falciparum* strain CS2, which is known to express VA2CSA after selection and does not switch as often as other wildtype strains (Maier et al., 2007). Before analyzing the binding of those transfectants *in vitro*, they need to be

selected regularly (three times) for binding to CSA to ensure the reliable expression of VA2CSA (Reeder et al., 1999). For this, 10 ml of sterile CSA solution (1 mg/ml in PBS pH 7.2) was left to absorb in a tissue culture flask (T74) overnight at 4 °C. The next day, the flask was washed three times with 10 ml PBS (pH 7.2) and blocked with 10 ml 1% BSA solution for one hour. Meanwhile, the synchronized trophozoite culture (4.4.5) was enriched using gelatine flotation (4.4.6) and resuspended in 10 ml cytoadhesion media. The flask was washed once with 10 ml cytoadhesion media before the enriched infected red blood cells were transferred into the flask and incubated for one hour at room temperature. After one hour, the flask was washed five times with 10 ml cytoadhesion media to remove the non-bound cells. The cells that were bound to CSA were removed from the flask with media and reseeded with A^+ blood. The enrichment and CSA binding selection were observed via Giemsa smears (4.4.2).

4.4.13 Chondroitin-sulphate A (CSA) binding assay

This static binding assay was used to analyze the effect of a knockdown of different *glmS* cell lines on the cytoadhesive capabilities to the PfEMP1 ligand CSA (Beeson et al., 1999). A synchronized *glmS* cell line (4.4.5) was cultivated for 72 h with 0 and 2.5 mM glucosamine with daily media changes. On the day before the assay, a petri dish (non-TC treated) was prepared with drops of 20 µl PBS (pH 7.2) for the PBS control, 20 µl of 1 mg/ml CSA for the CSA, and soluble CSA control in triplicates. The petri dish was sealed with parafilm and incubated at 4 °C overnight. The next day, each spot was washed three times with 20 µl PBS (pH 7.2) and blocked with 1% BSA in PBS (pH 7.2) for one hour at room temperature. Meanwhile, the infected red blood cells with trophozoites were enriched via gelatine flotation (4.4.6) and the parasitemia was determined in Giemsa blood smears (4.4.2). The parasitemia was diluted with cytoadhesion media to a concentration of $5x10^7$ iRBCs/ml. To ensure that the binding to CSA is specific, a soluble CSA solution was prepared (1 mg/ml CSA in PBS (pH 7.2) diluted 1:9 with cytoadhesion media) to dilute the parasitemia to $5x10^7$ iRBCs/ml for the control. After one hour of blocking, each spot was washed once with 20 µl cytoadhesion media, before 20 µl of diluted iRBCs were pipetted onto the respective spots and incubated for one hour at room temperature. Then, each spot was washed carefully with 20 µl cytoadhesion media and the non-bound cells were removed by adding 12 ml of cytoadhesion media and washing the plate on an orbital shaker at 70 rpm for 13 rounds. The cytoadhesion media was removed and the whole plate was washed once with 12 ml PBS (pH 7.2) without shaking. The cells were fixed by adding 12 ml of 2% glutaraldehyde in PBS (pH 7.2) for one hour at room temperature. Afterwards, the plate was washed twice with 12 ml PBS (pH 7.2), stained with Giemsa solution for 10 min, and washed two more times with PBS (pH 7.2)

and once with ddH_2O to remove the remaining staining solution. The plate was left to dry overnight. To analyze the binding of iRBCs to CSA, microscopic pictures (DIC, 100x magnification) were taken at a Kern OCM 161 with the Kern ODC832 microscope camera of each spot. The parasitemia was determined using a trained Ilastik program to distinguish background and iRBCs and ImageJ to count the iRBCs (Diehl, 2019).

4.4.14 PfEMP1 measurement by flow cytometry

The expression of PfEMP1 VAR2CSA on the surface of iRBCs was measured via flow cytometry. CSA-selected parasites (see 4.4.12) were synchronized (see 4.3.5) and cultivated for 72 h with and without 2.5 mM GlcN. Trophozoites were enriched by magnetic cell sorting (4.4.7) and incubated with a hematocrit of 1% with and without var2csa antiserum (11P, rabbit, a kind gift of Benoit Gamain) diluted in 0.3% BSA-PBS (pH 7.2) for 30 min at 4 °C. After three washing steps with PBS (pH 7.2), the samples were incubated with and without a secondary antibody conjugated to Cy3 for 30 min at 4 °C in the dark. The samples were washed again three times with PBS (pH 7.2) and incubated overnight in 4% PFA/0.0075% GA in PBS (pH 7.2) at 4 °C. The next day, it was washed three times with PBS (pH 7.2) and incubated with DAPI (1:10,000; stock 10 mg/ml) for 20 min at RT, followed by three washing steps with PBS (pH 7.2). The whole experiment was performed in 96-well plates with a 100 µl sample volume. It was measured and analyzed with a CytoflexS (Beckman Coulter).

4.5 Microscopy-based methods

4.5.1 Immunofluorescence assay (IFA)

The IFA was used to analyze the expression and localization of specific proteins in the blood stages of *P. falciparum*. A specific primary antibody binds to epitopes of the protein of interest against which a secondary antibody is directed that is conjugated to a fluorophore. The excited state of the respective fluorophores (Cy2, Cy3) emits light at different wavelengths. Depending on the antibody and the protein of interest, two methods were used to get an optimal result in fluorescence microscopy that are based on Tonkin et al., 2004.

IFA in solution (PFA fixation):

This fixation method preserves the three-dimensional structure of the cells as PFA forms covalent cross-links between molecules (Tonkin et al., 2004).

100 µl of infected red blood cells of a ~5% trophozoite stage culture were resuspended in 1 ml fixation solution and incubated with light shaking at 37 °C for 30 min. Then, the cells were pelleted

(1000 xg, 1 min, RT) and resuspended in 1 ml permeabilization solution. After 15 min of incubation at RT, it was pelleted (1000 xg, 1 min, RT) and incubated in 1 ml blocking buffer for 1 h at RT. The first antibody diluted in blocking solution was added to the blocked and pelleted cells and it was incubated overnight at 4 °C while rolling. The next day, the cells were washed three times for 15 min in PBS (pH 7.4) and incubated with the respective secondary antibody diluted in blocking buffer for 1 h at RT while rolling in the dark. After incubation, it was washed three times with PBS (pH 7.4), including DAPI (1:10,000; stock 10 mg/ml) in the final washing step (Tonkin et al., 2004). To preserve the fluorescence signal, it was post-fixed with a 1:3 fixation solution in PBS (pH 7.4) for 15 min at RT, resuspended in PBS, and stored at 4 °C until the microscopic pictures were taken at a Zeiss Observer Z1 with a ZEN 3.1 software.

IFA on slides (Acetone-Methanol fixation):

Acetone-methanol fixation dehydrates cells resulting in denatured and precipitated proteins. Using this method, the cells lose their three-dimensional structure but it might work better to visualize soluble proteins. (Tonkin et al., 2004).

Firstly, thin blood smears of a ~5% trophozoite stage culture were prepared and fixed in acetone with 10% methanol (-20 °C) for 10 min at -20 °C. To start the IFA, the slides were incubated in blocking buffer for 1 h while shaking. Then, the primary antibody diluted in blocking buffer was pipetted on parafilm and the slides were placed on top and incubated overnight at 4 °C. The next day, the slides were washed three times in PBS (pH 7.4) and the respective secondary antibody diluted in blocking buffer was pipetted on parafilm with the slides on top. This was incubated in the dark for 2 h at RT. Afterwards, the slides were washed again three times in PBS (pH 7.4), including DAPI (1:10,000; stock 10 mg/ml) in the final washing step with an additional washing step with ddH_2O at the end. Then, the slides were mounted using Fluoromount-G® (Southern Biotech, Birmingham, USA) and a cover slip to conserve the fluorescence signal and it was allowed to solidify at 4 °C overnight before they were imaged at a Zeiss Observer Z1 with a ZEN 3.1 software.

4.5.2 Scanning electron microscopy (SEM)

SEM was used to investigate if a knockdown of my proteins of interest affects the knob morphology.

Firstly, synchronized *glmS* and M9 control parasite cultures were cultivated for 72 h with 0 and 2.5 mM glucosamine. The trophozoite-stage infected red blood cells were purified via MACS (4.4.7) and fixed in 1% glutaraldehyde in PBS (pH 7.2) overnight at 4 °C. The next day, round

coverslips (12 mm diameter) were placed in a 12-well plate and coated with 20 µl 0.01% poly-L-lysine for 20 min at RT. Meanwhile, the fixed cells were washed two times with 0.1 M cacodylate buffer. 40 µl of washed and diluted cells were pipetted onto the coated coverslips and incubated for 20 min. Then, each well was washed twice with 0.1 M cacodylate buffer and it was incubated with 1% osmium tetroxide (OsO_4) in 0.1 M cacodylate buffer for 1 h at 4 °C to improve the contrast of the SEM image. After 1 h, each well was washed twice with 0.1 M cacodylate buffer and once with ddH_2O before the samples were dehydrated in a series of 25%, 50%, 75%, 95%, and 100% acetone for 10 min each. A Leica CPD300 was used for critical point drying and the samples were coated with 5 nm Au/Pd at a Leica ACE600 before being imaged at a Zeiss Lex15030 electron microscope.

4.5.3 Transmission electron microscopy (TEM)

TEM was used to investigate subcellular structures and knobs after a knockdown of my protein of interest.

Firstly, synchronized *glmS* and M9 control parasite cultures were cultivated for 72 h with 0 and 2.5 mM glucosamine. The trophozoite-stage infected red blood cells were enriched by gelatine flotation (4.4.6) and fixed in 100 mM cacodylate solution (CaCo) with 2% glutaraldehyde and 2% paraformaldehyde overnight at 4 °C. The next day, the cells were washed three times for 5 min with CaCo solution and incubated with 1% osmium in CaCo solution for 1 h at RT. After washing them two times with ddH_2O, the cells were incubated in 1% U-acetate in ddH_2O overnight at 4 °C to increase the contrast in the final image. The next day, the cells were washed again two times with ddH2O for 10 min at RT and dehydrated in a series of 25%, 50%, 70%, 90%, and 2x100% acetone for 10 min each. Then, they were incubated in a series of 25%, 50%, and 75% Spurr for 45 min each at RT and stored in 100% Spurr overnight before the sections were prepared and imaged at a Jeol JEM-1400 electron microscope at 80 kV.

References

Adisa, A., Rug, M., Klonis, N., Foley, M., Cowman, A. F., & Tilley, L. (2003). 'The signal sequence of exported protein-1 directs the green fluorescent protein to the parasitophorous vacuole of transfected malaria parasites', *Journal of Biological Chemistry*, 278/8: 6532–42.

Aguilar, R., Magallon-Tejada, A., Achtman, A. H., Moraleda, C., Joice, R., Cisteró, P., Li Wai Suen, C. S. N. et al. (2014). 'Molecular evidence for the localization of Plasmodium falciparum immature gametocytes in bone marrow', *Blood*, 123/7: 959-966.

Albano, F. R., Foley, M., Tilley, L. (1999). 'Export of parasite proteins in the erythrocyte cytoplasm: secretory machinery and traffic signals', *Novartis Foundation Symposia*, 226: 167-172.

Allison, A. C. (1954). 'Protection afforded to sickle-cell trait against subtertian malarial infection', *British Medical Journal*, 1(4857): 290-194.

Amino, R., Thiberge, S., Martin, B., Celli, S., Shorte, S., Frischknecht, F., & Ménard, R. (2006). 'Quantitative imaging of Plasmodium transmission from mosquito to mammal', *Nature Medicine*, 12/2: 220–224.

Amino, R., Giovannini, D., Thiberge, S., Gueirard, P., Boisson, B., Dubremetz, J.-F., Prévost, M.-C., et al. (2008). 'Host cell traversal is important for progression of the malaria parasite through the dermis to the liver', *Cell Host & Microbe*, 3/2: 88–96.

An, X. & Mohandas, N. (2008). 'Disorders of red cell membrane', *British Journal of Haematology*, 141: 367-375.

Antorini, S., Galimberti, L., Milazzo, L., Corbellino, M. (2012). 'Biology of human malaria Plasmodia including Plasmodium knowlesi', *Mediterranean Journal of Hematology and Infectious Diseases,* 4.

Archer, N. M., Petersen, N., Clark, M. A., Buckee, C. O., Childs, L. M., Duraisingh, M. T. (2018). 'Resistance to Plasmodium falciparum in sickle cell trait erythrocytes is driven by oxygen-dependent growth inhibition', *Proceedings of the National Academy of Sciences of the United States of America,* 115/28.

Ariso, N. & Hashimoto, T. (2015). 'Phylogeny and evolution of apicoplasts and apicomplexan parasites', *Parasitology International,* 64: 254-259.

Armstrong, C. M. & Goldberg, D. E. (2007). 'An FLBP destabilization domain modulates protein levels in Plasmodium falciparum', *Nature Methods*, 4:1007-1009.

Arora, N., Anbalagan, L. C., Pannu, A. K. (2021). 'Towards eradication of malaria: Is the WHO's RTS,S/AS01 vaccination effective enough?', *Risk Management and Healthcare Policy,* 14: 1033-1039.

Aurrrecoechea, C., Brestelli, J., Brunk, B. P., Dommer, J., Fischer, S., Gajrira, B. ,Gao, X. et al. (2009). 'PlasmoDB: a functional genomic database for malaria parasites', *Nucleic Acids Research*, 37: D539-D543.

Batolini, A. & Zammarchi, L. (2012). 'Clinical aspects of uncomplicated and severe malaria', *Mediterranean Journal of Hematology and Infectious Diseases,* 4.

Baer, K., Klotz, C., Kappe, S. H. I., Schnieder, T., Frevert, U. (2007). 'Release of hepatic Plasmodium yoelii merozoites into the pulmonary microvasculature', *PLoS Pathogens*, 3/11: e171.

Banaszynski, L. A., Chen, L.-C., Maynard-Smith, L. A., Ooi, A. G. L., Wandless, T. J. (2006). 'A rapid, reversible, and tunable method to regulate protein function in living cells using synthetic small molecules', *Cell*, 126/5: 995-1004.

Baruch, D. I., Pasloske, B. L., Singh, H. B., Bi, X., Ma, X. C., Feldman, M., Taraschi, T. F., Howard, R. J. (1995). 'Cloning the P. falciparum gene encoding PfEMP1, a malarial variant antigen and adherence receptor on the surface of parasitized human erythrocytes', *Cell*, 82: 77-87.

Baum, J., Papenfuss, A. T., Baum, B., Speed, T. P., Cowman, A. F. (2006). 'Regulation of apicomplexan actin-based motility', *Nature Reviews Microbiology*, 4: 621-628.

Baum, J., Chen, L., Healer, J., Lopaticki, S., Boyle, M., Triglia, T., Ehlgen, F. et al. (2009). 'Reticulocyte-binding protein homologue 5 – An essential adhesin involved in invasion of human erythrocytes by Plasmodium falciparum', *International Journal for Parasitology,* 39/3: 371-380.

Beck, J. R., Muralidharan, V., Oksman, A., Goldberg, D. E. (2014). 'PTEX component HSP101 mediates export of diverse malaria effectors into host erythrocytes', *Nature*, 511(7511): 592-595.

Beck, J. R. & Ho, C.-M. (2021). 'Transport mechanism at the malaria parasite-host cell interface', *PLoS Pathogens,* 17/4: e1009394.

Beeson, J. G., Chai, W., Rogerson, S. J., Lawson, A. M., Brown, G. V. (1998). 'Inhibition of binding of malaria-infected erythrocytes by a tetradecasaccharide fraction from chondroitin sulfate A', *Infection and Immunity*, 66/8: 3397-3402.

Beeson, J. G., Brown, G. V, Molyneux, M. E., Mhango, C., Dzinjalamala, F., & Rogerson, S. J. (1999). 'Plasmodium falciparum isolates from infected pregnant women and children are associated with distinct adhesive and antigenic properties', *The Journal of infectious diseases*, 180/2: 464–72.

Behari, R. & Haldar, K. (1994). 'Plasmodium falciparum: protein localization along a novel, lipid-rich tubovesicular membrane network in infected erythrocytes', *Experimental Parasitology*, 79/3: 250-259.

Bennett, T. N., Paguio, M., Gligorijevic, B., Seudieu, C., Kosar, A. D., Davidson, E., Roepe, P. D. (2004). 'Novel, rapid and inexpensive cell-based quantification of antimalarial drug efficacy', *Antimicrobial Agents and Chemotherapy,* 48/5: 1807-1810.

Bennink, S., Kiesow, M. J., Pradel, G. (2016). 'The development of malaria parasites in the mosquito midgut', *Cellular Microbiology,* 18/7: 905-918.

Berg, S., Kutra, D., Kroeger, T., Staehle, C. N., Kausler, B. X., Haubold, C., Schieegg, M. et al. (2019). 'ilastik: interactive machine learning for (bio)image analysis', *Nature Methods*, 16:12226-1232.

Biddau, M. & Sheiner, L. (2019). 'Targeting the apicoplast in malaria', *Biochemical Society Transactions,* 47:973-983.

Biggs, B. A., Goozé, L., Wycherley, K., Wollish, W., Southwell, B., Leech, J. H., & Brown, G. V. (1991). 'Antigenic variation in Plasmodium falciparum', *Proceedings of the National Academy of Sciences of the United States of America*, 88/20: 9171–4.

Billker, O., Shaw, M. K., Margos, G., Sinden, R. E. (1997). 'The roles of temperature, pH and mosquito factors as triggers of male and female gametogenesis of Plasmodium berghei in vitro', *Parasitology*, 115/1: 1-7.

Billker, O., Lindo, V., Panico, M., Etienne, A. E., Paxton, T., Dell, A. Rogers, M. et al. (1998). 'Identification of xanthurenic acid as the putative inducer of malaria development in the mosquito', *Nature*, 392: 289-292.

Birnbaum, J., Flemming, S., Reichard, N., Soares, A. B., Mesén-Ramírez, P., Jonscher, E., Bergmann, B., et al. (2017). 'A genetic system to study Plasmodium falciparum protein function', *Nature Methods*, 14/4: 450–6.

Boddey, J. A., Moritz, R. L., Simpson, R. J., Cowman, A. F. (2009). 'Role of the Plasmodium export element in trafficking parasite proteins to the infected erythrocyte'*, Traffic*, 10/3: 285-299.

Boddey, J. A., Hodder, A. N., Günther, S., Gilson, P. R., Patsiouras, H., Kapp, E. A., Pearce, J. A. et al. (2010). 'An aspartyl protease directs malaria effector proteins to the host cell', *Nature*, 463(7281): 627-631.

Böhme, U., Otto, T. D., Sanders, M. J., Newbold, C. I., Berriman, M. (2019). 'Progression of the canonical reference malaria parasite genome from 2002-2019', *Wellcome Open Research,* 4/58.

Boonyalai, N., Collins, C. R., Hackett, F., Withers-Martinez, C., & Blackman, M. J. (2018). 'Essentiality of Plasmodium falciparum plasmepsin V', *PLoS ONE*, 13/12: e0207621.

Butler, T. K. (2014). 'An exported Malaria protein regulates glucose uptake during intraerythrocytic infection', *All Theses and Dissertations (ETDs),,* 1224.

Carter, R. & Miller, L. H. (1979). 'Evidence for environmental modulation of gametocytogenesis in Plasmodium falciparum in continuous culture', *Bulletin of the World Health Organization,* 57(Suppl. 1): 37-52.

Chen, Q., Fernandez, V., Sundström, A., Schlichtherle, M., Datta, S., Hagblom, P., Wahlgren, M. (1998). 'Developmental selection of var gene expression in Plasmodium falciparum', *Nature*, 394: 392-395.

Chitnis, C. E. & Miller, L. H. (1994). 'Identification of the erythrocyte binding domain of Plasmodium vivax and Plasmodium knowlesi proteins involved in erythrocyte invasion', *Journal of Experimental Medicine*, 180/2: 497-506.

Cholera, R., Brittain, N. J., Gillrie, M. R., Lopera-Mesa, T. M., Diakité, S. A. S., Arie, T., Krause, M. A. et al. (2008). 'Impaired cytoadherence of Plasmodium falciparum-infected erythrocytes containing sickle hemoglobin', *Proceedings of the National Academy of Sciences of the United States of America,* 105/3: 991-996.

Clemens, R., Pramoolsinsap, C., Lorenz, R., Pukrittayakamee, S., Bock, H. L., White, N. J. (1994). 'Activation of the coagulation cascade in severe falciparum malaria through the intrinsic pathway', *British Journal of Hematology*, 87/1: 100-105.

Cockburn, I. A., Mackinnon, M. J., O'Donnell, A., Allen, S. J., Moulds, J. M., Baisor, M., Bockarie, M. et al. (2003). 'A human complement receptor 1 polymorphism that reduces Plasmodium falciparum rosetting confers protection against severe malaria', *Proceedings of the National Academy of Sciences of the United States of America,* 101/1: 272-727.

Coffey, M. J., Jennison, C., Tonkin, C. J., Boddey, J. A. (2016). 'Role of the ER and Golgi in protein export by Apicomplexa', *Current Opinion in Cell Biology,* 41: 18-24.

Collins, C. R., Das, S., Wong, E. H., Andenmatten, N., Stallmach, R., Hackett, F., Herman, J.-P. et al. (2013). 'Robust inducible Cre recombinase activity in the human malaria parasite Plasmodium falciparum enables efficient gene deletion within a single asexual erythrocytic growth cycle', *Molecular Microbiology*, 88/4: 687-701.

Cooke, B. M., Buckingham, D. W., Glenister, F. K., Fernandez, K. M., Bannister, L. H., Marti, M., Mohandas, N., et al. (2006). 'A Maurer's cleft-associated protein is essential for expression of the major malaria virulence antigen on the surface of infected red blood cells.', *The Journal of cell biology*, 172/6: 899–908.

Counihan, N. A., Modak, J. K., de Koning-Ward, T. F. (2021). 'How malaria parasites acquire nutrients from their host', *Frontiers in Cell and Developmental Biology,* 9:649184.

Cowman, A. F., Berry, D., & Baum, J. (2012). 'The cellular and molecular basis for malaria parasite invasion of the human red blood cell', *The Journal of cell biology*, 198/6: 961–71.

Cox, F.E. (2010). 'History of the discovery of the malaria parasites and their vectors', *Parasites & Vectors*, 3/1: 5.

Crabb, B. S., Cooke, B. M., Reeder, J. C., Waller, R. F., Caruana, S. R., Davern, K. M., Wickham, M. E., et al. (1997). 'Targeted gene disruption shows that knobs enable malaria-infected red cells to cytoadhere under physiological shear stress', *Cell*, 89/2: 287–96.

Culvenor, J. G., Langford, C. J., Crewther, P. E., Saint, R. B., Coppel, R. L., Kemp, D. J., Anders, R. F., Brown, G: V. (1987). 'Plasmodium falciparum: identification and localization of a knob protein antigen expressed by a cDNA clone', *Experimental Parasitology',* 63/1: 58-67.

Curt-Varesano, A., Braun, L., Ranquet, C., Hakimi, M.-A., Bougdour, A. (2016). 'The aspartyl protease TgASP5 mediates the export of the Toxoplasma GRA16 and GRA24 effectors into host cells', *Cellular Microbiology*, 18/2: 151-167.

Cyrklaff, M., Sanchez, C. P., Kilian, N., Bisseye, C., Simpore, J., Frischknecht, F., Lanzer, M. (2011). 'Hemoglobin S and C interfere with actin remodeling in Plasmodium falciparum-infected erythrocytes', *Science*, 334(6060): 1283-1286.

De Koning-Ward, T. F, Gilson, P. R., Boddey, J. A., Rug, M., Smith, B. J., Papenfuss, A. T., Sanders, P. R. et al. (2009). 'A newly discovered protein export machine in malaria parasites', *Nature*, 459: 945-949.

De Koning-Ward, T. F., Dixon, M. W. A., Tilley, L., Gilson, P. R. (2016). 'Plasmodium species: master renovators of their host cell', *Nature reviews Microbiology, 10.1038.*

Deponte, M., Hoppe, H. C., Lee, M. C. S., Maier, A. G., Richard, D., Rug, M., Spielmann, T., et al. (2012). 'Wherever I may roam: Protein and

Desai, M., ter Kuile, F. O., Nosten, F., McGready, R., Asamoa, K., Brabin, B., & Newman, R. D. (2007). 'Epidemiology and burden of malaria in pregnancy', *The Lancet Infectious Diseases*, 7/2: 93–104.

Dickerman, B. K., Elsworth, B., Cobbold, S. A., Nie, C. Q., McConville, M. J., Crabb, B. S., Gilson, P. R. (2016). 'Identification of inhibitors that dually target the new permeability pathway and dihydroorotate dehydrogenase in the blood stage of Plasmodium falciparum', *Nature Scientific Reports,* 6:37502.

Diehl, M. (2019). 'Using new genetic tools to elucidate the importance of exported proteins in intra-erythrocytic survival of the malaria parasite Plasmodium falciparum', *Heidelberg University.*

Diehl, M., Roling, L., Rohland, L., Weber, S., Cyrklaff, M., Sanchez, C. P., Beretta, C. A. et al. (2021). 'Co-chaperone involvement in knob biogenesis implicates host-derived chaperones in malaria virulence', *PLoS Pathogens,* 17/10: e1009969.

Divo, A. A., Geary, T. G., Davis, N. L., Jensen, J. B. (1985). 'Nutritional requirements of Plasmodium falciparum in culture. I. Exogenously supplied dialyzable components necessary for continuous growth', *The Journal of Protozoology*, 32/1: 59-64.

Dixon, M. W., Hawthorne, P. L., Spielmann, T., Anderson, K. L., Trenholme, K. R., Gardiner, D. L. (2008). 'Targeting of the ring exported protein 1 to the Maurer's clefts is mediated by a two-phase process', *Traffic*, 9/8: 1316-1326.

Dluzewski, A. R., Zicha, D., Dunn, G. A., Gratzer, W. B. (1995). 'Origins of the parasitophorous vacuole membrane of the malaria parasite: surface area of the parasitized red cell', *European Journal of Cell Biology,* 68/4: 446-449.

Dondorp, A. M., Angus, B. J., Chotivanich, K., Siamut, K., Ruangveerayuth, R., Hardeman, M. R., Kager, P A. et al. (1999). 'Red blood cell deformability as a predictor of anemia in severe falciparum malaria', *The American Journal off Tropical Medicine and Hygiene*, 60/5: 733-737.

Dondorp, A. M., Ince, C., Charunwatthana, P., Hanson, J., van Kuijen, A., Faiz, M. A., Rahman, M. R. et al. (2008). 'Direct in vivo assessment of microcirculatory dysfunction in severe falciparum malaria', *The Journal of Infectious Diseases*, 197/1: 79-84.

Downie, M. J., Kirk, K., Mamoun, C. B. (2008). 'Purine salvage pathways in the intraerythrocytic malaria parasite Plasmodium falciparum', *Eukaryotic Cell,* 7/8: 1231-1237.

Duraisingh, M. T., Triglia, T., Cowman, A. F. (2002). 'Negative selection of Plasmodium falciparum reveals targeted gene deletion by double-crossover recombination', *International Journal for Parasitology*, 32/1: 81-89.

Elhassan, I. M., Hviid, L., Satti, G., Akerstrom, B., Jakobsen, P. H., Jensen, J. B., Theander, T. G. (1994). 'Evidence of endothelial inflammation, T cell activation, and T cell reallocation in uncomplicated Plasmodium falciparum malaria', *The American Journal of Tropical Medicine and Hygiene*, 51/3: 372-379.

Elmendorf, H. G., Haldar, K. (1994). 'Plasmodium falciparum exports the golgi marker sohingomyelin synthase into a tubovesicular network in the cytoplasm of mature erythrocytes', *The Journal of Cell Biology*, 124/4: 449-462.

Elsworth, B., Matthews, K., Nie, C. Q., Kalanon, M., Charnaud, S. C., Sanders, P. R., Chisholm, S. A. et al. (2014). 'PTEX is an essential nexus for protein export in malaria parasites', *Nature*, 511: 587-591.

Elswoth, B., Sanders, P. R., Nebl, T., Batinovic, S., Kalanon, M., Nie, C. Q., Charnaud, S. C. et al. (2016). 'Proteomic analysis reveals novel proteins associated with the Plasmodium protein exporter PTEX and a loss of complex stability upon truncation of the core PTEX component, PTEX150', *Cellular Microbiology*, 18/11: 1551-1569.

Fast, N. M., Xue, L., Bingham, S., Keeling, P. J. (2002). 'Re-examining alveolate evolution using multiple protein molecular phylogenies', *Journal of Eucaryotic Microbiology,* 49/1: 30-37.

Fidock, D. A., & Wellems, T. E. (1997). 'Transformation with human dihydrofolate reductase renders malaria parasites insensitive to WR99210 but does not affect the intrinsic activity of proguanil', *Proceedings of the National Academy of Sciences of the United States of America*, 94/20: 10931–6.

Francis, S. E., Sullivan, D. J., Jr, Goldberg, D. E. (1997). 'Hemoglobin metabolism in the malaria parasite Plasmodium falciparum', *Annual Reviews of Microbiology,* 51: 97-123.

Fried, M. & Duffy, P. E. (1996). 'Adherence of Plasmodium falciparum to chondroitin sulfate A in the human placenta', *Science*, 272(5267): 1502-1504.

Gabriela, M., Matthews, K. M., Boshoven, C., Kouskousis, B., Jonsdottir, T. K., Bullen, H. E., Modak, J. et al. (2022). 'A revised mechanism for how Plasmodium falciparum recruits and exports proteins into its erythrocytic host cell', *Proceedings of the National Academy of Sciences of the United States of America Pathogens,* 18/2: e1009977.

Ganesan, S. M., Falla, A., Goldfless, S. J., Nasamu, A. S., Niles, J. C. (2016). 'Synthetic RNA-protein modules integrated with native translation mechanisms to control gene expression in malaria parasites', *Nature Communications,* 7: 10727.

Gardner, M. J., Hall, N., Fung, E., White, O., Berriman, M., Hyman, R. W., Carlton, J. M. et al. (2002). 'Genome sequence of the human malaria parasite Plasmodium falciparum', *Nature*, 419: 498-511.

Ghorbal, M., Gorman, M., Macpherson, C. R., Martins, R. M., Scherf, A., Lopez-Rubio, J.-J. (2014). 'Genome editing in human malaria parasite Plasmodium falciparum using the CRISPR-Cas9 system', *Nature Biotechnology*, 32: 819-821.

Ginsburg, H., Krugliak, M., Eidelman, O., Cabantchik, Z. I. (1983). 'New permeability pathways induced in membranes of Plasmodium falciparum infected erythrocytes', *Molecular and Biochemical Parasitology*, 8/2: 177-190.

Ginsburg, H., Stein, W. D. (1985). 'The new permeability pathways induced by the malaria parasite in the membrane of the infected erythrocyte: Comparison of results using different experimental techniques', *The Journal of Membrane Biology,* 197: 113-134.

Gold, D. A., Kaplan, A. D., Lis, A., Bett, G. C. L., Rosowski, E. E., Cirelli, K. M., Bougdour, A. et al. (2015). 'The Toxoplasma dense granule proteins GRA17 and GRA23 mediate the movement of small molecules between the host and the parasitophorous vacuole', *Cell Host & Microbe,* 17/5: 642-652.

Goldfless, S. J., Wagner, J. C., Niles, J. C. (2014). 'Versatile control of Plasmodium falciparum gene expression with an inducible protein-RNA interaction', *Nature Communications*, 5/5329.

Goodyer, I. D., Johnson, J., Eisenthal, R., & Hayes, D. J. (1994). 'Purification of mature-stage Plasmodium falciparum by gelatine flotation', *Annals of Tropical Medicine & Parasitology*, 88/2: 209–211.

Goonewardene, R., Daily, J., Kaslow, D., Sullivan, T. J., Duffy, P., Carter, R., Mendis, K., et al. (1993). 'Transfection of the malaria parasite and expression of firefly luciferase', *Proceedings of the National Academy of Sciences of the United States of America*, 90/11: 5234–5236.

Groomes, P. V., Kanjee, U., Duraisingh, M. T. (2022). 'RBC membrane biomechanics and Plasmodium falciparum invasion: probing beyond ligand-receptor interactions', *Trends in Parasitology,* 38/4: 302-315.

Guy, A. J., Irani, V., MacRaild, C. A., Anders, R. F., Norton, R. S., Beeson, J. G., Richards, J. S., Ramsland, P. A. (2015). 'Insights into the immunological properties of intrinsically disordered malaria proteins using proteome scale predictions', *PLoS One*, 10/10: e0141729.

Haase, S., Herrmann, S., Grürig, C., Heiber, A., Jansen, P. W., Langer, C., Treeck, M. et al. (2009). 'Sequence requirements for the export of the Plasmodium falciparum Maurer's clefts protein REX2', Molecular Microbiology, 71/4: 1003-1017.

Hammoudi, P.-M., Jacot, D., Mueller, C., Cristina, M. D., Dogga, S. K., Marq, J.-B., Romano, J. et al. (2015). 'Fundamental roles of the golgi-associated Toxoplasma aspartyl protease, ASP5, at the host-parasite interface', *PLoS Pathogens*, 11/10: e1005211.

Hanssen, E., Sougrat, R., Frankland, S., Deed, S., Klonis, N., Lippincott-Schwartz, J., Tilley, L. (2008a). 'Electron tomography of the Maurer's cleft organelles of Plasmodium falciparum-infected erythrocytes reveals novel structural features', *Molecular Micrrorbiology,* 67/4: 703-718.

Hanssen, E., Hawthorne, P., Dixon, M. W. A., Trernholme, K. R., McMillan, P. J., Spielmann, T., Gardiner, D. L., Tilley, L. (2008b). 'Targeted mutagenesis of the ring-exported protein-1 of Plasmodium falciparum disrupts the architecture of Maurer's cleft organelles', *Molecular Microbiology,* 69/4: 938-953.

Hanssen, E., Carlton, P., Deed, S., Klonis, J., Sedat, J., DeRisi, J., Tilley, L. (2010). 'Whole cell imaging reveals novel modular features of the exomembrane system of the malaria parasite Plasmodium falciparum', *International Journal of Parasitology,* 40/1: 123-134.

Hawking, F., Wilson, M. E., Gammage, K. (1971). 'Evidence for cyclic development and short-lived maturity in the gametocytes of Plasmodium falciparum', *Transactions of the Royal Society of Tropical Medicine and Hygiene*, 65/5: 549-559.

Hawthorne, P. L., Trenholme, K. R., Skinner-Adams, T. S., Spielmann, T., Fischer, K., Dixon, M. W. A., Ortega, M. R. et al. (2004). 'A novel Plasmodium falciparum ring stage protein, REX, is located in Maurer's clefts', *Molecular & Biochemical Parasitology,* 136: 181-189.

Heiber, A., Kruse, F., Pick, C., Grüring, C., Flemming, S., Oberli, A., Schoeler, H. et al. (2013). 'Identification of new PNEPs indicates a substantial non-PEXEL exportome and underpins common features in Plasmodium falciparum protein export', *PLoS Pathogens*, 9/8: e1003546.

Hill, R. J., Konigsberg, W., Guidotti, G., Craig, L. C. (1962). 'The structure of human hemoglobin', *The Journal of Biological Chemistry*, 237/5: 1549-1554.

Hiller, N. L., Bhattacharjee, S., van Ooij, C., Liolios, K., Harrison, T., Lopez-Estraño, C., & Haldar, K. (2004). 'A host-targeting signal in virulence proteins reveals a secretome in malarial infection', *Science*, 306/5703: 1934–1937.

Horuk, R., Chitnis, C. E., Darbonne, W. C., Colby, T. J., Rybicki, A., Hadley, T. J., Miller, L. H. (1993). 'A receptor for the malarial parasite Plasmodium vivax: the erythrocyte chemokine receptor', *Science*, 261(5125): 1182-1184.

Hsiao, C.-H. C., Hiller, N. L., Haldar, K., Knoll, L. J. (2013). 'A HT/PEXEL motif in Toxoplasma dense granule proteins is a signal for protein cleavage but not export into the host cell', *Traffic*, 14/5: 519-531.

Introini, V., Govendir, M. A., Rayner, J. C., Cicuta, P., Bernabeu, M. (2022). 'Biophysical tools and concepts enable understanding of asexual blood stage malaria', *Frontiers in Cellular and Infection Microbiology,* 12: 908241.

Janouskovec, J., Horák, A., Oborník, M., Lukes, J., Keeling, P. J. (2010). 'A common red algal origin of the apicomplexan, dinoflagellate, and heterokont plastids', *Proceedings of the National Academy of Sciences of the United States of America,* 107/24: 10949-10954.

Jinek, M., Chylinski, K., Fonfara, I., Hauer, M., Doudna, J. A., Charpentier, E. (2012). 'A programmable dual-RNA-guided DNA endonuclease in adaptive bacterial immunity', *Science,* 337/6096: 816-821.

Joice, R., Nilsson, S. K., Montgomery, J., Dankwa, S., Egan, E., Morahan, B., Seydel, K. B. (2014). 'Plasmodium falciparum transmission stages accumulate in the human bone marrow', *Science Translational Medicine,* 6/244.

Jones, M. L., Das, S., Belda, H., Collins, C. R., Blackman, M. J., Treeck, M. (2016). 'A versatile strategy for rapid conditional genome engineering using loxP sites in a small synthetic intron in Plasmodium falciparum', *Scientific Reports*, 6/21800.

Jonsdottir, T. K., Counihan, N. A., Modak, J. K., Kouskousis, B., Sanders, P. R., Gabriela, M., Bullen, H. E. et al. (2021). 'Characterisation of complexes formed by parasite proteins exported into the host cell compartment of Plasmodium falciparum infected red blood cells', *Cellular Microbiology,* e13332.

Knuepfer, E., Rug, M., Klonis, N., Tilley, L., Cowman, A. F. (2005). 'Trafficking of the major virulence factor to the surface of transfected P falciparum-infected erythrocytes', *Blood*, 105/10: 4078-4087.

Knuepfer, E., Rug, M., Klonis, N., Tilley, L., Cowman, A. F. (2005). 'Trafficking determinants for PfEMP3 export and assembly under the Plasmodium falciparum-infected red blood cell membrane', *Molecular Microbiology*, 58/4: 1039-1053.

Knuepfer, E., Napiorkowska, M., van Ooij, C., Holder, A. A. (2017). 'Generating conditional gene knockouts in Plasmodium – a toolkit to produce stable DiCre recombinase-expressing parasite lines using CRISPR/Cas9', *Scientific Reports,* 7/3881.

Korteweg, P. C. (1902). 'Klinische obsersvaties over malaria in den winter van 1901-,02', *herinneringsbundel voor Prof. Rosenstein. Leiden*. 263-281.

Külzer, S., Rug, M., Brinkmann, K., Cannon, P., Cowman, A., Lingelbach, K. Blatch, G. L. et al. (2010). 'Parasite-encoded Hsp40 proteins define novel mobile structures in the cytosol of the P. falciparum – infected erythrocyte', *Cellular Microbiology,* 12/10: 1398-1420.

Külzer, S., Charnaud, S., Dagan, T., Riedel, J., Mandal, P., Pesce, E. R., Blatch, G. L. et al. (2012). 'Plasmodium falciparum-encoded exported hsp70/hsp40 chaperone/co-chaperone complexes within the host erythrocyte', *Cellular Microbiology*, 14/11: 1784-1795.

Kudyba, H. M., Cobb, D. W., Vega-Rodriguez, J., Mualidharan, V. (2021). 'Some conditions apply: Systems for studying Plasmodium falciparum protein function', *PLoS Pathogens,* 17/4: e1009442.

Lambros, C., & Vanderberg, J. P. (1979). 'Synchronization of Plasmodium falciparum erythrocytic stages in culture', *The Journal of parasitology*, 65/3: 418–20.

Lanzer, M., Wickert, H., Krohne, G., Vincensini, L., Braun Breton, C. (2006). 'Maurer's clefts: A novel multi-functional organelle in the cytoplasm of Plasmodium falciparum-infected erythrocyte', *International Journal for Parasitology,* 36: 23-36.

Lee, M. C. S., Lindner, S. E., Lopez-Rubio, J.-J., Llinás, M. (2019). 'Cutting back malaria: CRISPR/Cas9 genome editing of Plasmodium', *Briefings in Functional Genomics,* 18/5: 281-289.

Lingelbach, K. & Joiner, K. A. (1998). 'The parasitophorous vacuole membrane surrounding Plasmodium and Toxoplasma: an unusual compartment in infected cells', *Journal of Cell Science,* 111: 1467-1475.

López-Barragán, M. J., Lemieux, J., Quiñones, M., Williamson, K. C., Molina-Cruz, A., Cui, K., Barillas-Mury, C. et al. (2011). 'Directional gene expression and antisense transcripts in sexual and asexual stages of Plasmodium falciparum', *BMC Genomics,* 12/587.

Luse, S. A., Miller, L. H. (1971). 'Plasmodium falciparum malaria. Ultrastructure of parasitized erythrocytes in cardiac vessels', *American Journal of Tropical Medicine and Hygiene,* 20/5: 655-660.

MacPherson, G. G., Warrell, M. J., White, N. J., Looareesuwan, S., Warrell, D. A. (1985). 'Human cerebral malaria. A quantitative ultrastructural analysis of parasitized erythrocyte sequestration', *The American Journal of Pathology*, 119/3: 385-401.

Maier, A. G., Braks, J. A. M., Waters, A. P., Cowman, A. F. (2006). 'Negative selection using yeast cytosine deaminase/uracil phosphoribosyl transferase in Plasmodium falciparum for targeted gene deletion by double crossover recombination', *Molecular and Biochemical Parasitology*, 150/1: 118-121.

Maier, A. G., Rug, M., O'Neill, M. T., Brown, M., Chakarvorty, S., Szestak, Tadge, Chesson, Joanne et al. (2008). 'Exported proteins required for virulence and rigidity of Plasmodium falciparum-infected human erythrocytes', *Cell,* 134: 48-61.

Maier, A. G., Cooke, B. M., Cowman, A. F., & Tilley, L. (2009). 'Malaria parasite proteins that remodel the host erythrocyte', *Nature Reviews Microbiology*, 7/5: 341–54. Nature Publishing Group.

Maier, A. G., Matuschewski, K., Zhang, M., Rug, M. (2019). 'Plasmodium falciparum', *Trends in Parasitology,* 35/6: 481-482.

Marapana, D. S., Dagley, L. F., Sandow, J. J., Nebl, T., Triglia, T., Pasternak, M., Dickerman, B. K. et al. (2018). 'Plasmepsin V cleaves malaria effector proteins in a distinct endoplasmatic reticulum translocation interactome for export to the erythrocyte', *Nature Microbiology*, 3: 1010-1022.

Marti, M., Good, R. T., Rug, M., Knuepfer, E., & Cowman, A. F. (2004). 'Targeting Malaria Virulence and Remodeling Proteins to the Host Erythrocyte', *Science*, 306/5703: 1930–3.

Matthews, K. M., Pitman, E. L., de Koning-Ward, T. F. (2018). 'Illuminating how malaria parasites export proteins into host erythrocytes', *Cellular Microbiology,* 21: e13009.

Matz, J. M., Beck, J. R., Blackman, M. J. (2020). 'The parasitophorous vacuole of the blood-stage malaria parasite', *Nature Reviews Microbiology,* 18/10.1038.

Maurer, G. (1902). 'Die Malaria perniciosa', *Centralblatt für Bakteriologie. Parasitenkunde und Infektionskrankheiten*, 32: 695-719.

Mayer, D. C. G. (2021). 'Protein sorting in Plasmodium falciparum', *Life,* 11/937.

McHugh, E., Batinovic, S., Hanssen, E., McMillan, P. J., Kenny, S., Griffin, M. D. W., Crawford, S. et al. (2015). 'A repeat sequence domain of the ring-exported protein-1 of Plasmodium falciparum controls export machinery architecture and virulence protein trafficking', *Molecular Microbiology,* 98/6: 1101-1114.

McHugh, E., Carmo, O. M. S., Blanch, A., Looker, O., Liu, B., Tiash, S., Andrew, D. et al. (2020). 'Role of Plasmodium falciparum protein GEXP07 in Maurer's cleft morphology, knob architecture, and P. falciparum EMP1 trafficking', *mBio,* 11:e03320-19.

Ménard, R., Sultan, A. A., Cortes, C., Altszuler, R., van Dijk, M. R., Janse, C. J., Waters, A. P. et al. (1997). 'Circumsporozoite protein is required for development of malaria sporozoites in mosquitoes', *Nature*, 385: 336-340.

Ménard, D., Barnadas, C., Bouchier, C., Henry-Halldin, C., Gray, L. R., Ratsimbasoa, A., Thonier, V. et al. (2010). 'Plasmodium vivax clinical malaria is commonly observed in Duffy-negative Malagasy people', *Proceedings of the National Academy of Sciences of the United States of America,* 107/13: 5967-5971.

Mesen-Ramirez, P., Bergmann, B., Tran, T.T., Garten, M., Stäcker, J., Naranjo-Prado, I., Höhn, K. et al. (2019). 'EXP1 is critical for nutrient uptake across the parasitophorous vacuole membrane of malaria parasites', *PLoS Biology,* 17/9: e3000473.

Mikkelsen, R. B., Kamber, M., Wadwa, K. S., Lin, P.-S., Schmidt-Ullrich, R. (1988). 'The role of lipids in Plasmodium falciparum invasion of erythrocytes: A coordinated biochemical and microscopic analysis', *Proceedings of the National Academy of Sciences of the United States of America,* 85: 5956-5960.

Mitchell, D., Bell, A. (2003). 'PEST sequences in the malaria parasite Plasmodium falciparum: a genomic study', *Malaria Journal,* 2/16.

Moore, R. B., Oborník, M., Janouskovek, J., Chrudimsky, T., Vancová, M., Green, D. H., Wright, S. W. et al. (2008). 'A photosynthetic alveolate closely related to apicomplexan parasites', *Nature*, 451: 959-963.

Oborník, M., Vancová, M., Lai, D.-H., Janouskovek, J., Keeling, P. J., Lukes, J. (2011). 'Morphology and ultrastructure of multiple life cycle stages of the photosynthetic relative of Apicomplexa, Chromera velia', *Protist*, 162/1: 115-130.

Oborník, M., Modry, D., Lukes, M., Cerrnotíková-Strbrná, E., Cihlár, J., Tesarová, M., Kotabová, E. et al. (2012). 'Morphology, ultrastructure and life cycle of Vitrella brassicaformis n. sp., n. gen., a novel chromerid from the great barrier reef', *Protist*, 163/2: 306-323.

Ochola, L. B., Siddondo, B. R., Ocholla, H., Nkya, S., Kimani, E. N., Williams, T. N., Makale, J. O. et al. (2011). 'Specific receptor usage in Plasmodium falciparum cytoadherence is associated with disease outcome', *PLoS ONE*, 6/3: e14741.

O'Donnell, R. A., Preiser, P. R., Williamson, D. H., Moore, P. W., Cowman, A. F., Crabb, B. S. (2001). 'An alteration in concatameric structure is associated with efficient segregation of plasmids in transfected Plasmodium falciparum parasites', *Nucleid Acids Research*, 29/3: 716-724.

Omelianczyk, R. I., Loh, H. P., Chew, M., Hoo, R., Baumgarten, S., Renia, L., Chen, J., Preiser, P., R. (2020). 'Rapid activation of distinct members of multigene families in Plasmodium spp', Nature *Communications Biology, 3:* 351.

O'Neal, A., J., Butler, L. R., Rolandelli, A., Gilk, S. D., Pedra, J. H. F. (2020). 'Lipid hijacking: A unifying theme in vector-borne diseases', *eLife,* 9: e61675.

Ouayoue Noutong, A. M. (2021). 'Elucidating the function of exported proteins important for the survival of the malaria parasite Plasmodium falciparum during its intra-erythrocytic development', *Heidelberg University.*

Pasloske, B. L., Baruch, D. I., van Schravendijk, M. R., Handunnetti, S. M., Aikawa, M., Fujioka, H., Taraschi, T. F. et al. (1993). 'Cloning and characterization of a Plasmodium falciparum gene encoding a novel high-molecular weight host membrane-associated protein, PfEMP3', *Molecular and Biochemical Parasitology,* 59/1: 59-72.

Pellé, K. G., Jiang, R. H. Y., Mantel, P.-Y., Xiao, Y.-P., Hjelmqvist, D., Gallego-Lopez, G. M., Lau, A., O. T. et al. (2015). 'Shared elements of host-targeting pathways among apicomplexan parasites of different lifestyles', *Cellular Microbiology*, 17/11: 1618-1639.

Piel, F. B., Hay, S. I., Gupta, S., Weatherall, D. J., Williams, T. N. (2013). 'Global burden of sickle cell anemia in children under five, 2010-2050: modelling based on demograrphics, excess mortality, and interventions', *PLoS Medicine*, 10/7: e1001484.

Pimenta, P. F., Touray, M., Miller, L. (1994). 'The journey of malaria sporozoites in the mosquito salivary gland', *The Journal of Eukaryotic Microbiology*, 41/6: 608-824.

Polino, A. J., Nasamu, A. S., Niles, J. C., Goldberg, D. E. (2020). 'Assessment of biological role and insight into druggability of the Plasmodium falciparum protease Plasmepsin V', *ACS Infectious Diseases,* 6: 738-746.

Pologe, L. G., Ravetch, J. V. (1986). 'A chromosomal rearrangement in a P. falciparum histidine-rich protein gene is associated with the knobless phenotype', *Nature,* 322:474-477.

Popovici, J., Roesch, C., Rougeron, V. (2020). 'The enigmatic mechanism by which Plasmodium vivax infects Duffy-negative individuals', *PLoS Pathogens,* 16/2: e1008258.

Prommana, P., Uthaipibull, C., Wongsombat, C., Kamchonwongpaisan, S., Yuthavong, Y., Knuepfer, E., Holder, A. A., et al. (2013). 'Inducible knockdown of Plasmodium gene expression using the glmS ribozyme', *PLoS ONE*, 8/8: e73783.

Prudêncio, M., Rodriguez, A., Mota, M. M. (2006). 'The silent path to thousands off merozoites: the Plasmodium liver stages', *Nature,* 4: 849-856.

Przyborski, J. M., Wickert, H., Krohne, G., Lanzer, M. (2003). 'Maurer's clefts – a novel secretory organelle?', *Molecular and Biochemical Parasitology*, 132/1: 17-26.

Przyborski, J. M., Nyboer, B., & Lanzer, M. (2016). 'Ticket to ride: export of proteins to the Plasmodium falciparum -infected erythrocyte', *Molecular Microbiology*, 101/1: 1–11.

Rajaram, K., Liu, H. B., Prigge, S. T. (2020). 'Redesigned TetR-aptamer system to control gene expression in Plasmodium falciparum', *mSphere,* 5:e00457-20.

Reddy, B. L. & Saier Jr., M. H. (2016). 'Properties and phylogeny of 76 families of bacterial and eukaryotic organellar outer membrane pore-forming proteins', *PLoS ONE*, 11/4: e0152733.

Reeder, J. C., Cowman, A. F., Davern, K. M., Beeson, J. G., Thompson, J. K., Rogerson, S. J., & Brown, G. V. (1999). 'The adhesion of Plasmodium falciparum-infected erythrocytes to chondroitin sulfate A is mediated by P. falciparum erythrocyte membrane protein 1', *Proceedings of the National Academy of Sciences of the United States of America*, 96/9: 5198–202.

Rocamora, F., Winzeler, E. A. (2020). 'Genomic approaches to drug resistance in malaria', *Annual Review in Microbiology,* 74:761-786.

Rogerson, S. J., Desai, M., Mayor, A., Sicuri, E., Taylor, S. M., van Eijk, A. M. (2018). 'Burden, pathology, and costs of malaria in pregnancy: new developments for an old problem', *Lancet Infectious Diseases,* 10/1016.

Rudzinska, M. A., Trager, W., Lewengrub, S. J., Gubert, E. (1976). 'An electron microscopic study of Babesia microti invading erythrocytes', *Cell and Tissue Research*, 169: 323-334.

Russo, I., Babbitt, S., Muralidharan, V., Butler, T., Oksman, A., Golsberg, D. E. (2010). 'Plasmepsin V licenses Plasmodium proteins for export into the host erythrocyte', *Nature*, 463: 632-636.

Saliba, K. J., Horner, H. A., Kirk, K. (1998). 'Transport and metabolism of the essential vitamin pantothenic acid in human erythrocytes infected with the malaria parasite Plasmodium falciparum', *Journal of Biological Chemistry,* 273/17: 10190-5.

Salmon, B. L., Oksman, A., Goldberg, D. E. (2000). 'Malaria parasite exit from the host erythrocyte: A two-step process requiring extraerythrocytic proteolysis , *Proceedings of the National Academy of Sciences,* 98/1: 271-276.

Sanchez, C. P., Karathanasis, C., Sanchez, R., Cyrklaff, M., Jäger, J., Buchholz, B., Schwarz, U. S. et al. (2019). 'Single-molecule imaging and quantification of the immune-variant adhesin VAR2CSA on knobs of Plasmodium falciparum-infected erythrocytes', *Nature Communications Biology,* 2/172.

Sanchez, C. P., Patra, P., Chang, S.-Y. S., Karathanasis, C., Hanebutte, L., Kilian, N., Cyrklaff, M. et al. (2021). 'KAHRP dynamically relocalizes to remodeled actin junctions and associates with knob spirals in Plasmodium falciparum-infected erythrocytes', *Molecular Biology,* 117: 274-292.

Sargeant, T. J., Marti, M., Caler, E., Carlton, J. M., Simpson, K., Speed, T. P., Cowman, A. F. (2006). 'Lineage-specific expansion of proteins exported to erythrocytes in malaria parasites', *Genome Biology*, 7/2.

Saridaki, T., Fröhlich, K. S., Braun-Breton, C., Lanzer, M. (2009). 'Export of PfSBP1 to the Plasmodium falciparum Maurer's clefts', *Traffic*, 10: 137-152.

Sato, S. (2021).'Plasmodium – a brief introduction to the parasite causing human malaria and their basic biology', *Journal of Physiological Anthropology,* 40/1.

Scherf, A., Hernandez-Rivas, R., Buffet, P., Bottius, E., Benatar, C., Pouvelle, B., Gysin, J., Lanzer, M. (1998). 'Antigenic variation in malaria: in situ switching, relaxed and mutually exclusive transcription of var genes during intra-erythrocytic development in Plasmodium falciparum', *The EMBO Journal*, 17/18: 5418-5426.

Schureck, M. A., Darling, J. E., Merk, A., Shao, J., Daggupati, G., Srinivasan, P., Olinares, P. D. B. et al. (2021). 'Malaria parasites use a soluble RhopH complex for erythrocyte invasion and an integral form for nutrient uptake', *eLife,* 10: e65282.

Shears, M. J., Nirujogi, R. S., Swearingen, K. E., Renuse, S., Mishra, S., Reddy, P. J., Moritz, R. L. et al. (2019). 'Proteomic analysis of Plasmodium merosomes: The link between liver and blood stages in malaria', *Journal of Proteome Research,* 18/9: 3404-3418.

Sidjanski, S. & Vanderberg, J. P. (1997). 'Delayed migration of Plasmodium sporozoites from the mosquito bite site to the blood', *American Journal of Tropical Medicine and Hygiene*, 57/4: 426-429.

Sinden, R. E., Talman, A., Marques, S. R., Wass, M. N., Sternberg, M. J. E. (2010). 'The flagellum in malarial parasites', *Current Opinion in Microbiology*, 13/4: 491-500.

Sleebs, B. E., Lopaticki, S., Marapana, D. S., O'Neill, M. T., Rajasekaran, P., Gazdik, M., Günther, S. et al. (2014). 'Inhibition of Plasmepsin V activity demonstrates its essential role in protein export, PfEMP1 display, and survival of malaria parasites', *PLoS Biology,* 12/7: e1001897.

Smith, J. D., Chitnis, C. E., Craig, A. G., Roberts, D. J., Hudson-Taylor, D. E., Peterson, D. S., Pinches, R. et al. (1995). 'Switches in expression of Plasmodium falciparum var genes correlate with changes in antigenic and cytoadherent phenotypes of infected erythrocytes', *Cell*, 82/1: 101-110.

Spycher, C., Rug, M., Pachlatko, E., Hanssen, E., Ferguson, D., Cowman, A. F., Tilley, L. et al. (2008). 'The Maurer's cleft protein MAHRP1 is essential for trafficking of PfEMP1 to the surface of Plasmodium falciparum-infected erythrocytes', *Molecular Microbiology,* 68: 1300-1314.

Sterling, C. R., Aikawa, M., Vanderberg, J. P. (1973). 'The passage of Plasmodium berghei sporozoites through the salivary glands of Anopheles stephensi: an electron microscope study', *Journal of Parasitology*, 59/4: 593-605.

Su, X.-Z., Heatwole, V. M., Wertheimer, S. P., Guinet, F., Herrfeldt, J. A., Peterson, D. S., Raveetch, J. A., Wellems, T. E. (1995). 'The large diverse gene family var encodes proteins involved in cytoadherence and antigenic variation of plasmodium falciparum-infected erythrocytes', *Cell*, 82/1: 89-100.

Surolia, N. & Padmanaban, G. (1992). 'De novo biosynthesis of heme offers a new chemotherapeutic target in the human malaria parasite', *Biochemical and Biophysical Research Communication*, 187/2: 744-750.

Tavares, J., Formaglio, P., Thiberge, S., Mordelet, E., van Rooijen, N., Medvinsky, A., Menard, R., Amino, R. (2013). 'Role of host cell traversal by the malaria sporozoite during liver infection', *Journal of Experimental Medicine,* 210/5: 905-915.

Taylor, S. M., Cerami, C., Fairhurst, R. M. (2013). 'Hemoglobinopathies: Slicing the gordian knot of Plasmodium falciparum malaria pathogenesis', *PLoS Pathogens,* 9/5: e1003327.

Thurnburn Manson, P. (1901). 'Experimental Malaria: Recurrence after Nine Months', *British Medical Journal*, 2(2115): 77.

Tinto, H., D'Alessandro, U., Sorgho, H., Valea, I., Tahita, M. C., Kabore, W., Kiemde, F. et al. (2015). 'Efficacy and safety of RTS,S/AS01 malaria vaccine with or without a booster dose in infants and children in Africa: final results of a phase 3, individually randomized, controlled trial', The *Lancet,* 386: 31-45.

Tonkin, C. J., van Dooren, G. G., Spurck, T. P., Struck, N. S., Good, R. T., Handman, E., Cowman, A. F., McFadden, G. I. (2004). 'Localization of organellar proteins in Plasmodium falciparum using a novel set of transfection vectors and a new immunofluorescence fixation method', *Molecular and Biochemical Parasitology,* 137: 13-21.

Treeck, M., Zacherl, S., Herrmann, S., Cabrera, A., Kono, M., Struck, N. S., Engelberg, K. et al. (2009). 'Functional analysis of the leading malaria vaccine candidate AMA-1 reveals an essential role for the cytoplasmic domain in the invasion process', *PLoS Pathogens,* 5/3: e1000322.

Tu, Z., Gormley, J., Sheth, V., Seydel, K. B., Taylor, T., Beare, N., Barrera, V. et al. (2021). 'Cerebral malaria: insight into pathology from optical coherence tomography', *Nature Scientific Reports,* 11:15722.

Turner, G. D., Ly, V. C., Nguyen, T. H., Tran, T. H., Nguyen, H. P., Bethell, D., Wyllie, S. et al. (1998). 'Systemic endothelial activation occurs in both mild and severe malaria. Correlating dermal microvascular endothelial cell phenotype and soluble cell adhesion molecules with disease severity', The *American Journal of Pathology*, 152/6: 1477-1487.

Turner, L., Lavstsen, T., Berger, S. S., Wang, C. W., Petersen, J. E. V., Avril, M., Brazier, A. J. et al. (2013). 'Severe malaria is associated with parasite binding to endothelial protein C receptor', *Nature*, 498(7455): 502-505.

Van der Pluijm, R. W., Tipura, R., Hoglund, R. M., Pyae Phyo, A., Lek, D., ul Islam, A., Ankivar, A. R. et al. (2020). 'Triple artemisinin-based combination therapies versus artemisinin-based combination therapies for uncomplicated Plasmodium falciparum malaria: a multicentre, open-label, randomized clinical trial', *The Lancet*, 395/10233: 1345-1360.

Van der Pluijm, R. W., Amaratunga, C., Dhorda, M., Dondorp, A. M. (2021). 'Triple artemisinin-based combination therapies for malaria – a new paradigm?', *Trends in Parasitology,* 10.1016.

Van Schaijk, B. C. L., Kumar, T. R. S., Vos, M. W., Richman, A., van Gemert, G.-J., Li, T., Eappen, A. G. et al. (2014). 'Type II fatty acid biosynthesis is essential for Plasmodium falciparum sporozoite development in the midgut of Anopheles mosquitoes', *Eukaryotic Cell*, 13/5: 550-559.

Vaughn, A. M., O'Neill, M. T., Tarun, A. S., Camargo, N., Phuong, T. M., Aly, A. S. I., Cowman, A. F., Kappe, S. H. I. (2009). 'Type II fatty acid synthesis is essential only for malaria parasite late liver stage development', *Cellular Microbiology*, 11/3: 506-520.

Vinetz, J. M. (2005). 'Plasmodium ookinete invasion of the mosquito midgut', *Current Topics in Microbiology and Immunology*, 295: 357-382.

Wahlgren, M., Goel, S., Akhouri, R. R. (2017). 'Variant surface antigens of Plasmodium falciparum and their roles in severe malaria', *Nature Reviews Microbiology,* 15:479-491.

Waller, R. F., Reed, M. B., Cowman, A. F., & McFadden, G. I. (2000). 'Protein trafficking to the plastid of Plasmodium falciparum is via the secretory pathway', *The EMBO Journal*, 19/8: 1794–1802.

Wang, P., Wang, Q., Sims, P. F. G., Hyde, J. E. (2007). 'Characterisation of exogenous folate transport in Plasmodium falciparum', *Molecular and Biochemical Parasitology,* 154/1: 40-51.

Ward, G. E., Miller, L. H., Dvorak, J. A. (1993). 'The origin of parasitophorous vacuole membrane lipids in malaria-infected erythrocytes', *Journal of Cell Science,* 106/1: 237-248.

WHO. (2021). 'Word Malaria report 2021'

Wickham, M. E., Rug, M., Ralph, S. A., Klonis, N., McFadden, G. I., Tilley, L., & Cowman, A. F. (2001). 'Trafficking and assembly of the cytoadherence complex in Plasmodium falciparum-infected human erythrocytes', *The EMBO journal*, 20/20: 5636–5649.

Williams, T. N., Mwangi, T. W., Wambua, S., Alexander, N. D., Kortok, M., Snow, R. W., Marsh, K. (2013). 'Sickle cell trait and the risk of Plasmodium falciparum malaria and other childhood diseases', *The Journal of Infectious Diseases*, 192/1: 178-186.

Winkler, W. C., Nahvi, A., Roth, A., Collins, J. A., Breaker, R. R. (2004). 'Control of gene expression by a natural metabolite-responsive ribozyme', *Nature*, 428: 281-286.

Wrenger, C., Eschbach, M.-L., Müller, I. B., Laun, N. P., Begley, T. P., Walter, R. D. (2006). 'Vitamin B1 de novo synthesis in the human malaria parasite Plasmodium falciparum depends on external provision of 4-amino-5-hydroxymethyl-2-metthylpyrimidine', *Journal of Biological Chemistry,* 387/1: 41-51.

Wu, Y., Sifri, C. D., Lei, H. H., Su, X. Z., & Wellems, T. E. (1995). 'Transfection of Plasmodium falciparum within human red blood cells', *Proceedings of the National Academy of Sciences*, 92/4: 973–977.

Wu, Y., Kirkman, L. A., Wellems, T. E. (1996). 'Transformation of Plasmodium falciparum malaria parasites by homologous integration of plasmids that confer resistance to pyrimethamine', *Proceedings of the National Academy of Sciences,* 93/3: 1130-1134.

Yeh, E. & DeRisi, J. L. (2011). 'Chemical rescue of malaria parasites lacking an apicoplast defines organelle function in blood-stage Plasmodium falciparum', PLoS Biology, 9/8: e1001138.

Yu, M., Santha Kumar, T. R., Nkrumah, L. J., Coppi, A., Retzlaff, S., Li, C. D., Kelly, B. J. et al. (2008). 'The fatty acid biosynthesis enzyme FabI plays a key role in the development of liver stage malarial parasites', *Cell Host & Microbe*, 4/6: 567-578.

Zhang, C., Xiao, B., Jiang, Y., Zhao, Y., Li ,Z., Gao, H., Ling, Y. et al. (2014). 'Efficient editing of malaria parasite genome using the CRISPR/Cas9 system', *mBio*, 5/4: e01414-14.

Zhang, Q., Ma, C., Oberli, A., Zinz, A., Engels, S., Przyborski, J. M. (2017). 'Proteomic analysis of exported chaperone/co-chaperone complexes of P. falciparum reveals an array of complex protein-potein interactions', *Scientific Reports*, 7/42188.

Zhang, M., Wang, C., Otto, T. D., Oberstaller, J., Liao, X., Adapa, S. R., Udenze, K. et al. (2018). 'Uncovering the essential genes of the human malaria parasite Plasmodium falciparum by saturation mutagenesis', *Science,* 360: eaap7847.

Zhu, G., Marchewka, M. J., Keithly, J. S. (2000). 'Cryptosporidium parvum appears to lack a plastid genome', *Microbiology*, 146/2: 315-321.

Supplements

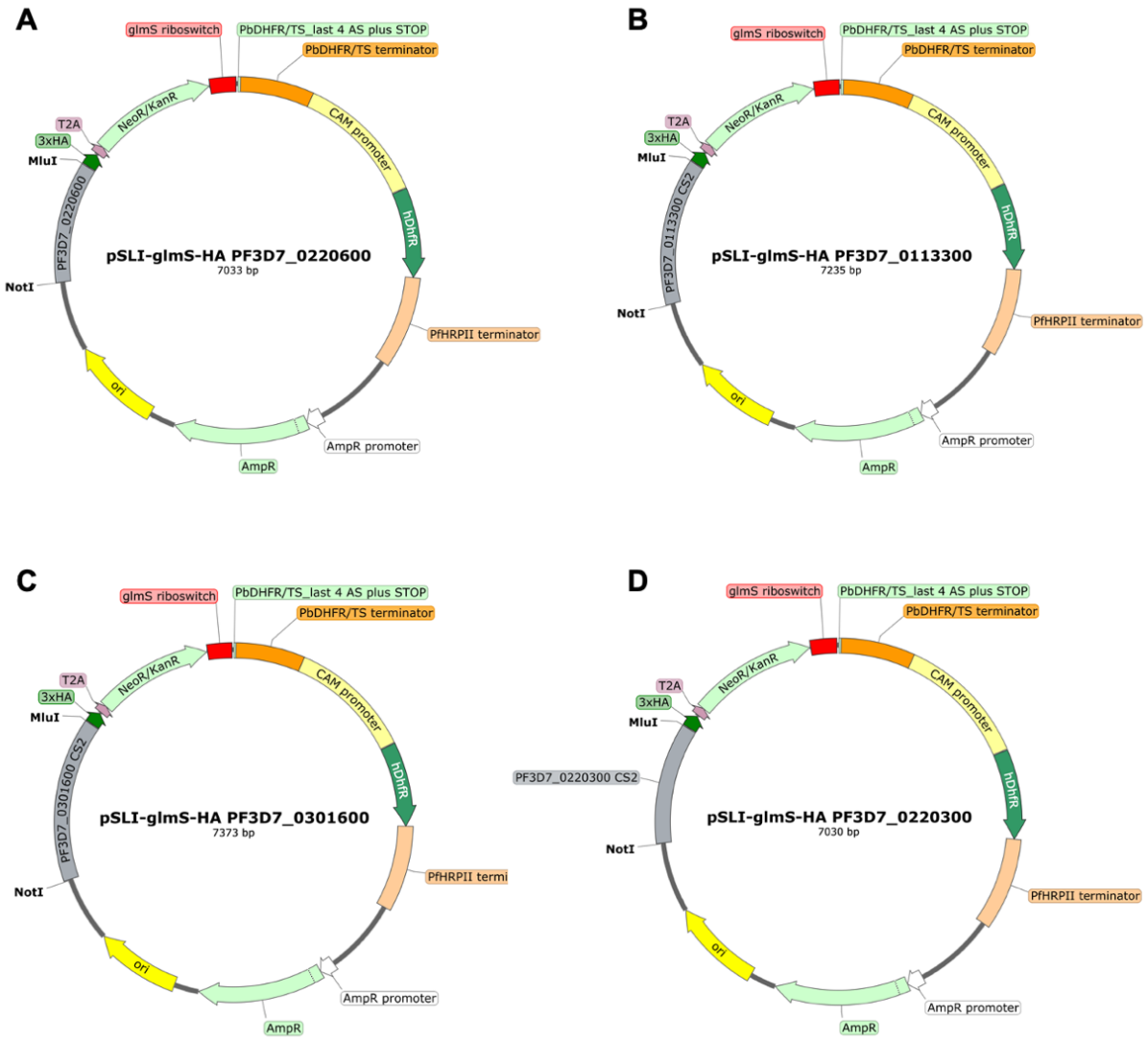

Suppl. 1: Maps of *glmS* plasmids used in this study. (A) pSLI-glmS-HA PF3D7_0220600 **(B)** pSLI-glmS-HA PF3D7_0113300 **(C)** pSLI-glmS-HA PF3D7_0301600 **(D)** pSLI-glmS-HA PF3D7_0220300. The gene sequence of the ortholog gene in CS2 was cloned into the plasmids. M9 control plasmids have a mutation in the *glmS* self-cleavage site (made with SnapGene).

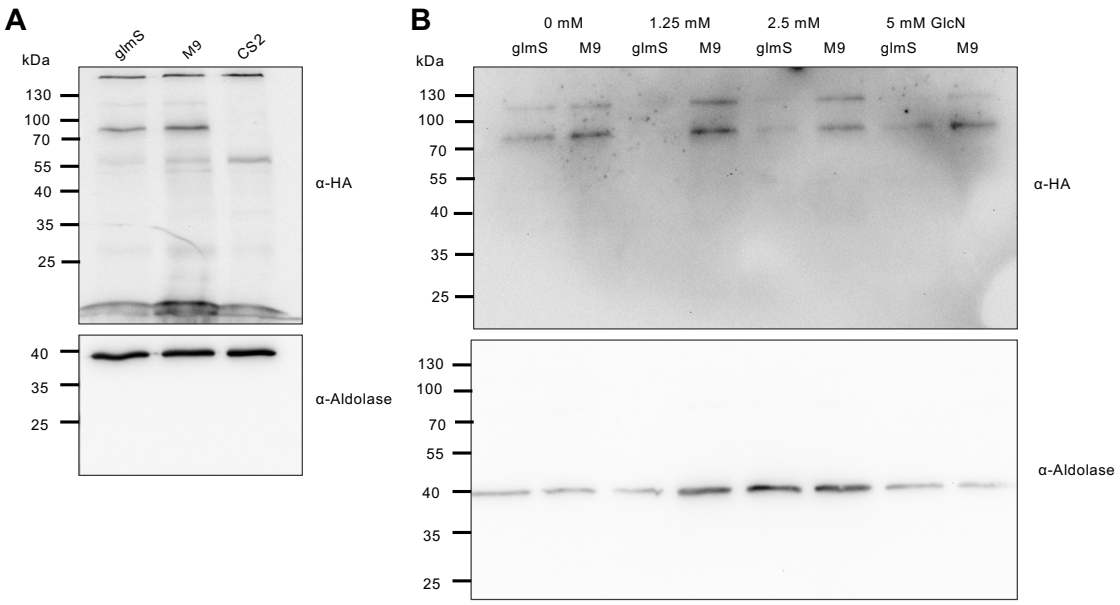

Suppl. 2: Full-size Western Blots: Verification of CS2PF3D7_0113300$^{glmS/M9}$ and efficiency of knockdown. A) Western blot analysis of enriched trophozoites shows the expression of the HA-tagged POI using α-HA (expected size ~66 kDa) and α-Aldolase (expected size ~40 kDa) as a loading control. The higher HA-band is an unskipped version of the HA-tagged POI bound to neomycin phosphotransferase (~30 kDa) **B)** Downregulation in asexual blood stages after cultivation with 0, 1.25, 2.5, and 5 mM glucosamine (GlcN) for 72 h. Western blot analysis of enriched trophozoites using α-HA (expected size ~66 kDa) and α-Aldolase (expected size ~40 kDa) as a loading control. Representative of three independent experiments.

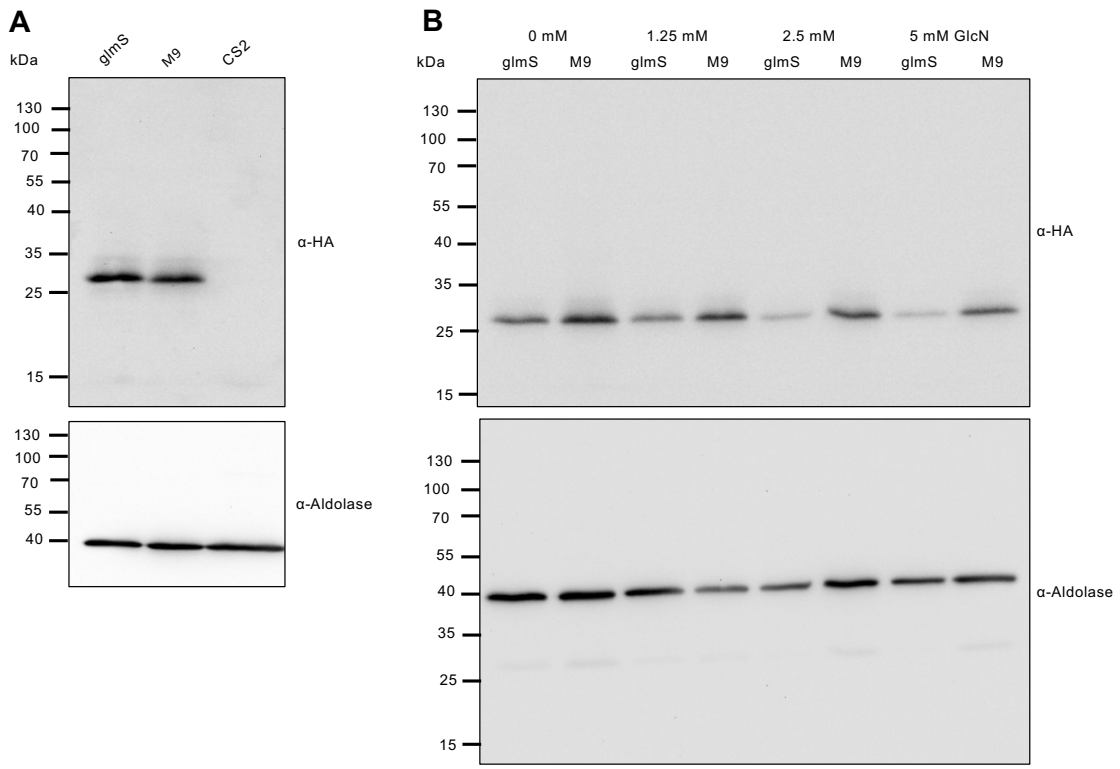

Suppl. 3: Full-size Western Blots: Verification of CS2PF3D7_0220300$^{glmS/M9}$ and efficiency of knockdown. A) Western blot analysis of enriched trophozoites shows the expression of the HA-tagged POI using α-HA (expected size ~22 kDa) and α-Aldolase (expected size ~40 kDa) as a loading control. **B)** Downregulation in asexual blood stages after cultivation with 0, 1.25, 2.5, and 5 mM glucosamine (GlcN) for 72 h. Western blot analysis of enriched trophozoites using α-HA (expected size ~22 kDa) and α-Aldolase (expected size ~40 kDa) as a loading control. Representative of three independent experiments.

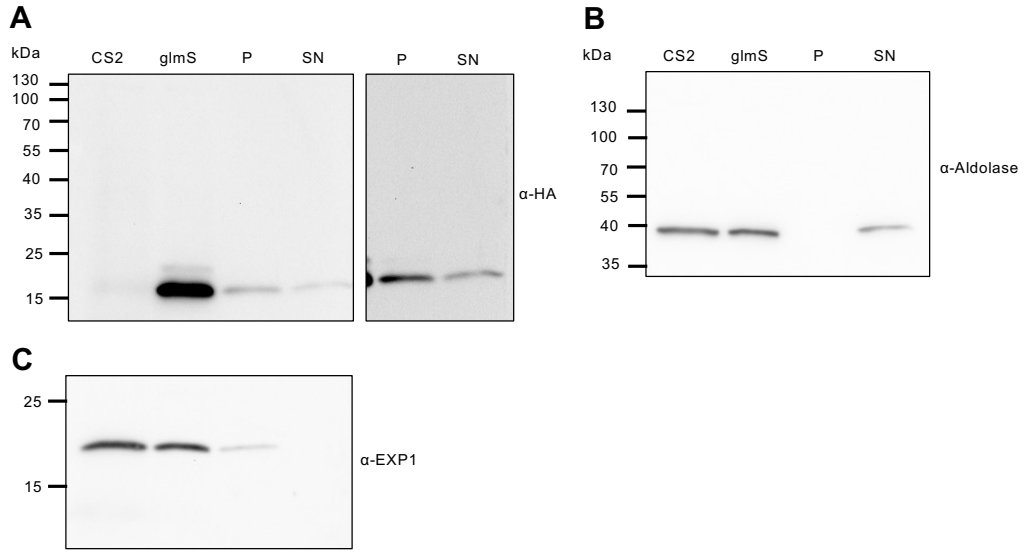

Suppl. 4: Full-size Western Blots: CS2PF3D7_0220300 is a membrane-bound protein. Enriched trophozoite-stage parasites were hypotonically lysed and analyzed in a Western blot. **A)** The HA-tagged POI was detected in the pellet (P) and supernatant (SN) fraction using α-HA (expected size ~22 kDa). **B)** Aldolase (expected size ~40 kDa) and C) EXP1 (expected size ~16 kDa) served as a control for soluble and membrane-bound proteins, respectively. Western Blots with two different exposure times for HA.

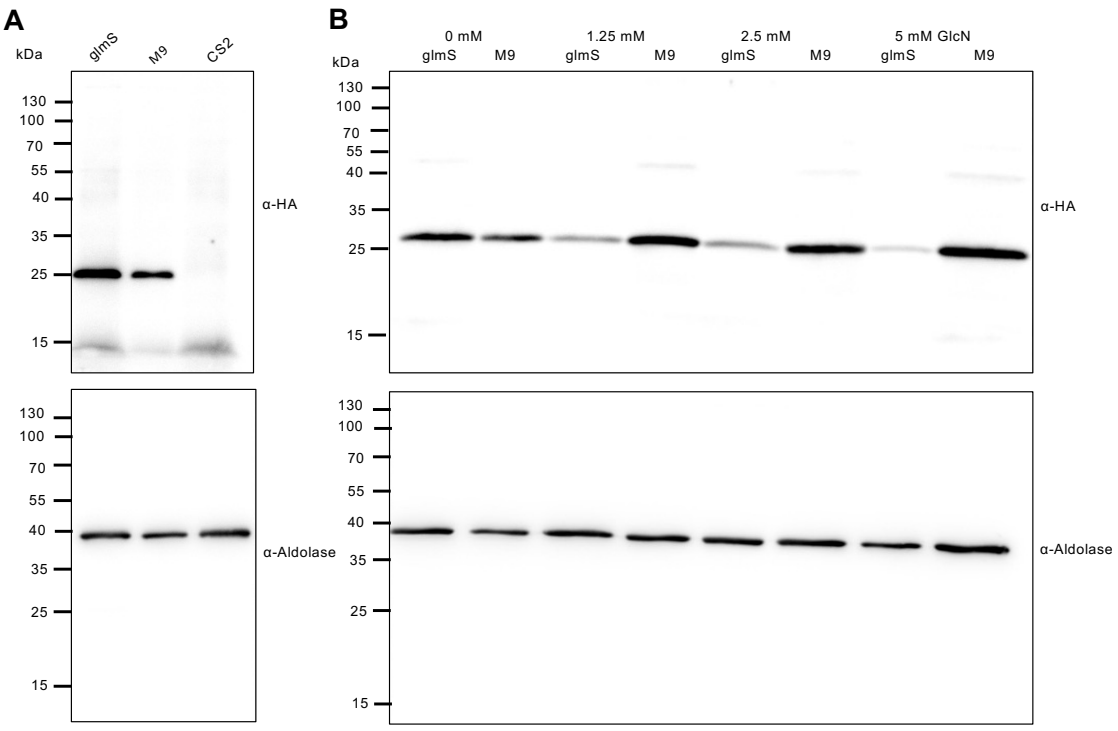

Suppl. 5: Full-size Western Blots: Verification of CS2PF3D7_0220600$^{glmS/M9}$ and efficiency of knockdown. A) Western blot analysis of enriched trophozoites shows the expression of the HA-tagged POI using α-HA (expected size ~24 kDa) and α-Aldolase (expected size ~40 kDa) as a loading control. **B)** Downregulation in asexual blood stages after cultivation with 0, 1.25, 2.5, and 5 mM glucosamine (GlcN) for 72 h. Western blot analysis of enriched trophozoites using α-HA (expected size ~24 kDa) and α-Aldolase (expected size ~40 kDa) as a loading control. Representative of three independent experiments.

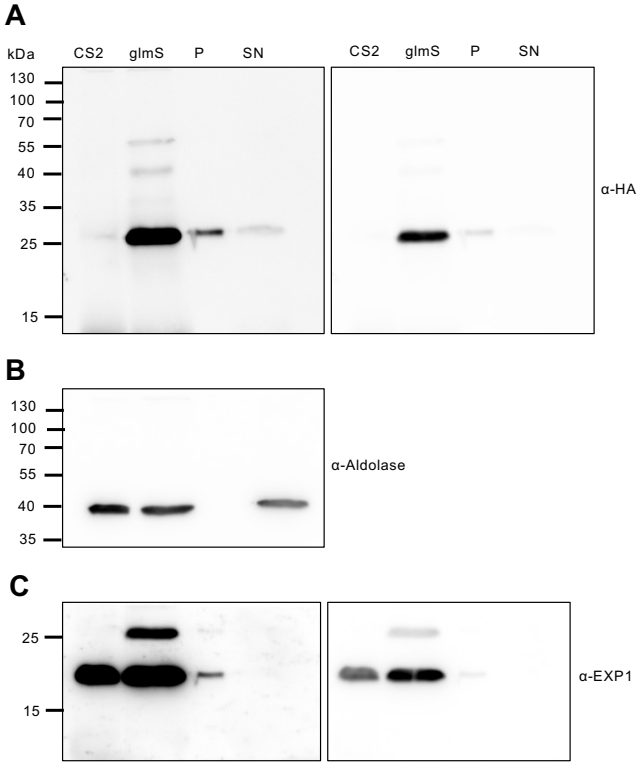

Suppl. 6: Full-size Western Blots: CS2PF3D7_0220600 is a membrane-bound protein. Enriched trophozoite-stage parasites were hypotonically lysed and analyzed in a Western blot. **A)** The HA-tagged POI was detected in the pellet (P) and supernatant (SN) fraction using α-HA (expected size ~24 kDa). **B)** Aldolase (expected size ~40 kDa) and **C)** EXP1 (expected size ~16 kDa) served as a control for soluble and membrane-bound proteins, respectively. Western Blots with two different exposure times for HA and EXP1.

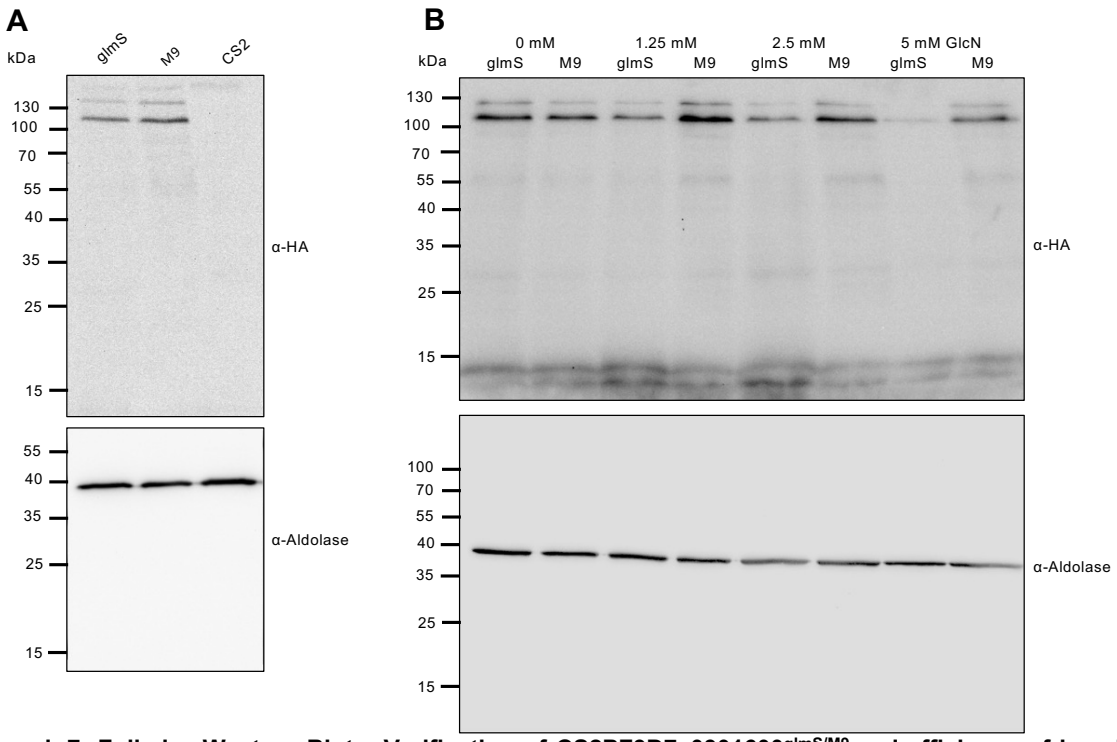

Suppl. 7: Full-size Western Blots: Verification of CS2PF3D7_0301600$^{glmS/M9}$ and efficiency of knockdown. A) Western blot analysis of enriched trophozoites shows the expression of the HA-tagged POI using α-HA (expected size ~82 kDa) and α-Aldolase (expected size ~40 kDa) as a loading control. The higher HA-band is an unskipped version of the HA-tagged POI bound to neomycin phosphotransferase (~30 kDa) **B)** Downregulation in asexual blood stages after cultivation with 0, 1.25, 2.5, and 5 mM glucosamine (GlcN) for 72 h. Western blot analysis of enriched trophozoites using α-HA (expected size ~22 kDa) and α-Aldolase (expected size ~40 kDa) as a loading control. Representative of three independent experiments.

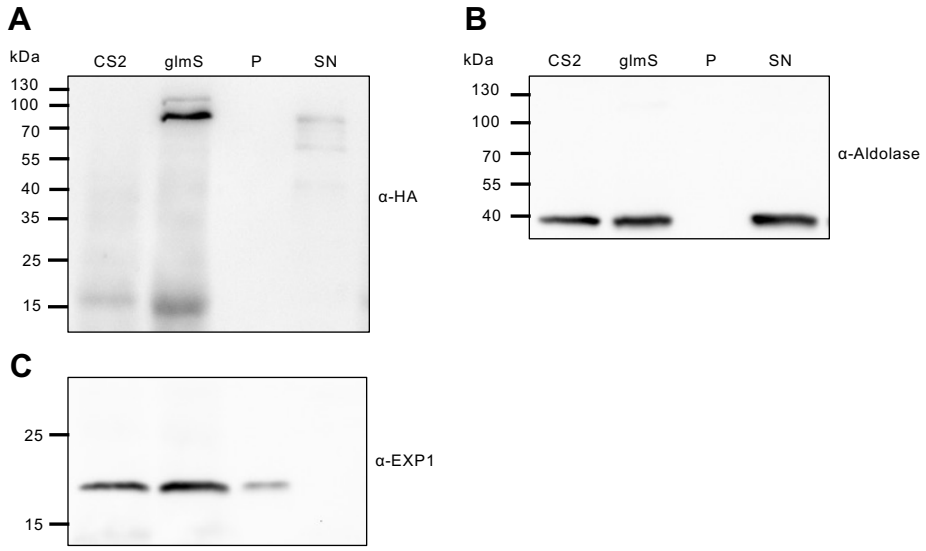

Suppl. 8: Full-size Western Blots: CS2PF3D7_0301600 is a soluble protein. Enriched trophozoite-stage parasites were hypotonically lysed and analyzed in a Western blot. **A)** The HA-tagged POI was detected in supernatant (SN) fraction using α-HA (expected size ~ 82 kDa). **B)** Aldolase (expected size ~40 kDa) and **C)** EXP1 (expected size ~16 kDa) served as a control for soluble and membrane-bound proteins, respectively.

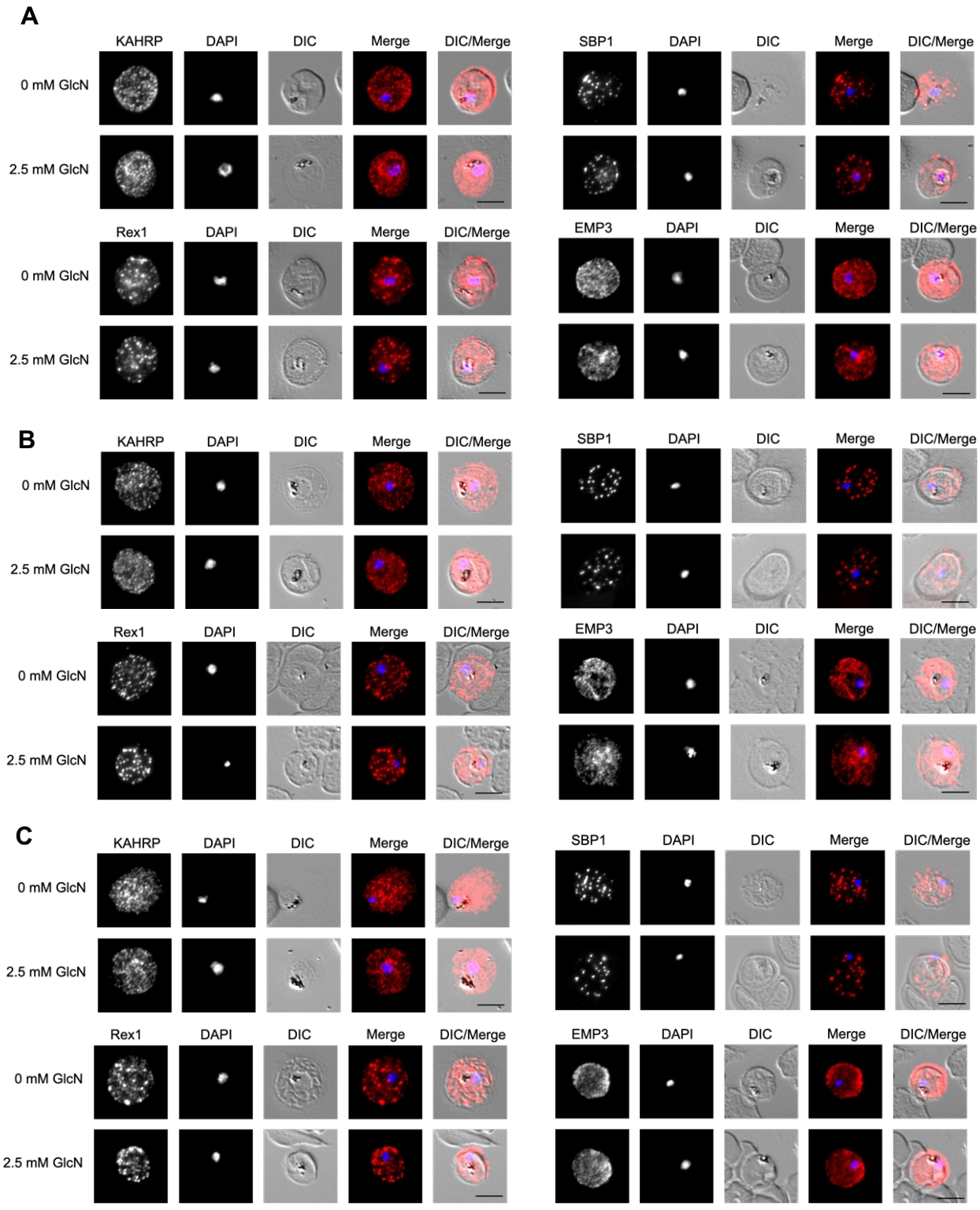
A
KAHRP
DAPI
DIC
Merge
DIC/Merge
SBP1
0 mM GlcN
2.5 mM GlcN
Rex1
EMP3
B
C

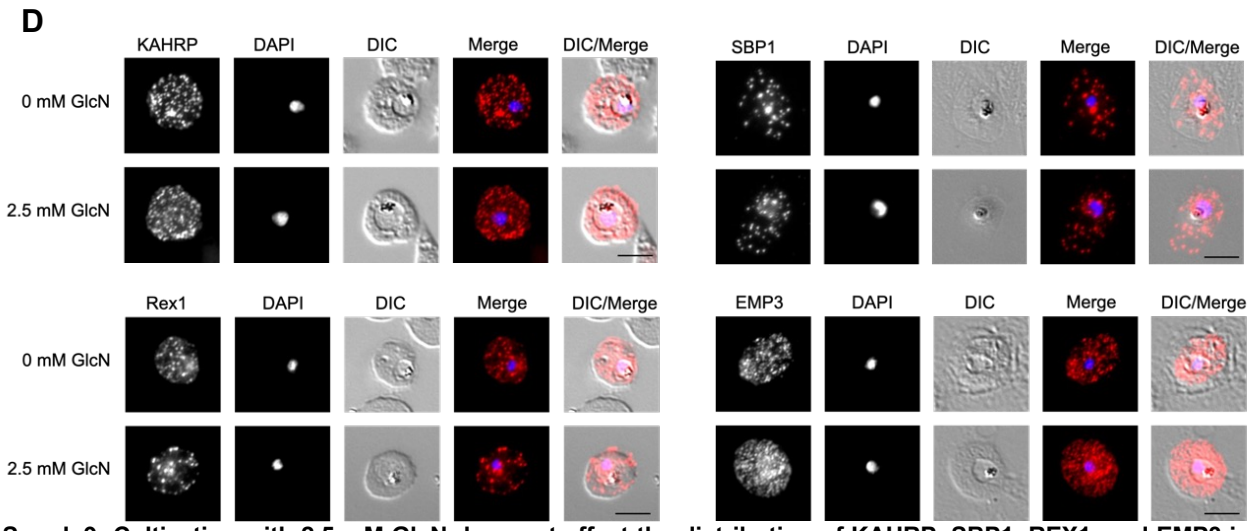

Suppl. 9: Cultivation with 2.5 mM GlcN does not affect the distribution of KAHRP, SBP1, REX1, and EMP3 in *glmS* cell lines. Immunolabelling of the exported proteins KAHRP, SBP1, REX1, and EMP3 with the respective primary antibodies and Cy3-conjugated secondary antibodies (red) in CS2PF3D7_0220600^{glmS} **(A)**, CS2PF3D7_0113300^{glmS} **(B)**, CS2PF3D7_0220300^{glmS} **(C)** and CS23D7_0301600^{glmS} **(D)**. The nuclei were highlighted with DAPI (blue). Erythrocytes infected with trophozoites were fixed on slides with acetone/10% MeOH after cultivation ±2.5 mM GlcN for 72 h. Images were edited in ImageJ 2.3.0. Scale bar 5 µm.

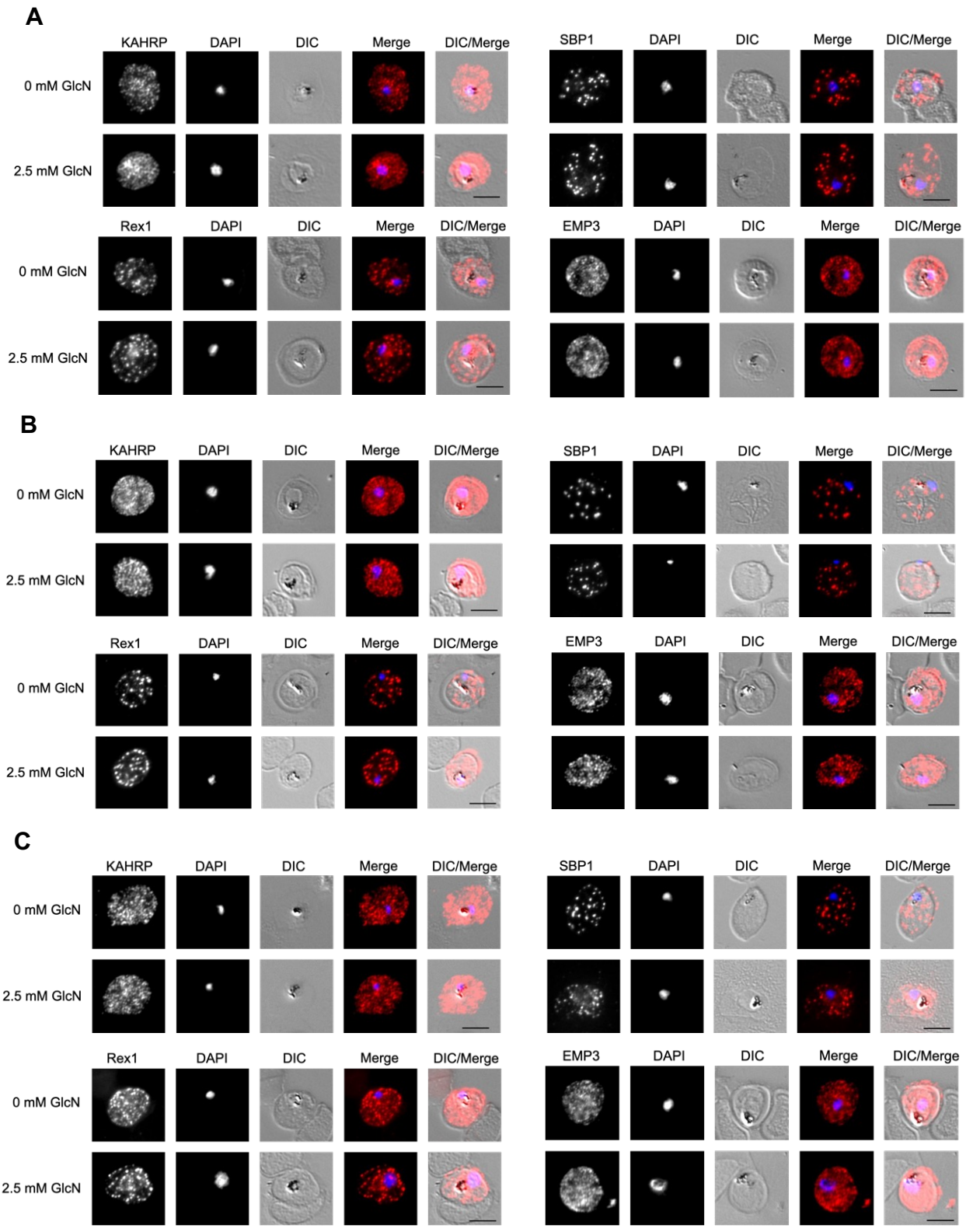
A
KAHRP
DAPI
DIC
Merge
DIC/Merge
SBP1
0 mM GlcN
2.5 mM GlcN
Rex1
EMP3
B
C

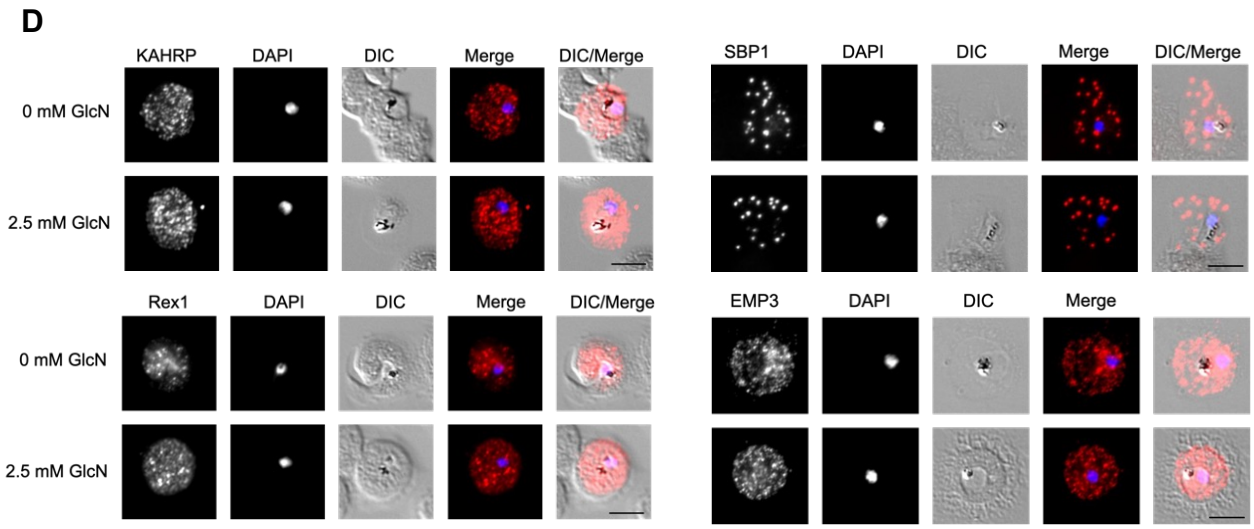

Suppl. 10: Cultivation with 2.5 mM GlcN does not affect the distribution of KAHRP, SBP1, REX1, and EMP3 in M9 cell lines. Immunolabelling of the exported proteins KAHRP, SBP1, REX1, and EMP3 with the respective primary antibodies and Cy3-conjugated secondary antibodies (red) in CS2PF3D7_0220600^{M9} **(A)**, CS2PF3D7_0113300^{M9} **(B)**, CS2PF3D7_0220300^{M9} **(C)** and CS23D7_0301600^{M9} **(D)**. The nuclei were highlighted with DAPI (blue). Erythrocytes infected with trophozoites were fixed on slides with acetone/10% MeOH after cultivation ±2.5 mM GlcN for 72 h. Images were edited in ImageJ 2.3.0. Scale bar 5 µm.

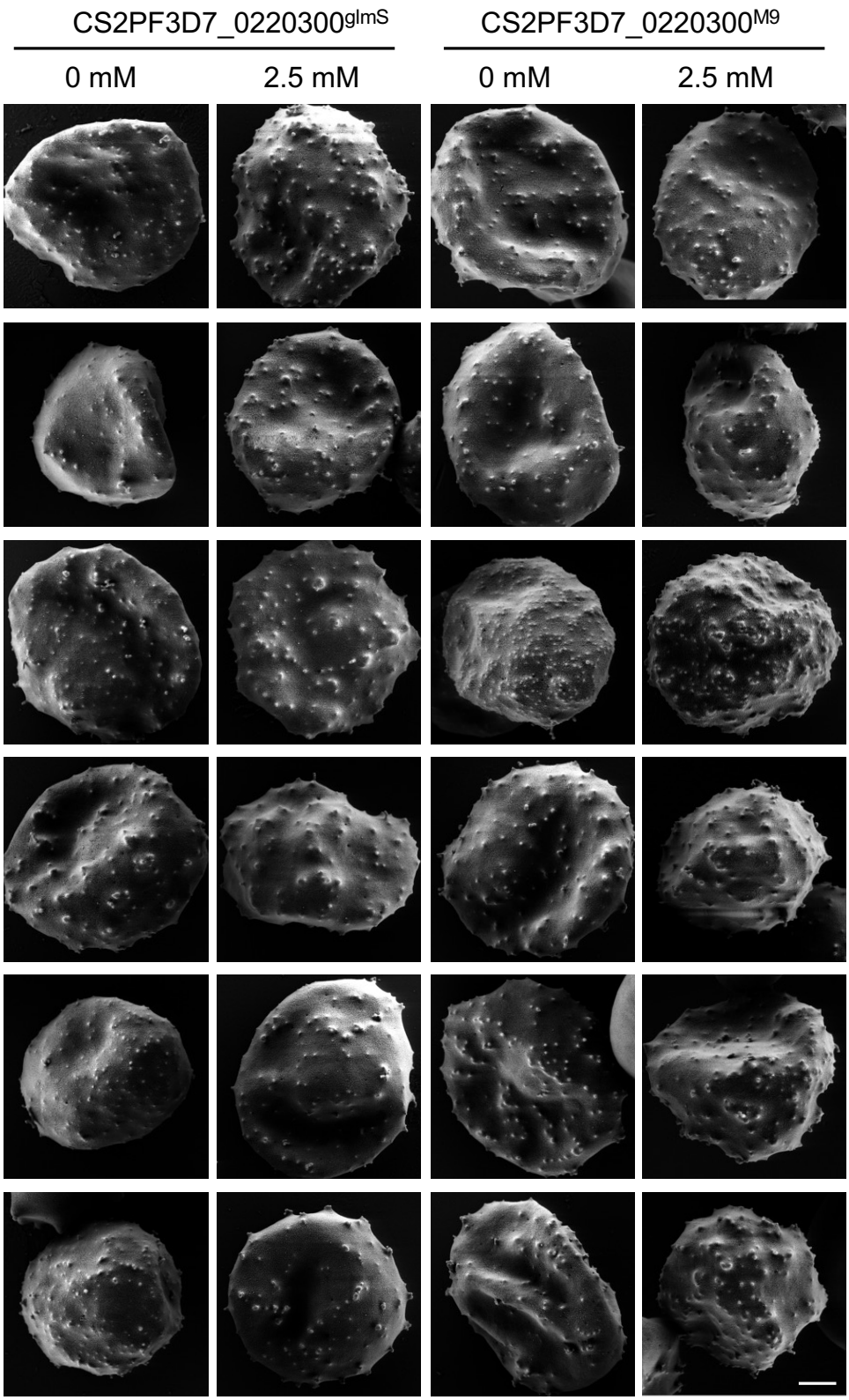

Suppl. 11: Scanning electron microscopy (SEM) images of CS2PF3D7_0220300$^{glmS/M9}$. Parasite-infected erythrocytes ± 2.5 mM GlcN. Scale bar 1 µm.

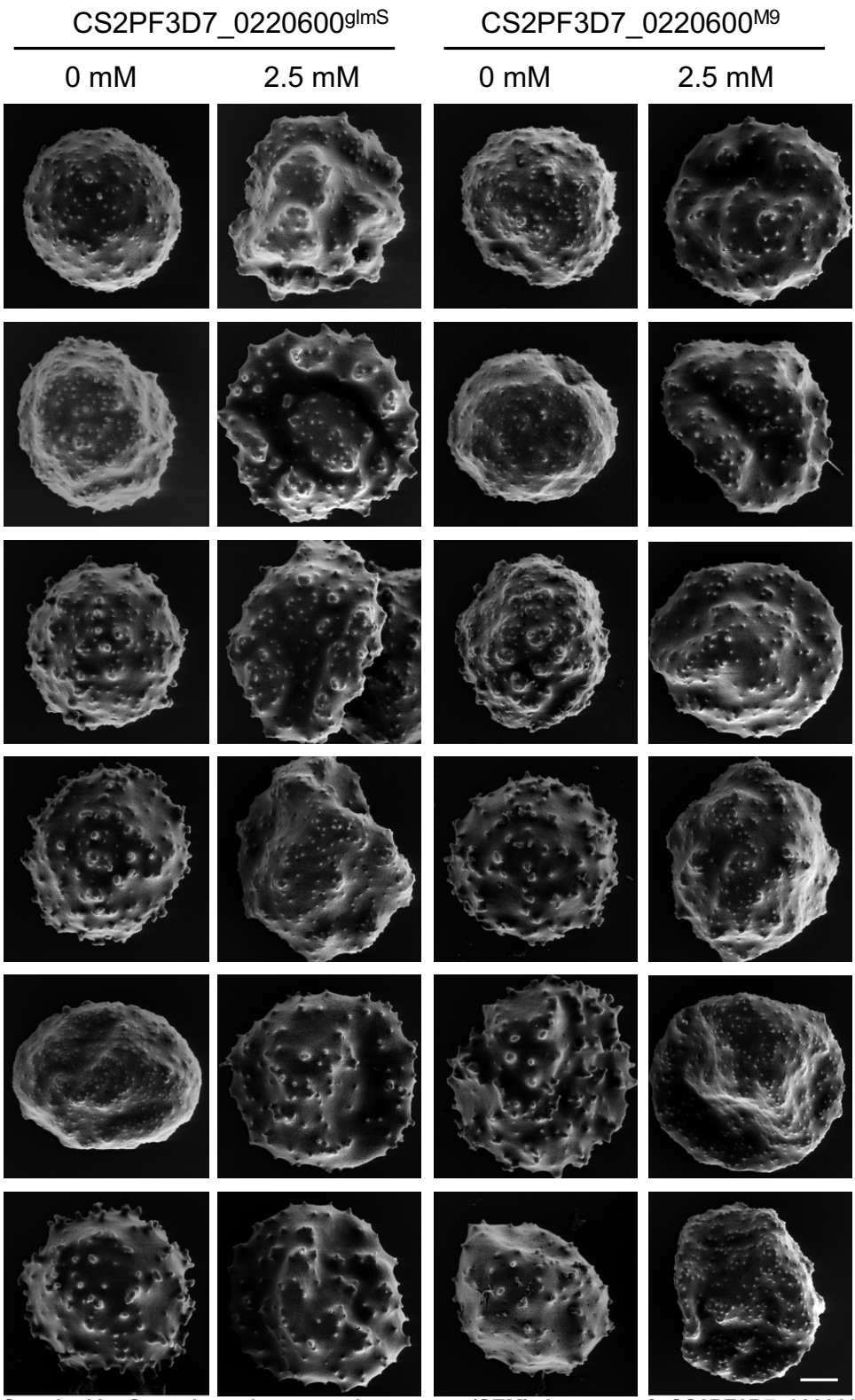

Suppl. 12: Scanning electron microscopy (SEM) images of CS2PF3D7_0220600$^{glmS/M9}$. Parasite-infected erythrocytes ± 2.5 mM GlcN. Scale bar 1 µm.

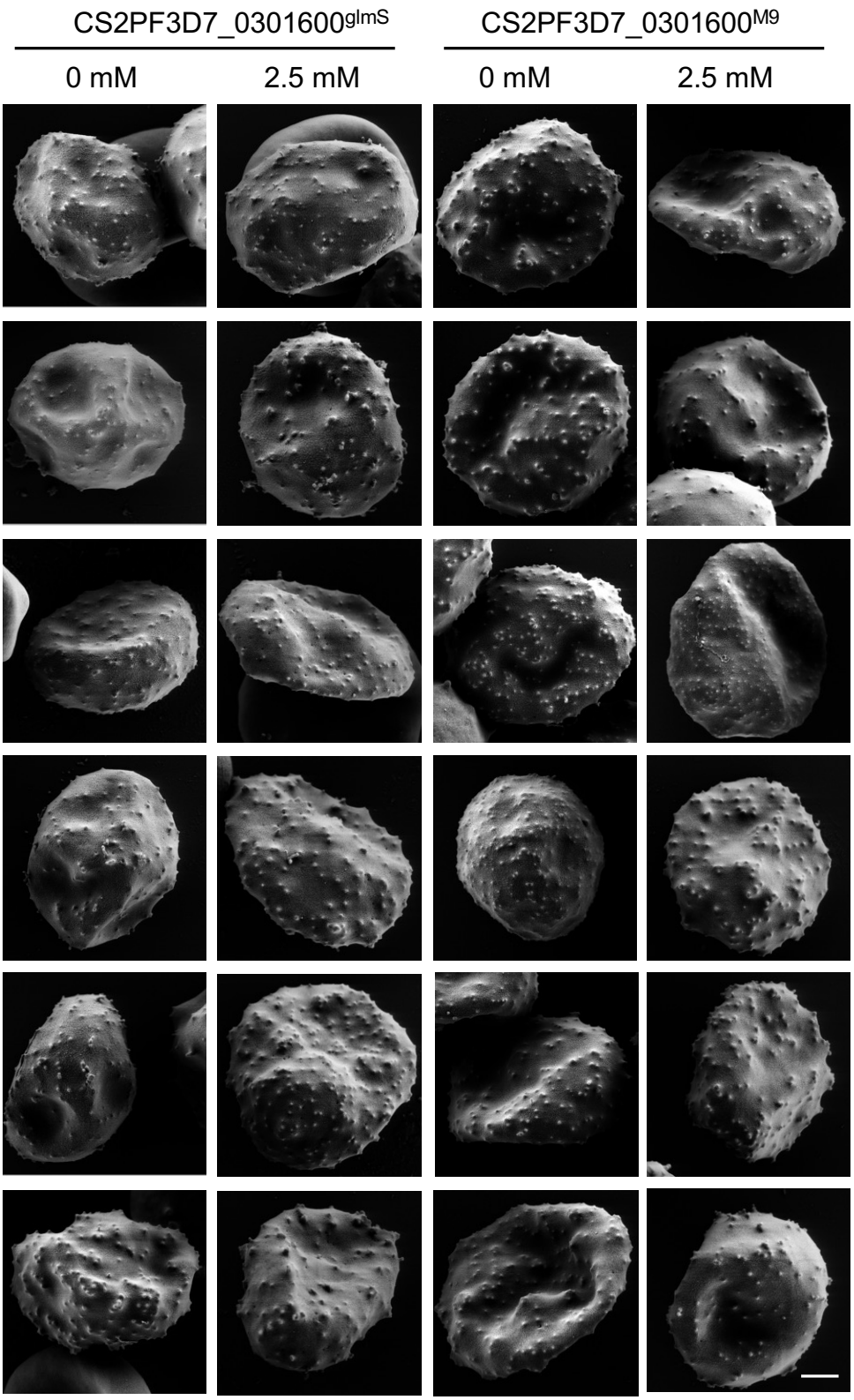

Suppl. 13: Scanning electron microscopy (SEM) images of CS2PF3D7_0301600$^{glmS/M9}$. Parasite-infected erythrocytes ± 2.5 mM GlcN. Scale bar 1 µm.

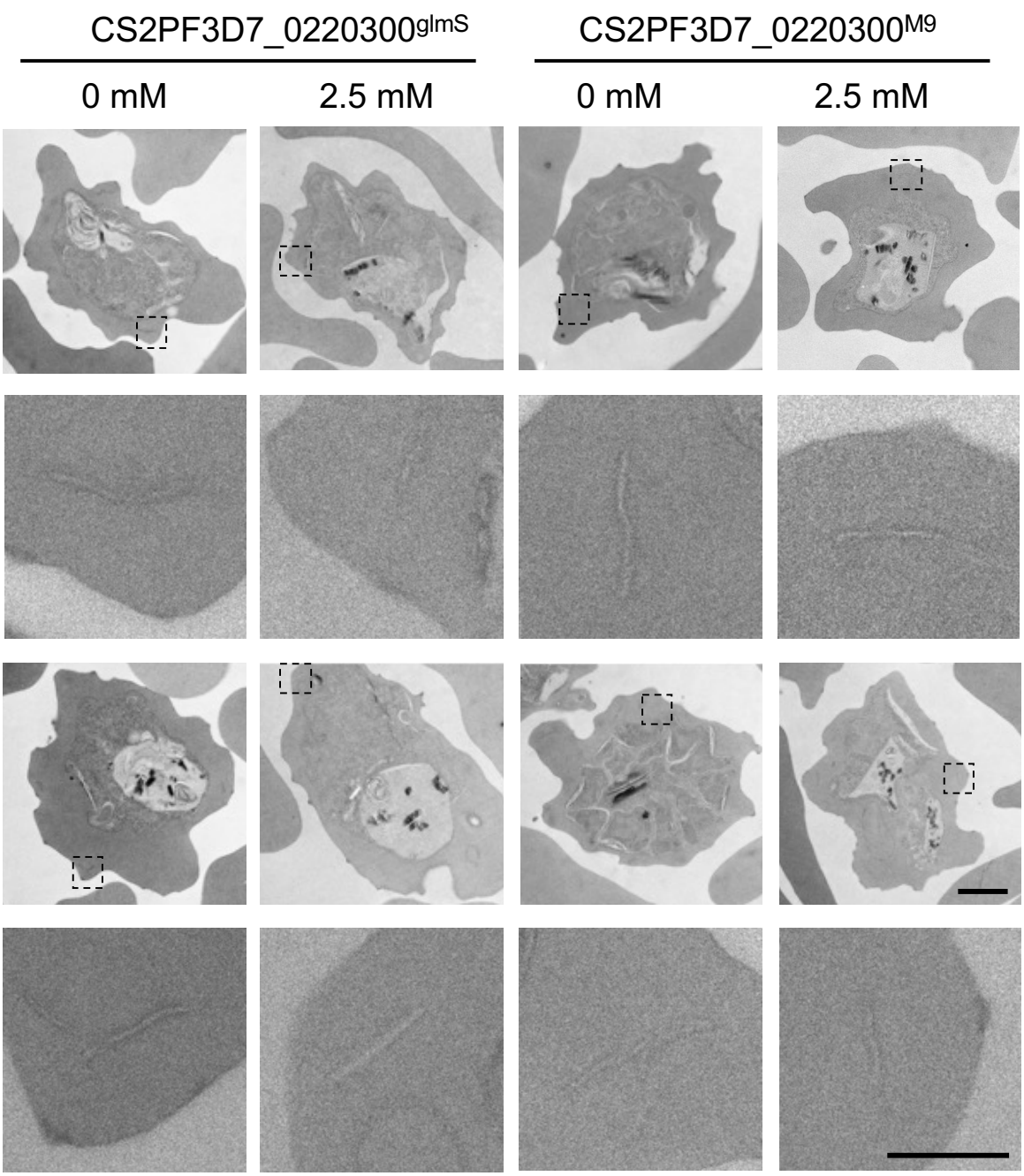
CS2PF3D7_0220300glmS
CS2PF3D7_0220300M9
0 mM
2.5 mM
0 mM
2.5 mM

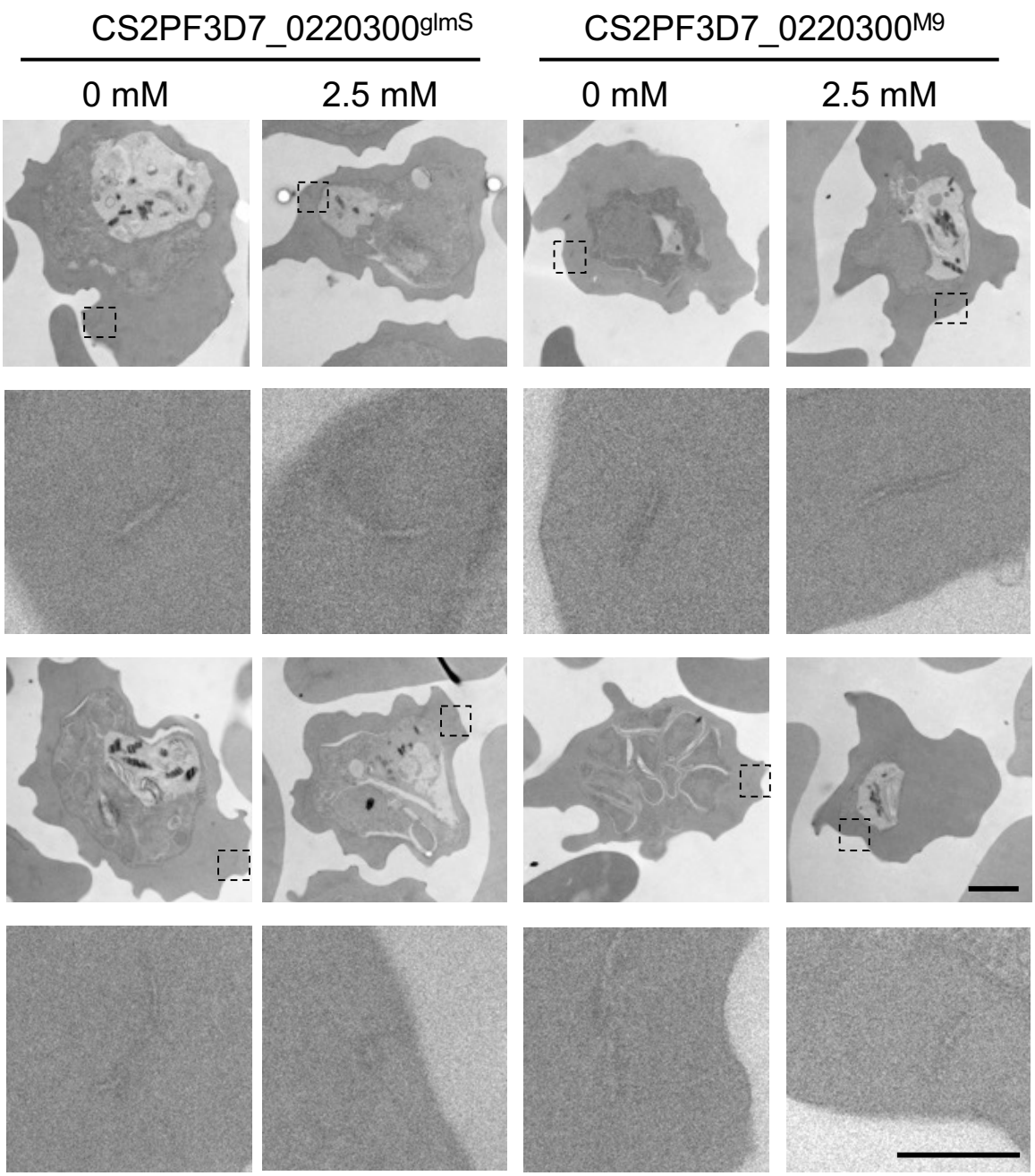

Suppl. 14: Transmission electron microscopy (TEM) images of CS2PF3D7_0220300$^{glmS/M9}$. Parasite-infected erythrocytes ± 2.5 mM GlcN. Detailed images of Maurer's clefts. Scale bar 1 µm (full size image), 0.2 µm (detail image).

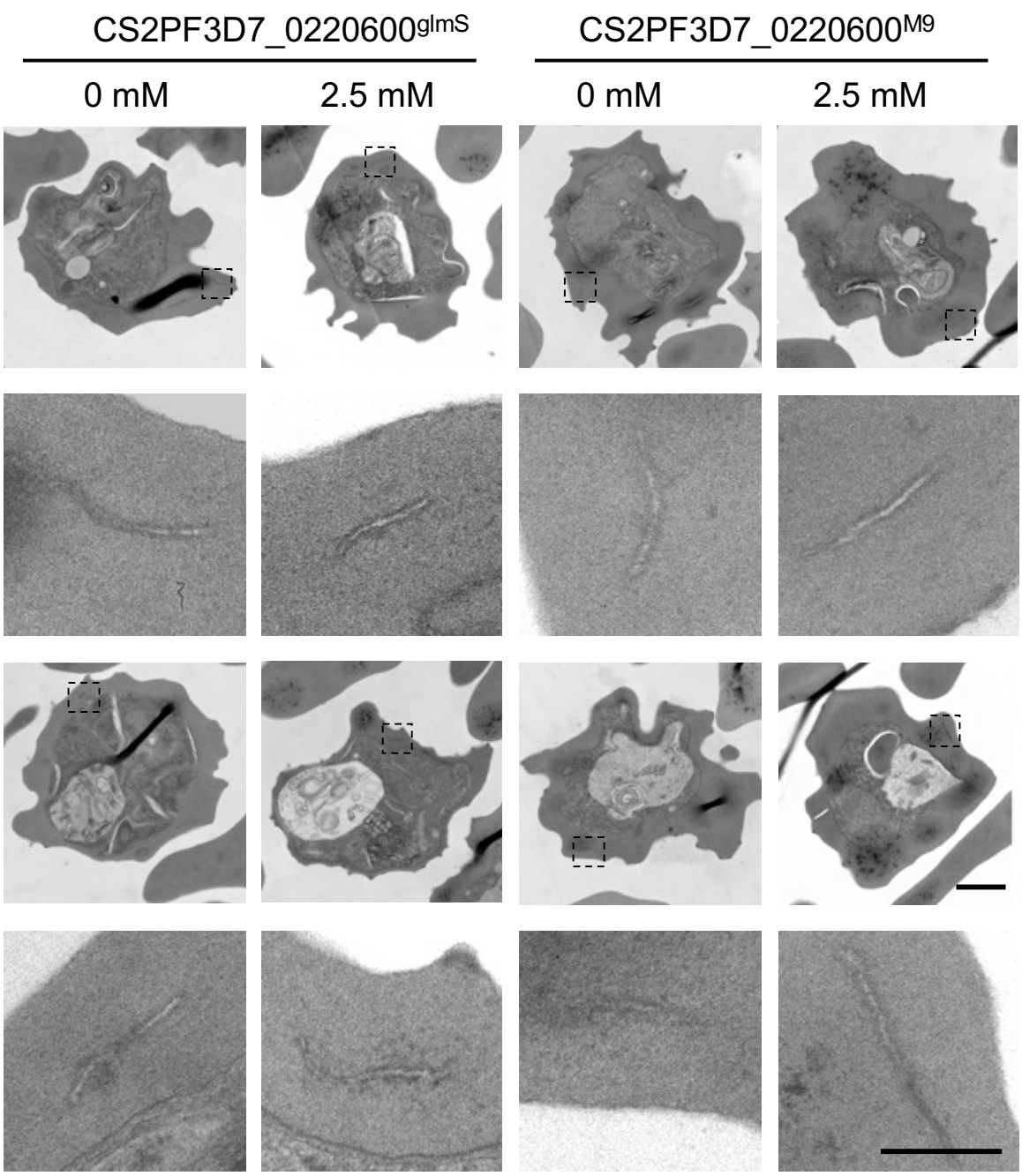
CS2PF3D7_0220600glmS
CS2PF3D7_0220600M9
0 mM
2.5 mM
0 mM
2.5 mM

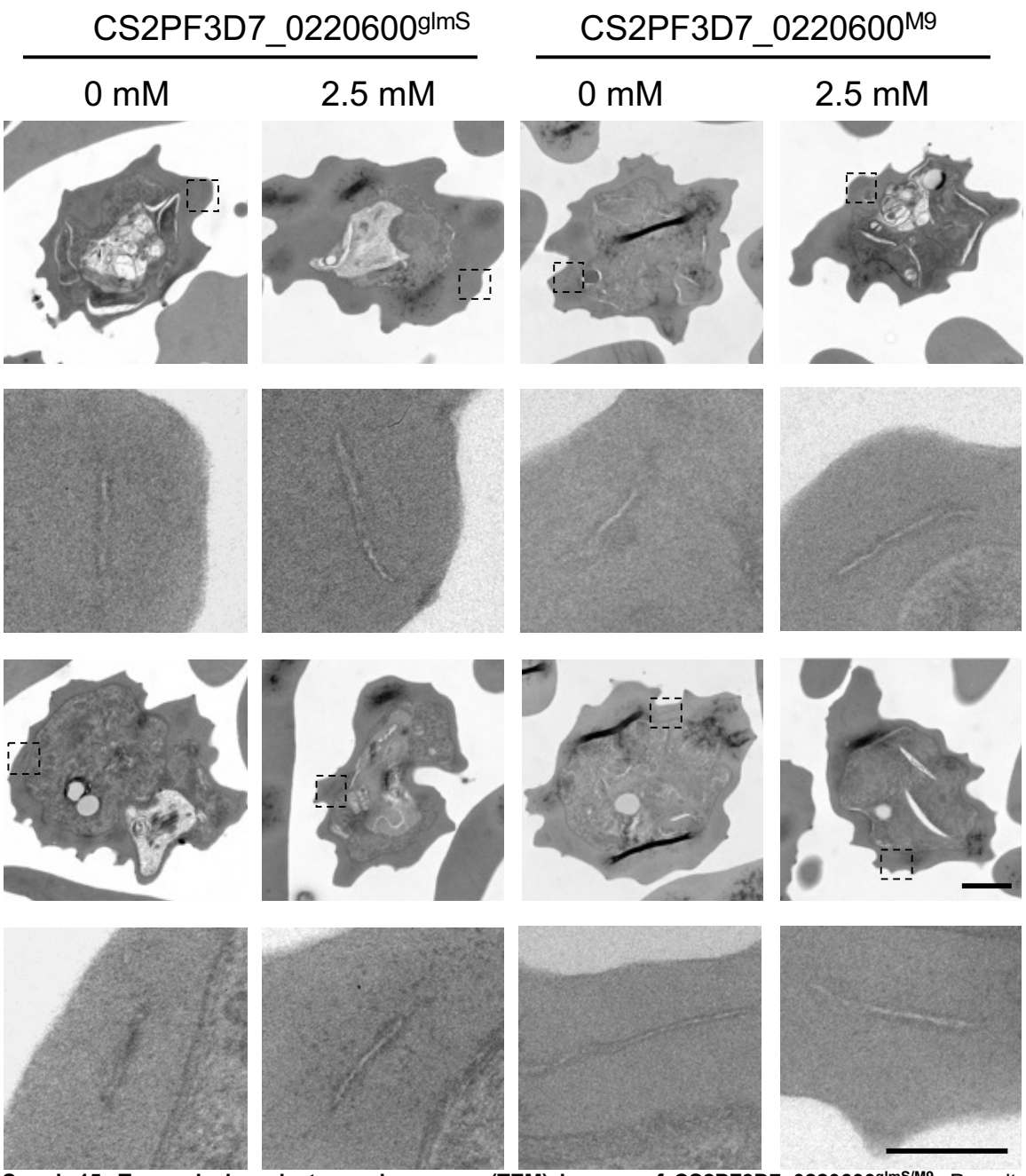

Suppl. 15: Transmission electron microscopy (TEM) images of CS2PF3D7_0220600$^{glmS/M9}$. Parasite-infected erythrocytes ± 2.5 mM GlcN. Detailed images of Maurer's clefts. Scale bar 1 µm (full size image), 0.2 µm (detail image).

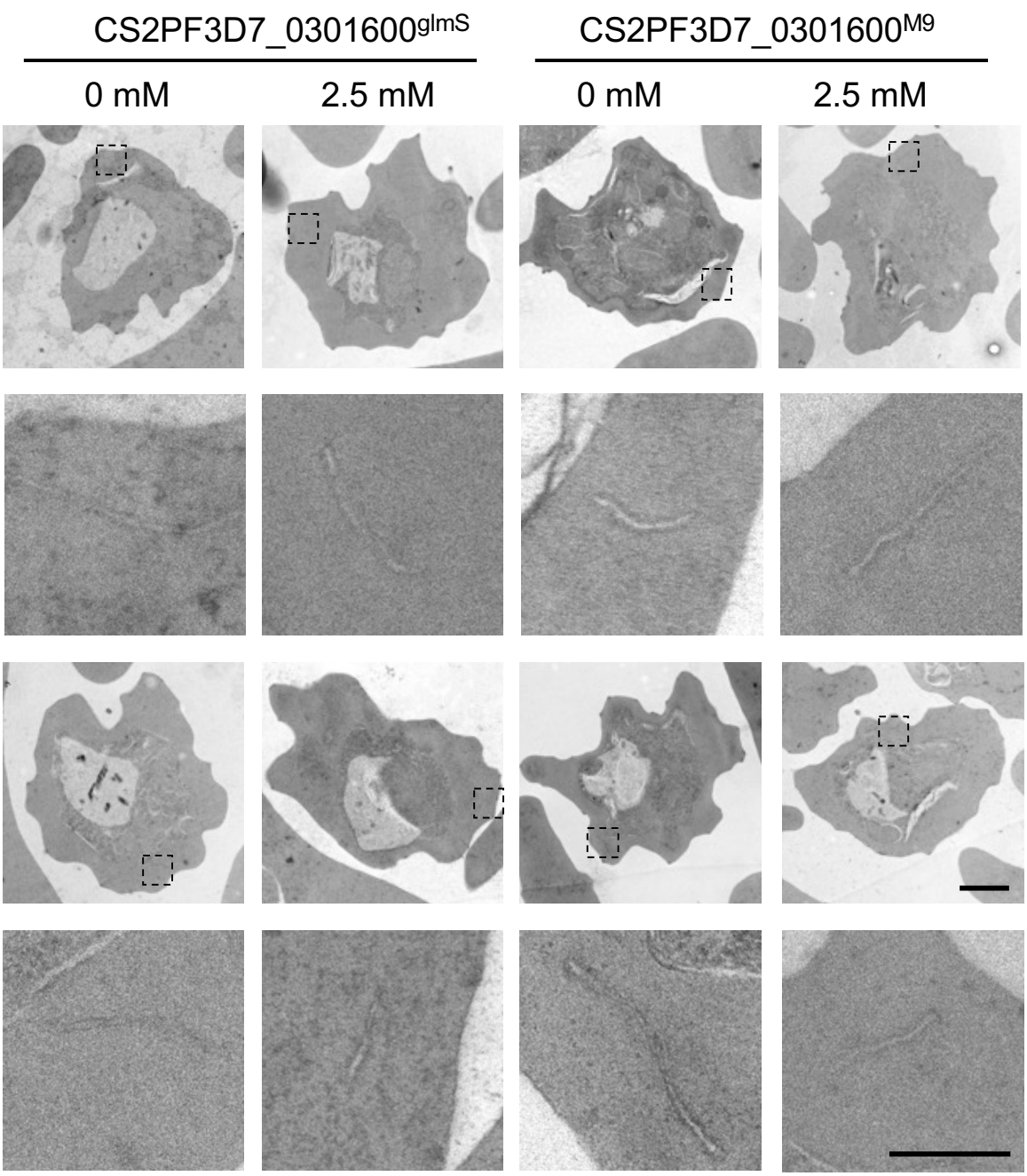
CS2PF3D7_0301600glmS
CS2PF3D7_0301600M9
0 mM
2.5 mM
0 mM
2.5 mM

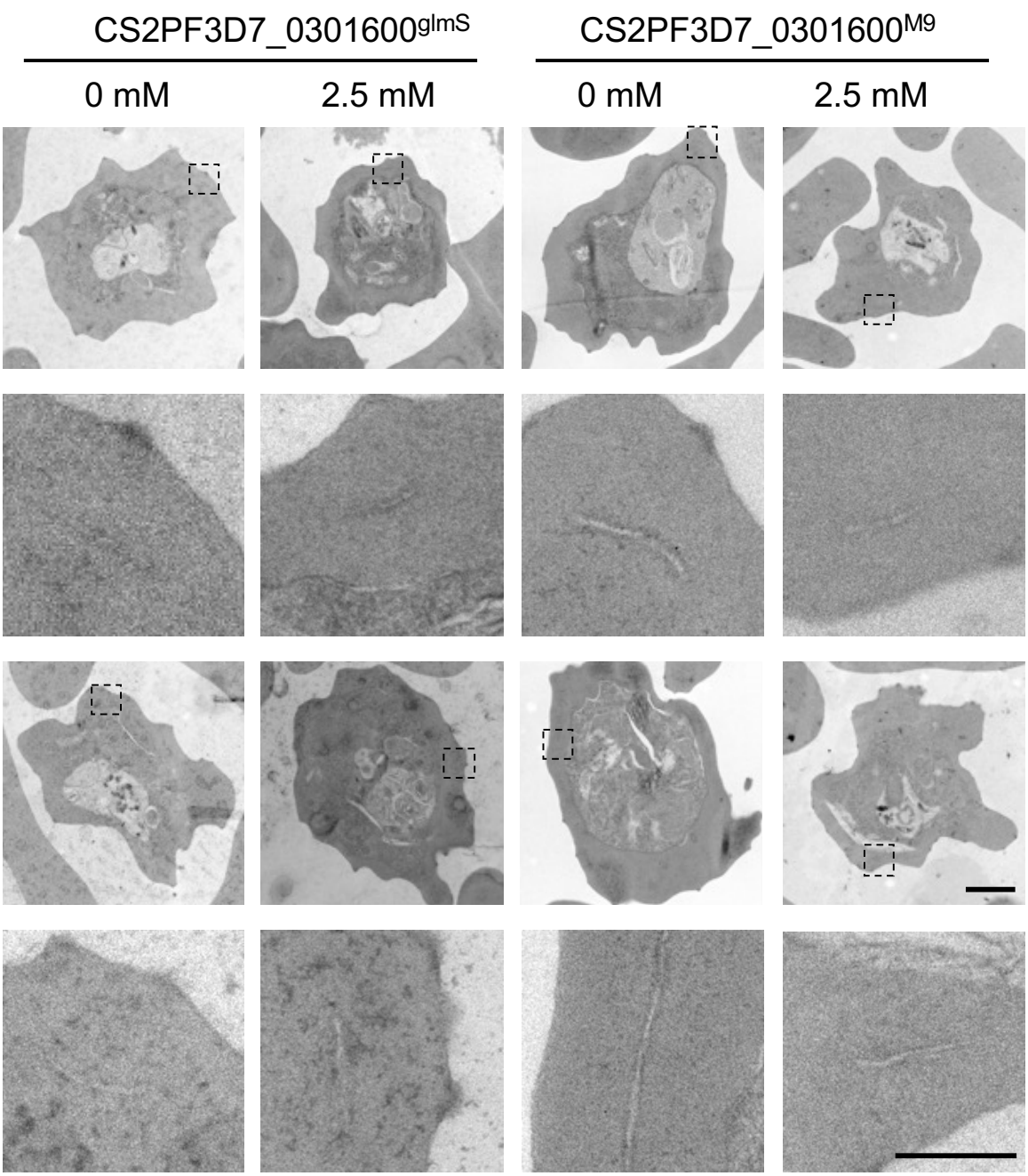

Suppl. 16: Transmission electron microscopy (TEM) images of CS2PF3D7_0301600$^{glmS/M9}$. Parasite-infected erythrocytes ± 2.5 mM GlcN. Detailed images of Maurer's clefts. Scale bar 1 µm (full size image), 0.2 µm (detail image).